

UNESCO-IHE INSTITUTE FOR WATER EDUCATION



Modelling of Cohesive Sediment Transport in the Maasmond Area

Wang, Li

MSc Thesis (WSE-HI.07-18)
April 2007

UNESCO-IHE
Institute for Water Education



Modelling of Cohesive Sediment Transport in the Maasmond Area

Master of Science Thesis
by
Wang, Li

Supervisors
Dr. B. Bhattacharya (UNESCO-IHE)
Dr. T. van Kessel (WL | Delft Hydraulics)

Examination committee
Prof. Dr. R.K. Price (UNESCO-IHE), Chairman
Prof. Dr. D. Zhang (Hohai University)
Dr. B. Bhattacharya (UNESCO-IHE)
Dr. T. van Kessel (WL | Delft Hydraulics)

This research is done for the partial fulfilment of requirements for the Master of Science degree at the UNESCO-IHE Institute for Water Education, Delft, the Netherlands

Delft
April, 2006

The findings, interpretations and conclusions expressed in this study do neither necessarily reflect the views of the UNESCO-IHE Institute for Water Education, nor of the individual members of the MSc committee, nor of their respective employers.

Abstract

In the Dutch coastal zone, where the marine environment is highly dynamic owing to tidal currents, wind-driven, wave-driven, and density-driven currents and waves, the cohesive sediment dynamics is always a great concern to transportation authority and coastal managers. So far, a lot research has been contributed on the cohesive sediment dynamics such as transportation, deposition and resuspension. In addition, the origin of the cohesive sediment is also of a great interest to researchers. In this study, I will explore some underlying mechanics governing cohesive sediment dynamics with the help of numerical models based on Delft3D which is a powerful software package developed by WL | Delft Hydraulics.

This study starts with the large-scale modelling of the North Sea using ZUNO grid, which has been verified by WL | Delft Hydraulics. During this research the original model is simplified due to the limitation of relevant data. Through the comparison with the measured water level, both of the simplified and original ZUNO models present a good performance. The simplification doesn't cause significant change on the simulated results compared with the original model. Based on scale-based philosophy of Vriend, the simulated water level and current velocity on corresponding grids are provided to another model based on the RIJMAMO grid as boundary conditions. The RIJMAMO model is a local refinement for the Dutch coastal area.

The hydrodynamics of the RIJMAMO model is completed with the boundary condition extracted from the ZUNO model. Upon the calibration and verification against SILTMAN data which contains measured data regarding to flow velocity and sediment concentration near the mouth of Maasmond which is adjacent to the approaching channel of the port of Rotterdam, it indicates that boundary conditions provided by the ZUNO model are appropriate for the RIJMAMO model. The wave and sediment models are introduced to the RIJMAMO model successively. After the calibration and verification of the wave and sediment models, the coupled model presents that the sediment dynamics relates much to the significant wave height.

As a new function of Delft3D, WAQ model coupled with FLOW and WAVE models is applied into this study. Amongst them, WAQ model is used for versatile water quality modelling including physical, (bio)chemical and biological processes; FLOW model is used for simulation of multi-dimensional hydrodynamic flow and transport phenomena including sediments; WAVE model is used for simulation of short-crested waves nearshore. Compared with the modelled results by FLOW model used previously in which sediment model is executed as a process, WAQ model presents some improvement on the modelled results. During the calm period, the sediment has more response to the tide-induced shear stress in WAQ model than that in FLOW model, which can be attributed to the more processes included in WAQ model. Nevertheless, due to the limited time, WAQ model has not been calibrated further, in which there is more potential to be exploited.

Keywords: cohesive sediments, dynamics, wave, Delft3D, FLOW, Maasmond, RIJMAMO, SILTMAN data, WAQ, ZUNO.

Acknowledgements

Writing this page, my MSc. study is going to the end of the six months. At this moment, I would like to express my sincere gratitude to many people. Without their help and assistance, this study would not have been completed.

I would like to thank my supervisors, Dr. Biswanath Bhattacharya and Dr. Thijs van Kessel for providing such a nice opportunity to start my MSc. study, during which I got a lot of careful instructions and valuable ideas from you.

I would like to thank Prof. Roland Price and Prof. Arthur Mynett for all directions of discussion which inspired me too much on my research.

Many thanks go to Dr. Dimitri Solomatine and Dr. J.M. de Kok. During every meeting I obtained a lot of precious suggestions from you.

Many thanks go to Prof. J.A. Roelvink and Mick van Der Wegen for leading me into the fantastic simulation of Deflt3D.

Many thanks go to the staffs from WL | Delft Hydraulics, Arjen Luijendijk, Arjen markus, Adri Mourits, Dr. Jacco Groeneweg, Jan Mooiman, and Jan van Beek for your warmhearted help and technical support.

Many thanks go to Dr. I. Popescu, Dr. A. Jonoski, Dr. A.H. Lobbrecht, and Dr. Z. Vojinovic for your consistent help and support.

I am grateful to the PhD researchers and post-doctor fellow from WL | Delft Hydraulics, Ye Qinghua, Li Hong and Huang Ziwen for your frank advices and interesting discussion.

Many thanks go to master students from WL | Delft Hydraulics, Nazli Aral Celik, Paulien van Slingerland, Elisabeth Lee, Al Azhar Mohammed, Bas van Leeuwen, Hendrik Meuwese, Wouter Kranenburg. We shared a lot of fun in office, and constructed a friendly international environment.

Many thanks go to every player of DCF. We enjoyed the happiness brought by football on every Saturday and found more warmness in the past warming winter.

Many thanks go to the colleagues of 2005-2007 Hydroinformatics group. We shared pleasure and pain together in the past year, which turn to be a triumph for all of us so far.

I am thankful to my tutor Prof. Yao Qi of Institute of Environmental & Hydraulic Science at Hohai University for leading me into the field of numerical modelling. I also thank my colleagues at Hohai University for your continuous help and encouragement in the past few years.

Finally, I would like to thank my family for your endless encouragement and love.

Table of Contents

Abstract.....	i
Acknowledgements	iii
List of symbols	vii
Chapter 1 Introduction	1
1.1 Background.....	1
1.2 Objectives of the study	2
1.3 Research Methodology	2
1.3.1 Literature review	2
1.3.2 Different-scale models setting and physical processes simulation.....	2
1.3.3 Schematic representation of research methodology	3
1.4 Definitions used in this study	4
1.5 Outline of the thesis.....	4
Chapter 2 Numerical Model and Model Structure.....	7
2.1 Basic concepts of cohesive sediments	7
2.1.1 Cohesive sediment properties and behaviours	7
2.1.2 Cohesive sediment deposition	11
2.1.3 Cohesive sediment erosion	12
2.2 Hydrodynamics model.....	12
2.2.1 Governing equations.....	12
2.2.2 Boundary conditions.....	15
2.2.3 Solving process.....	16
2.3 WAVE model	17
2.3.1 Basic equations	18
2.3.2 Wave effects on flow	18
2.4 Cohesive sediment dynamics implemented in FLOW model	19
2.4.1 Cohesive sediment settling velocity	19
2.4.2 Cohesive sediment dispersion	20
2.4.3 Cohesive sediment erosion and deposition.....	20
2.4.4 Influence of waves on cohesive sediment transport	21
2.5 Morphodynamics model.....	21
2.5.1 Feedback to hydrodynamics	21
2.5.2 Effect of sediment on fluid density	22
2.6 Water quality model (Delft3D-WAQ).....	22
2.6.1 Mass balances	22
2.6.2 Mass transport by advection and dispersion.....	23
2.6.3 Boundary conditions.....	25
2.6.4 Sediment module implemented in Delft3D-WAQ	25
2.7 Conclusions	27
Chapter 3 Developing the Simplified ZUNO Model	29
3.1 Introduction to the Dutch coastal zone	29
3.2 Model setup	30
3.2.1 Grid and bathymetry	30
3.2.2 Open boundary condition	31
3.2.3 River discharge	31

3.3	Simplified model verification.....	31
3.4	Original model verification	35
3.5	Conclusion.....	37
Chapter 4 RIJMAMO Model Calibration and Verification.....		39
4.1	Introduction to the Maasmond area	39
4.2	Model setup	41
4.2.1	FLOW model.....	41
4.2.2	WAVE model	43
4.3	Model calibration.....	44
4.3.1	Calibration of hydrodynamic model.....	44
4.3.2	Calibration of cohesive sediment model	51
4.4	Model verification	60
4.4.1	Verification of hydrodynamic model	61
4.4.2	Verification of cohesive sediment model	63
4.5	Conclusions	68
Chapter5 WAQ Model		71
5.1	Calibration of WAQ model	71
5.2	Conclusions	76
Chapter 6 Conclusions and Recommendations.....		79
6.1	Conclusions	79
6.2	Recommendations	80
References		81

List of symbols

- a : reference height for suspended sediment concentration (m)
 A : surface area (m^2)
 c : suspended sediment concentration (kg/m^3)
 $c_b^{(\ell)}$: averaged sediment concentration in the near bottom computational layer
 \bar{c} : depth-averaged concentration (kg/m^3)
 $c_{a,e}$: equilibrium concentration (kg/m^3)
 c_b : near-bed concentration (kg/m^3)
 c_{gel} : gelling concentration (kg/m^3)
 c_v : consolidation coefficient of the soil
 $c_x, c_y, c_\sigma, c_\theta$: propagation velocities in x, y and σ, θ space (m/s)
 C_{x_0} : concentration at $x = x_0$ (g/m^3)
 D : diameter of the sediment (mm); deposition rate (kg/m^2s)
 $D^{(\ell)}$: deposition flux ($kg/m^2/s$)
 D_* : dimensionless particle diameter
 D_{50} : median grain size (m)
 D_H, D_V : horizontal and vertical eddy diffusivities (m^2/s)
 D_V^{back} : background turbulent eddy viscosity in vertical direction (m^2/s)
 $E(\sigma, \theta)$: energy density spectrum
 $E^{(\ell)}$: erosion flux ($kg/m^2/s$)
 F_ζ, F_η : horizontal Reynold's stresses determined by using eddy viscosity concept (m/s^2)
 h : water depth (m)
 k : diffusion coefficient (m^2/s)
 ℓ : length scale of the deformation process
 M : erosion rate parameter (kg/m^2s)
 $M^{(\ell)}$: user specified erosion parameter for sediment fraction (ℓ) (kg/m^2s)
 M_i^t : mass in volume i at time t (g)
 M_ξ, M_η : contributions due to external sources or sinks of momentum (m/s^2)
 $N(\sigma, \theta)$: the action density spectrum
 p : porosity of bed layer
 p^w : total pore water pressure (kg/ms^2)
 p_e : hydrostatic pore water pressure (kg/ms^2)
 Pe : Peclet number
 P_x, P_y : horizontal pressure terms, which is given by Boussineq approximation (kg/m^2s^2)
 Ri : Richardson number
 Re : Reynolds
 Re_e : effective Reynolds number
 S : source or sink term per unit area; salinity (ppt)
 S_{max} : maximal salinity at which $w_{s,max}^{(\ell)}$ is specified (ppt)

$S(\tau_{cw}, \tau_{cr,e}^{(\ell)})$: erosion step function:

$$S(\tau_{cw}, \tau_{cr,e}^{(\ell)}) = \begin{cases} \left(\frac{\tau_{cw}}{\tau_{cr,e}^{(\ell)}} - 1 \right), & \text{when } \tau_{cw} > \tau_{cr,e}^{(\ell)}, \\ 0 & \text{when } \tau_{cw} \leq \tau_{cr,e}^{(\ell)}. \end{cases}$$

$S(\tau_{cw}, \tau_{cr,d}^{(\ell)})$: deposition step function:

$$S(\tau_{cw}, \tau_{cr,d}^{(\ell)}) = \begin{cases} \left(1 - \frac{\tau_{cw}}{\tau_{cr,d}^{(\ell)}} \right), & \text{when } \tau_{cw} < \tau_{cr,d}^{(\ell)}, \\ 0 & \text{when } \tau_{cw} \geq \tau_{cr,d}^{(\ell)}. \end{cases}$$

W_s : sediment settling velocity (m/s)

Q_{x_0} : flow at $x = x_0$ (m³/s)

U, V : Generalized Lagrangian Mean (GLM) velocity components (m/s)

\bar{U}, \bar{V} : Depth-averaged GLM velocity components (m/s)

U_m : mean velocity in the fluid mud layer (m/s)

u_* : shear velocity (m/s)

V : velocity of the deformation process

ν : kinematic viscosity (m²/s)

ν_m : viscosity of fluid mud (m²/s)

ν_V : vertical eddy viscosity (m²/s)

v_{x_0} : velocity at $x = x_0$ (m/s)

W_s : settling velocity (m/s)

$W_{s,b}$: settling velocity of the sediment at the bed (m)

$w_s^{(\ell)}$: fall velocity (hindered) (m/s)

$w_{s,0}^{(\ell)}$: non-hindered settling velocity of sediment fraction (ℓ)

$w_{s,f}^{(\ell)}$: fresh water settling velocity of sediment fraction (ℓ) (m/s)

$w_{s,\max}^{(\ell)}$: settling velocity of sediment fraction (ℓ) at salinity concentration SALMAX (m/s)

β : Rouse number

δ_b : thickness of bed layer (m)

δ_m : thickness of fluid mud layer (m)

δ_{nb} : thickness of near-bed layer (m)

ε_s^ℓ : vertical sediment mixing coefficient for sediment fraction (ℓ) (m²/s)

ε_f : vertical fluid mixing coefficient calculated by turbulence closure model (m²/s)

κ : von Kármán constant

ρ : local fluid density (kg/m³)

ρ_0 : reference density of water (kg/m³)

ρ_m : density of fluid mud (kg/ms²)

ρ_s : density of solid sediment particles (kg/m³)

ρ_s^ℓ : specific density of sediment fraction (ℓ) (kg/m^3)
 ρ_w : specific density of water with salinity concentration S (kg/m^3)
 ζ : water surface elevation above reference datum (m)
 σ : externally applied stress; vertical “sigma” coordinate
 σ_{mol} : Prandtl-Schmidt number for molecular mixing
 σ_T : turbulent Prandtl-Schmidt number
 τ_B : Bingham strength of fluid mud (N/m^2)
 τ_b : bed shear stress (N/m^2)
 $\tau_{b,w}$: wave-induced bottom shear stress (N/m^2)
 $\tau_{b,f}$: tidal flow-induced bottom shear stress (N/m^2)
 $\tau_{c,w}$: critical shear stress for erosion of bed layer (N/m^2)
 $\tau_{c,f}$: critical shear stress for erosion of near-bed layer (N/m^2)
 τ_{cw} : mean bed stress due to current and waves as calculated by the wave-current interaction model (N/m^2)
 $\tau_{cr,e}^{(\ell)}$: user specified critical erosion shear stress (N/m^2)
 $\tau_{cr,d}^{(\ell)}$: user specified critical deposition shear stress (N/m^2)
 τ_d : critical shear stress for deposition (N/m^2)
 τ_e : critical shear stress for erosion (N/m^2)
 τ_v : yield strength (N/m^2)
 ν_{mol} : kinematic viscosity (molecular) coefficient (m^2/s)
 ω : vertical velocity component in sigma coordinate system (s^{-1})
 ϕ : fineness factor of sediment
 $\left. \frac{\partial C}{\partial x} \right|_{x_0}$: concentration gradient at $x = x_0$ (g/m^4)
 (ℓ) : sediment fraction (ℓ)
 Δt : time step (s)

Chapter 1 Introduction

1.1 Background

Coastal zone directly supports a growing part of the world population. Highest densities of urbanisation are found along coastal areas which are multiform, infinitely complex, quasi-fractal, always changing and unpredictable in many aspects. Understanding complex interactions among waves, current, and sediment in energetic coastal and estuarine settings has been of interests to coastal oceanography and engineering; e.g. coastal protection, land reclamation, dredging of deepwater navigational channels, and water quality management. Both coastal oceanographers and coastal engineers would like to understand the underlying physical process governing the cohesive sediment transport in coastal and estuarine energetic waters. Coastal oceanographers focus on erosion and deposition on the coastal mudflat and saltmarshes. Coastal engineers are more interested in siltations in the harbours and the deep water navigational channel.

So far, a lot of work has been done for the sediment transport problem. As a kind of important study tool, the numerical model is playing more and more role in revealing patterns of cohesive sediment transportation, deposition and resuspension. Therefore, with the help of the numerical model, we are able to have a better insight in the coastal processes and corresponding sediment processes, which makes it possible to provide some constructive suggestions to decision-makers by modellers.

For instance, the mud deposits and high turbidity in the Belgian-Dutch coastal zone, southern part of the North Sea from the Dover strait to Zeebrugge, were investigated with integrated 2D hydrodynamic and sediment model. It is found the formation of high turbidity zone can be attributed to the currents and the influx of SPM (suspended particulate matter) through the Dover Strait. Due to the decreasing capacity of residual transport and the shallowness of the area, the SPM is concentrated in the Belgian-Dutch coastal water and forms a turbidity maximum in front of Zeebrugge. Mud was found continuously deposited and resuspended. Significant variations occur during tidal cycles and during neap-spring cycles. Seasons and meteorological conditions have an influence on mud behaviours as well. Because of the many processes involved, it still remained difficult to compare the model output with the measured data on quantity (Fettweis, 2003). Moreover, Ye (2006) developed a schematized model and examined the influence of waves upon the cohesive sediment in the Haringvliet Mouth. The model results show the wave dynamics is one of the most significant processes behind the sediment movements in the Haringvliet Mouth.

For the port of Rotterdam being one of the largest ports over the world, the access channel and harbour basins need to be maintained by frequent dredging, especially during and after the rough weather periods, a large amount of cohesive sediments (mud) are deposited in short time interval. A 1DV POINT MODEL which is a fully 3D sediment transport model omitting horizontal advection terms was applied. Within this model, salinity-induced and sediment-induced stratification effects, and wave-induced mixing are represented. The result is that the collapse of concentration profile is not sufficient condition to form high concentrated near-bed suspension and it is

hypothesized that the collapse of suspension triggers the generation of sediment-driven density current causing the rapid siltation through the transport and accumulation of fluid mud into the channel and harbour basins (Winterwerp, 1998). Moreover, Bhattacharya (2005) investigated the sedimentation problem of the port of Rotterdam and built a data-driven model which predicted the transport rate of cohesive sediment.

In order to improve the understanding of the physical dynamics and sediment environments along the Dutch coast, one Delft Cluster project sponsored by the Dutch government is aimed to develop a hybrid sedimentation modelling combining data-driven modelling approach with physically-based (numerical) models to predict sediment transport rates and accretion rates in channels, estuaries or harbour basins. In fact, this study is a component of the project mentioned above, which will be detailed in the following sections. Of course, the research on cohesive sediment dynamics along the coast is not limited to The Netherlands but is applicable anywhere.

1.2 Objectives of the study

The main objective of this study is to understand the underlying processes which govern cohesive sediment dynamics such as deposition and resuspension with the help of numerical models.

Considering the ZUNO model is too coarse, the study will utilize the finer RIJMAMO model to obtain more detailed information regarding to velocity and SPM concentration in the Maasmond area adjacent to the approaching channel of the port of Rotterdam.

With the hydrodynamic boundary condition extracted from ZUNO model, the hydrodynamic results of the RIJMAMO model will be calibrated and verified against SILTMAN data.

On the premise that the hydrodynamic results simulated by RIJMAMO model are reliable, the study will reveal how much of the observed variability on SPM concentration in SILTMAN data can be explained by the well-established numerical models.

1.3 Research Methodology

1.3.1 Literature review

The literature review aims at understanding the cohesive sediments properties and behaviours, the relevant physical processes of the system being studied and underlying theories on topics, such as, the FLOW model, the WAVE model, the cohesive sediment transportation model as a process included in the FLOW model, and the water quality (WAQ) model used to calculate the cohesive sediment, all of which are implemented in Delft3D systems.

1.3.2 Different-scale models setting and physical processes simulation

According to the scale-based theory developed by de Vriend (1991), bigger scale model provides the boundary conditions for the smaller scale model. In order to account for the wave-induced effect on cohesive sediment dynamics, a wave model is introduced to be

online-coupled with the flow model. In the interest of describing cohesive sediment characteristics and with the benefit of faster calibration, a water quality model which includes more physical processes for the cohesive sediment compared with the FLOW model is used in this study.

1.3.3 Schematic representation of research methodology

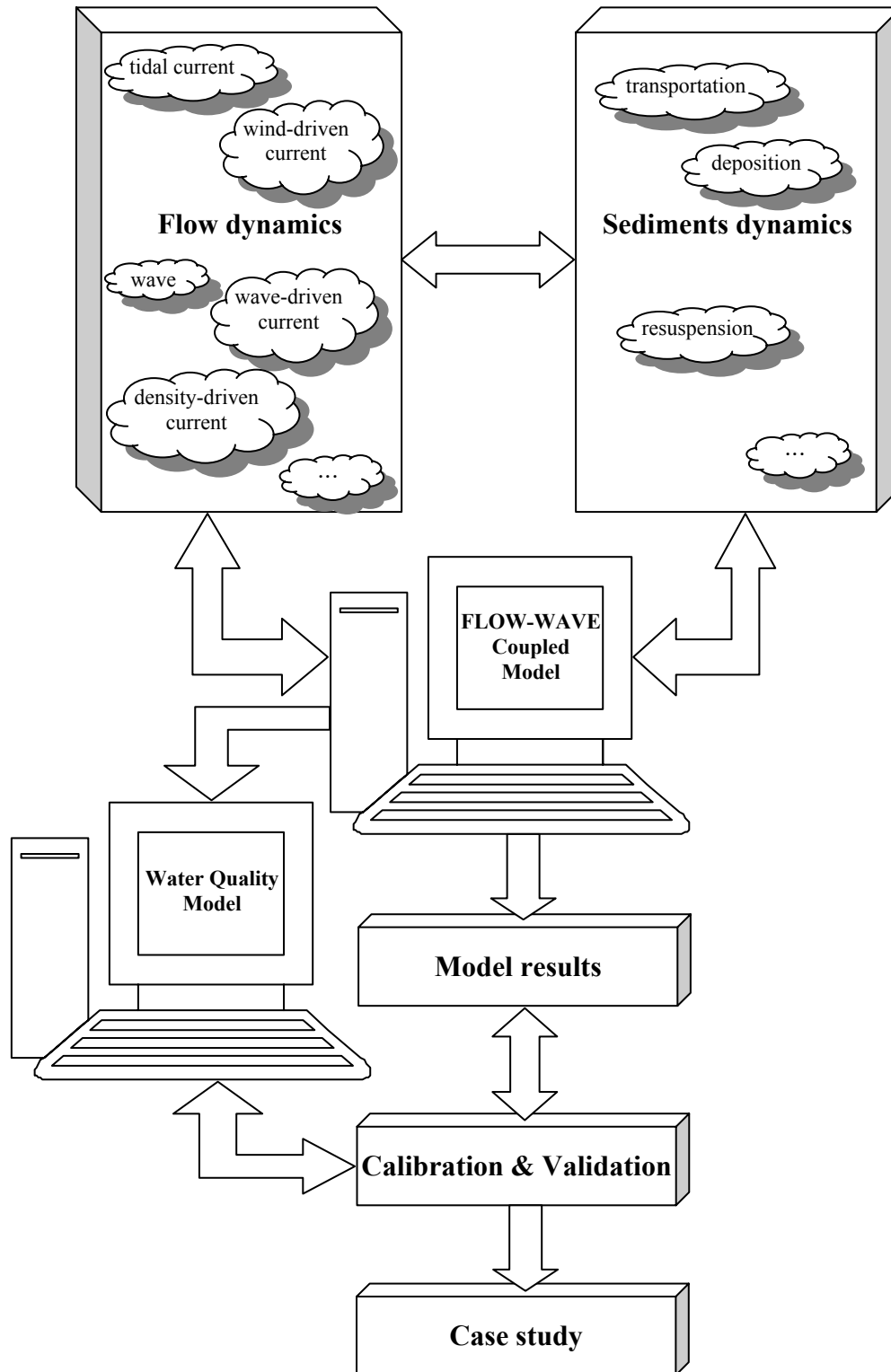


Fig 1.1 The schematization of research methodology

1.4 Definitions used in this study

In this study, some numerical models and measurement database with special names and functions are utilized, which are specified as follows:

ZUNO coarse grid model

This study starts from the ZUNO coarse grid which covers the area from the south Dover strait to the north of Scotland and most northern points of Denmark with about 9,000 computational elements. The grid is originally provided by the Dutch Ministry of Public Works and then to WL | Delft Hydraulics. The model setup based on the ZUNO grid, which is named ZUNO model in this thesis, is useful in the beginning to provide hydrodynamic boundary conditions for the finer model.

RIJMAMO model

Compared with the ZUNO model, it is much finer grid with more than 20,000 computational elements and only a local refinement for the Dutch coast. The length of the model section is about 60 km, the width about 30 km excluding the channel and harbour.

SILTMAN data

In order to develop a modelling system for studying the sediment transport processes in the vicinity of the Maasmond area, Rijkswaterstaat initiated the SILTMAN-project. Four semi-permanent measuring stations were installed by Rijkswaterstaat near the mouth of the Maasmond to monitor the flow velocity and the suspended sediment concentration which were recorded in the period November 1995 – May 1996 and November 1996 – May 1997.

Coupled model / Online simulation of Delft3D

The latest version used in this study, the flow, wave, sediment and morphology models are simulated in a coupled way, which is also termed as online simulation.

Delft3D modelling system

Delft3D modelling system is a unique, fully integrated modelling framework for a multi-disciplinary approach and 3D computations for coastal zone, river, lake and estuarine areas provided by WL | Delft Hydraulics. The Delft3D framework is composed of several modules, such as Delft3D-FLOW for hydrodynamics, salinity, temperature, online sediment transport and morphology, WAVE for short wave propagation, WAQ-SED for cohesive and non-cohesive sediment transport, etc.

1.5 Outline of the thesis

The basic structure is comprised of the following parts:

Chapter 1 introduces the objectives of the study and the methodology used in this study.

Chapter 2 presents working principles and involved processes of the numerical model, including some basic concepts of cohesive sediments.

Chapter 3 verifies the simplified ZUNO model developed in this study and original ZUNO model through the comparison between the simulated and observed values of water level. At the same time, hydrodynamic boundary conditions for RIJMAMO model are extracted from the results calculated by the simplified and original ZUNO models.

Chapter 4 is dedicated to calibrate and verify RIJMAMO model firstly from hydrodynamics, followed by sediment concentration after coupling with the wave model.

Chapter 5 utilizes a new function of Delft3D to develop a water quality model by coupling the flow model with the wave and WAQ models simultaneously for carrying out further comparison with the observed data.

Chapter 6 presents some conclusions in view of this study done, and some recommendations for further study are put forward as well.

Chapter 2 Numerical Model and Model Structure

Numerical model is our approach to build physically-based model in this study. In our study, the integrated model consists of hydrodynamics model, WAVE model and the sediment model which will be introduced respectively in this chapter.

2.1 Basic concepts of cohesive sediments

The cohesive sediment is generally characteristics of being sticky, muddy, stinky and sometimes gassy. Actually all the cohesive sediment consists of organic and mineral solids in a liquid phase. Both the solids and the time scale of flow of the liquid phase dominate the cohesive feature of the sediment.

2.1.1 Cohesive sediment properties and behaviours

Cohesive sediment, or mud, as encountered in the marine environment, consists of a mixture of clay, silt, (fine) sand, organic material, water, and sometimes gas. In order to understand the cohesive sediment property, some work should be started from its composition.

The solid phase is characterised by its particle size distribution. For practical purposes many classifications were defined. In sedimentology, the particle diameter is often given in terms of the fineness factor ϕ (Krumbein, 1941), defined by:

$$\phi = -\log_2 D \quad \text{with } D \text{ in mm} \quad (2.1)$$

it is remarked that all fractions can contain mineral and organic solids whatever is clay, silt, sand or gravel. In common application, there is an important fraction definition: fines ($< 45 \mu\text{m}$) and mud fraction ($< 63 \mu\text{m}$).

In its mineral ingredients, clay minerals are to a large extent responsible for cohesion mainly because of the size and flat shape of the particles, yielding a very high specific surface area and an electrical charge distribution, which interacts with the ambient water. Moreover, as the most significant property of cohesive sediment is that it can form flocs when the sediment is put in contact with a fluid especially in marine environments, the salinity tends to aggravate its flocculation.

However, behaviours and properties of cohesive sediment on a larger scale are not only dependent on the composition itself, but also on a number of environmental parameters. Upon the increasing order of sediment concentration c , different modes of cohesive sediment appearance are defined as shown as Table 2.1

Table 2.1 Classification of cohesive sediment modes in the marine environment

	concentr.	flow characteristics		governing scale numbers		
LCMS	$c \ll c_{gel}$	turbulent	Newtonian	Re	β	
HCMS	$c < c_{gel}$	turbulent	Newtonian	Re	Ri	
turbidity current	$c \approx c_{gel}$	turbulent	non-Newt.	Re_e	Ri	
mobile fluid mud	$c \approx c_{gel}$	trans./lam	non-Newt.	Re_e	Ri	Pe
stationary fluid mud	$c \approx c_{gel}$	tans./creep	non-Newt.		p^w/p_e	Pe
consolidation bed	$c > c_{gel}$	creep	non-Newt.		p^w/p_e	Pe σ/τ_v
consolidated bed	$c \gg c_{gel}$	stationary	non-Newt.			σ/τ_v

where the following symbols have been used:

c = suspended sediment concentration p^w = total pore water pressure
 c_{gel} = gelling concentration p_e = hydrostatic pore water pressure
 Re = Reynolds Pe = Peclet number
 Re_e = effective Reynolds number σ = externally applied stress
 β = Rouse number τ_v = yield strength
 Ri = Richardson number

The modes of cohesive sediment appearance in the first column of Table 2.1 are illustrated as below:

- LCMS: abbreviation for Low-Concentration Mud Suspensions, the concentrations are too low to affect the flow field.
- HCMS: abbreviation for High-Concentration Mud Suspensions, the turbulent flow is (largely) affected by the suspended sediment.
- Turbidity current: a current of rapidly moving, sediment-laden water moving down a slope through another fluid. The current moves because it has a higher density and turbidity than the fluid through which it flows.
- Fluid mud: a suspension of cohesive sediment at a concentration at or beyond the gelling point of the order of several 10 to 100 g/l.
- Consolidation and consolidated beds: during sedimentation, more and more mud flocs accumulate on the bed, and the flocs that arrived first are squeezed by the ones on top. Pore water is driven out of the flocs and out of the space between the flocs.

It is remarked that no absolute c -values can be assigned to the first column, as the mud appearances are determined by sediment and pore water properties and the stress history of the sediment.

The gelling concentration c_{gel} is hereby defined as the concentration at which a network structure exits. The Rouse number β determines the vertical suspended sediment concentration profile, and is defined as:

$$\beta = \sigma_T W_s / \kappa u_* \quad (2.2)$$

where σ_T is the turbulent Prandtl-Schmidt number, W_s is settling velocity, κ is the von Kármán constant and u_* the shear velocity.

The Reynolds number Re defines whether the flow is laminar or turbulent. For non-Newtonian, Bingham plastic flow, the effective Reynolds number Re_e is defined as:

$$\frac{1}{Re_e} = \frac{1}{Re} + \frac{1}{Re_y} \quad \text{where } Re = \frac{4U_m \delta_m}{\nu_m} \quad \text{and } Re_y = \frac{8\rho_m U_m^2}{\tau_B} \quad (2.3)$$

where U_m is the mean velocity in the fluid mud layer with thickness δ_m , τ_B is the Bingham strength of fluid mud, ν_m and ρ_m are viscosity and density of fluid mud.

The Richardson number Ri determines whether (sediment-induced) buoyancy effects (stratification) on the turbulent properties of the flow are important.

The difference between the total pore water pressure p^w and the hydrostatic pore water pressure p_e is called excess pore water pressure.

The Peclet number Pe is a measure to determine whether a deformation process should be regarded as drained or undrained, and is defined as:

$$Pe = V\ell / c_v \quad (2.4)$$

where V is the velocity of the deformation process, ℓ is a length scale of the deformation process, and c_v is the consolidation coefficient of the soil.

The ratio of the (externally) applied stresses σ and the yield strength τ_y determines whether the soil may flow under the influence of mentioned stresses.

Furthermore, there are a number of processes which determine the vertical concentration profile such as plotted in Fig 2.1.

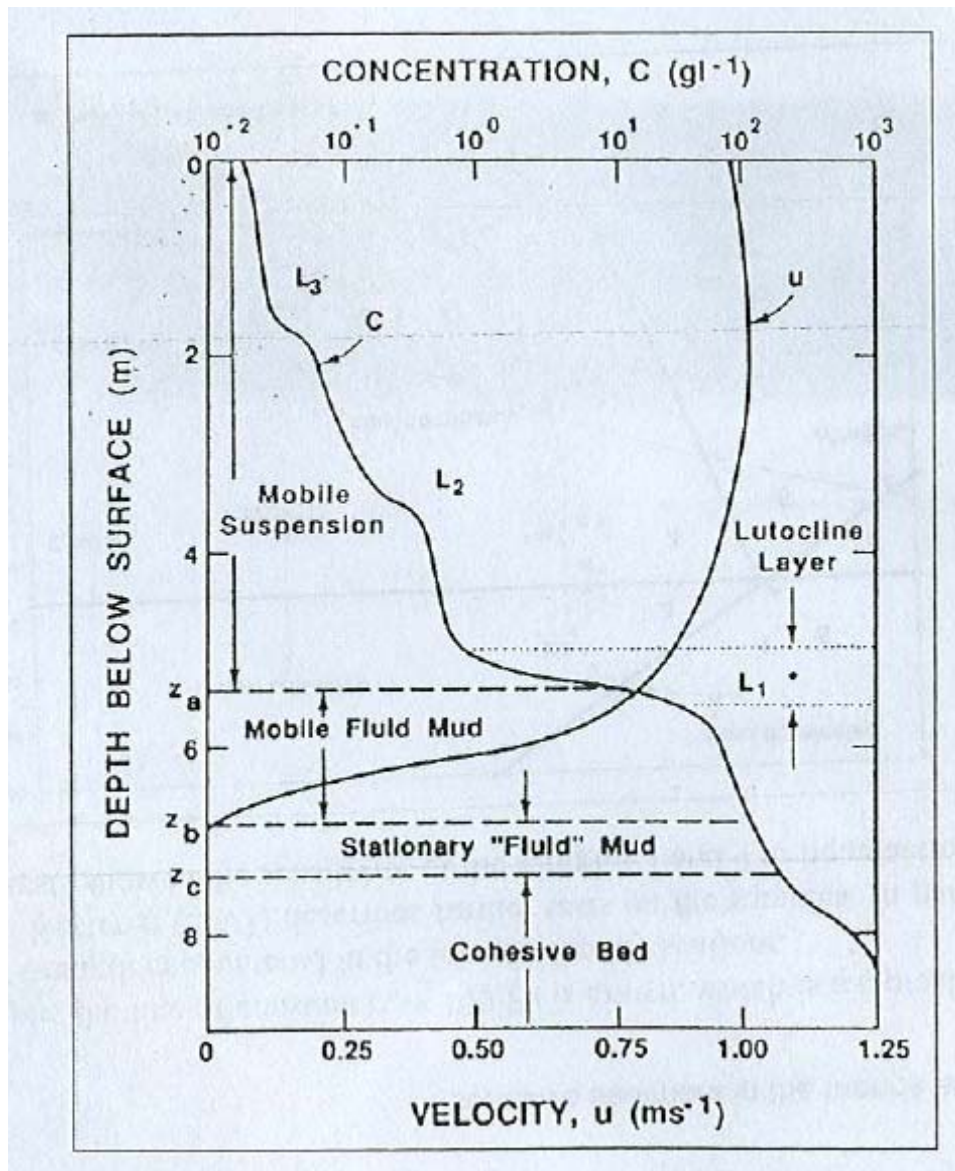


Fig 2.1 Typical vertical profiles of suspended sediment concentration and velocity for high-concentration conditions (after Ross and Mehta, 1989).

- Flocculation: because of the cohesive nature of mud, flocs are formed, affecting the settling velocity and bed structure,
- Settling and mixing: mud particles fall through the water column due to gravity, opposed by mixing processes generated by the turbulent water movement,
- Deposition: settling mud particles may become part of the bed,
- Resuspension: during accelerating flow, particles freshly deposited on the bed may be re-entrained into the water column by the turbulent flow,
- Entrainment: turbulent flow over or underneath a less turbulent fluid entrains water and matter from this less turbulent layer,
- Gelling: deposited mud particles, when left still for sufficient time, will form a structure, causing the build-up of strength that can resist re-entrainment,
- Consolidation: another step in bed formation is self-weight consolidation, when pore water is squeezed out of the bed, and the strength of the bed increases further,

- Liquefaction: when subject to cyclical loading, bonds between particles can be broken gradually, reversing the consolidation process, weakening the bed,
- Erosion: even when the bed has achieved a considerable strength, it can still be eroded by turbulent flow or waves.

These processes may act simultaneously or successively. Often however, only some of these play a role, depending on the dominant conditions. In this study, deposition and erosion are main processes taken into account, for which some brief description is made in the following part.

2.1.2 Cohesive sediment deposition

Settling of mud flocs is one of the most important aspects in assessing the transport and fate of cohesive sediment suspensions in the marine environment. Yet, this settling velocity is difficult to determine. It should be recognized that a uniquely defined settling velocity for cohesive sediment does not exist. In order to circumvent these difficulties, some meaningful definitions are made:

W_s : a characteristics settling velocity without further specification, constant in time and space,

$w_{s,r}$: settling velocity of a single mud flocs in still water; $w_{s,r}$ may vary in time and space as a result of flocculation processes,

w_s : effective settling velocity of a particle in a suspension of cohesive sediment.

In addition, there are two definitions we should distinguish from each other:

Deposition: the gross flux of cohesive sediment flocs on the seabed,

Sedimentation: the net increase in bed level (accretion or shoaling), i.e. the sedimentation rate is the deposition rate minus the erosion rate.

A formula for the deposition rate of cohesive sediment used world-wide is defined as:

$$\frac{dh\bar{c}}{dt} = -D = -W_s c_b \left(1 - \frac{\tau_b}{\tau_d} \right) \text{ for } \tau_b < \tau_d \quad (2.5)$$

where D is the deposition rate, \bar{c} is the depth-averaged concentration, c_b is the near-bed concentration, τ_b the bed shear stress and τ_d the so-called critical shear stress for deposition.

However, this formulation is valid under laboratory conditions only, but cannot explain many field observations. So an alternative description is put forward. It is assumed that erosion and deposition can occur simultaneously. The deposition rate D is given by the sediment flux at the bed, thus:

$$D = W_{s,b} c_b \quad (2.6)$$

where c_b and $W_{s,b}$ are the suspended sediment concentration and settling velocity of the sediment at the bed. Actually, it is equivalent to equation (2.6) if we set τ_d large enough, which can guarantee there is continuous deposition being occurring.

2.1.3 Cohesive sediment erosion

The transport and fate of cohesive sediment in the marine environment is governed to a large extent by water-bed exchange processes, i.e. deposition and erosion. In fact, the erodibility of freshly deposited cohesive sediment particles decreases with time, as the critical shear stress of erosion increases with time because of consolidation and physico-chemical effects, which means some parameters in formulations are also dependant on the time scale. Similar to deposition process, there is a classical formula describing erosion as well, which is developed by Partheniades based on systematic experiments and parameterized by Ariathurai (1974):

$$E = M \left(\frac{\tau_b - \tau_e}{\tau_e} \right) \text{ for } \tau_b > \tau_e \quad (2.7)$$

where M is an erosion rate parameter, τ_b the turbulent-mean bed shear stress, and τ_e a critical (threshold) shear stress for erosion. This formula was combined with the deposition formula aforementioned to compute the water-bed exchange rate in a numerical model for the transport of cohesive sediment.

2.2 Hydrodynamics model

In Delft3D, hydrodynamic model is executed by ‘FLOW’ module in which the optional sediment model is embedded as well. The Flow module of this system, Delft3D-FLOW provides the hydrodynamic results for other modules such as water quality, ecology, waves and morphology.

Delft3D-FLOW is a multi-dimensional (2D or 3D) hydrodynamic (and transport) simulation program which calculates non-steady flow and transport phenomenon that result from tidal meteorological forcing on a rectilinear or a curvilinear, boundary fitted grid. In this study, we are interested in the cohesive sediment distribution along the depth of the water column especially in its concentration near to the bottom. Therefore 3D hydrodynamic model is established based on a curvilinear boundary fitted grid.

2.2.1 Governing equations

Delft3D-FLOW solves the Navier Stokes equations for an incompressible fluid, under shallow water and Boussinesq assumptions. Because of neglecting vertical accelerations in the vertical momentum, we get the hydrostatic equation. There are two kinds of horizontal co-ordinates we can choose in Delft3D-FLOW. In this study, the Cartesian co-ordinate is utilized. In the vertical directions, there are also two different vertical grid systems, we choose the σ co-ordinate system (σ -grid) which is boundary fitted both to the bottom and to the moving free surface.

2.2.1.1 The σ co-ordinate system

The number of vertical layer specified by users is constant over the entire horizontal computational area, which is independent of the local depth. The thickness of each layer can be non-uniform, which allows for more resolution for the zones of interest.

The σ co-ordinate system is defined as:

$$\sigma = \frac{z - \zeta}{H} \quad (2.8)$$

The value of σ varies between -1 and 1, which can be demonstrated as Fig 2.2.

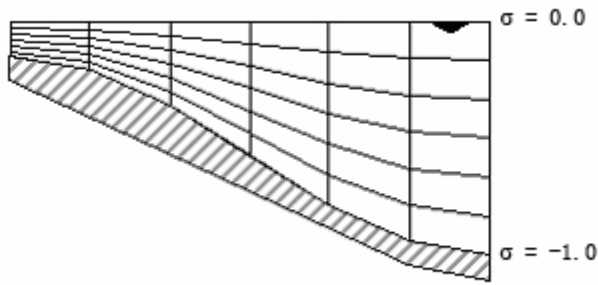


Fig 2.2 A layout of a vertical grid consisting of six equal thickness σ -layers

2.2.1.2 Continuity Equation

The depth-averaged continuity equation is given by:

$$\frac{\partial \zeta}{\partial t} + \frac{\partial [h\bar{U}]}{\partial x} + \frac{\partial [h\bar{V}]}{\partial y} = S \quad (2.9)$$

in which S represents the contributions per unit area due to the discharge or withdrawal of water, evaporation, and precipitation.

2.2.1.3 Horizontal momentum equations

The momentum equations in two horizontal directions are given by

$$\frac{\partial U}{\partial t} + U \frac{\partial U}{\partial x} + v \frac{\partial U}{\partial y} + \frac{\omega}{h} \frac{\partial U}{\partial \sigma} - fV = -\frac{1}{\rho_0} P_x + F_x + M_x + \frac{1}{h^2} \frac{\partial}{\partial \sigma} \left(\nu_v \frac{\partial u}{\partial \sigma} \right) \quad (2.10)$$

and

$$\frac{\partial V}{\partial t} + U \frac{\partial V}{\partial x} + V \frac{\partial V}{\partial y} + \frac{\omega}{h} \frac{\partial V}{\partial \sigma} - fU = -\frac{1}{\rho_0} P_y + F_y + M_y + \frac{1}{h^2} \frac{\partial}{\partial \sigma} \left(\nu_v \frac{\partial v}{\partial \sigma} \right) \quad (2.11)$$

in which the horizontal pressure terms, P_x and P_y , are given by (Boussinesq approximation)

$$\frac{1}{\rho_0} P_x = g \frac{\partial \zeta}{\partial x} + g \frac{h}{\rho_0} \int_{\sigma}^0 \left(\frac{\partial \rho}{\partial x} + \frac{\partial \sigma'}{\partial x} \frac{\partial \rho}{\partial \sigma'} \right) d\sigma' \quad (2.12)$$

$$\frac{1}{\rho_0} P_y = g \frac{\partial \zeta}{\partial y} + g \frac{h}{\rho_0} \int_{\sigma}^0 \left(\frac{\partial \rho}{\partial y} + \frac{\partial \sigma'}{\partial y} \frac{\partial \rho}{\partial \sigma'} \right) d\sigma' \quad (2.13)$$

F_ξ, F_η : horizontal Reynold's stresses determined by using eddy viscosity concept

M_ξ, M_η : contributions due to external sources or sinks of momentum (external forces by hydraulic structures, discharge or withdrawal of water, wave stresses, etc.)

2.2.1.4 Hydrostatic pressure assumption (for σ -grid)

Based on the shallow water assumption, the vertical momentum equation is reduced to a hydrostatic pressure equation. Vertical accelerations due to buoyancy effects and due to sudden variation in the bottom topography are not taken into account. The resulting expression is:

$$\frac{\partial P}{\partial \sigma} = -g\rho h \quad (2.14)$$

2.2.1.5 Transport equation

The flows in rivers, estuaries, and coastal seas are able to deliver some dissolved substances, salinity and heat. These processes can be simulated by the advection-diffusion equation in three co-ordinate directions. Source and sink terms are used to simulate discharges and withdrawals. In addition, first-order decay processes can be included in this equation as well.

The transport equation here is formulated in a conservative form in orthogonal curvilinear co-ordinate in the horizontal direction and σ co-ordinates in the vertical:

$$\begin{aligned} & \frac{\partial [hc]}{\partial t} + \frac{\partial [hUc]}{\partial x} + \frac{\partial [hVc]}{\partial y} + \frac{\partial [\omega c]}{\partial \sigma} \\ & = h \left[\frac{\partial}{\partial x} \left(D_H \frac{\partial c}{\partial x} \right) + \frac{\partial}{\partial y} \left(D_H \frac{\partial c}{\partial y} \right) \right] + \frac{1}{h} \frac{\partial}{\partial \sigma} \left[D_v \frac{\partial c}{\partial \sigma} \right] + hS \end{aligned} \quad (2.15)$$

where:

S : source and sink terms per unit area

D_H, D_V : horizontal and vertical eddy diffusivities

In Delft3D-FLOW, the horizontal viscosity and diffusivity are assumed to be a superposition of three parts: (1) molecular viscosity, (2) “3D turbulence”, and (3) “2D turbulence”. The molecular viscosity of the fluid (water) is a constant value $O(10)^{-6}$. “2D turbulence” is associated with the horizontal mixing that is not resolved by advection on the horizontal computational grid. 2D turbulence values may either be specified by users, or can be computed using a subgrid model for horizontal large eddy simulation (HLES). In a 3D simulation, “3D turbulence” is computed by the turbulence closure model selected by users.

For utilization in the transport equation, the vertical eddy diffusivity is defined by:

The vertical eddy diffusivity coefficient D_V is defined by:

$$D_V = \frac{\nu_{mol}}{\sigma_{mol}} + \max(D_V^{back}, D_{3D}) \quad (2.16)$$

In the case of stratified flows, apart from molecular diffusion, there should be other forms of unresolved mixing, of which is caused by internal waves. Therefore, for all turbulence closure models, a background mixing coefficient D_V^{back} may be specified by users.

2.2.2 Boundary conditions

To solve the systems of equations, the following boundary conditions are required.

2.2.2.1 Bed and free surface boundary conditions

In the σ co-ordinate system, the bed and the free surface correspond with σ -planes. Therefore, the vertical velocities at these boundaries are simply:

$$\omega|_{\sigma=-1} = 0 \text{ and } \omega|_{\sigma=0} = 0$$

Friction is applied at bed as follows:

$$\frac{\nu_V}{h} \frac{\partial u}{\partial \sigma} \Big|_{\sigma=-1} = \frac{1}{\rho} \tau_{bx} \text{ and } \frac{\nu_V}{h} \frac{\partial v}{\partial \sigma} \Big|_{\sigma=-1} = \frac{1}{\rho} \tau_{by} \quad (2.17)$$

where τ_{bx} and τ_{by} are bed stress components that include the effect of wave-current interaction.

2.2.2.2 Lateral boundary conditions

Along closed boundaries, the velocity component perpendicular to the closed boundary is set to zero (a free-slip condition). At open boundaries, one of the following types of boundary conditions must be specified: water level, velocity (in the direction normal to the boundary), discharge, or linearised Riemann invariant (weakly reflective boundary

condition; Verboom and Slob, 1984). Additionally, in the case of 3D models, the user must prescribe the use of either a uniform or logarithmic velocity profile at inflow boundaries.

For the transport boundary conditions, we assume that the horizontal transport of dissolved substance is dominated by advection. This means that at an open inflow boundary, a boundary condition is needed. During outflow, the concentration must be free. Delft3D-FLOW allows the user to prescribe the concentration at every σ -layer using a time series. For sand sediment fractions, the local equilibrium sediment concentration profile may be used.

2.2.3 Solving process

Delft3D-FLOW is a numerical model based on finite differences. To discretize the 3D shallow water equations in space, the model area is covered by a rectangular, curvilinear, or spherical grid. It is assumed that the grid is orthogonal and well structured. The variables are arranged in a pattern called the Arakawa C-grid (a staggered grid). In this arrangement, the water level points (pressure points) are defined in the center of a (continuity) cell; the velocity components are perpendicular to the grid cell faces where they are situated (see Fig 2.3).

2.2.3.1 Hydrodynamics

For the simulations applied in this study, an alternating direction implicit (ADI) method is used to solve the continuity and horizontal momentum equations (Leendertse, 1987). The advantage of ADI method is that the implicitly integrated water levels and velocities are coupled along grid lines, leading to systems of equations with a small band width. Stelling (1984) extended the ADI method of Leendertse with a special approach for horizontal advection terms. This approach splits the third-order upwind finite-difference scheme for the first derivative into two second-order consistent discretizations, a central discretization, and an upwind discretization, which are successively used in both stages of the ADI scheme. The scheme is denoted as a “cyclinc method” (Stelling and Leendertse, 1991). This leads to a method that is computationally efficient, at least second-order accurate, and stable at Courant number of up to approximately 10.

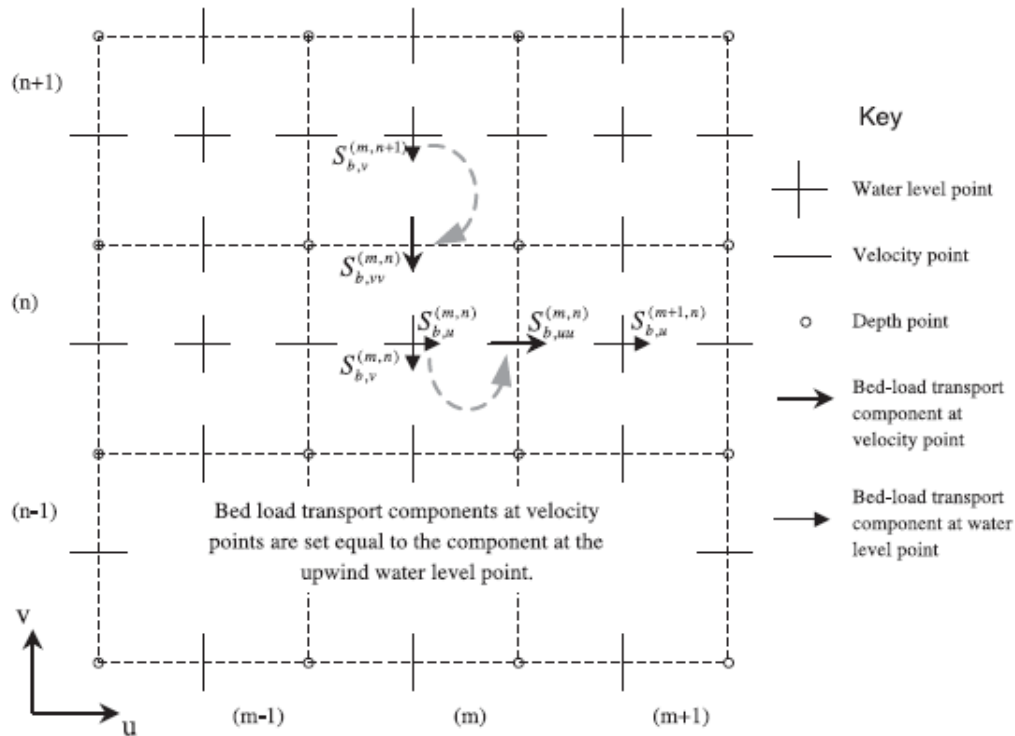


Fig 2.3 The Delft3D staggered grid showing the upwind method of setting bedload sediment transport components at velocity points. Water level points are located in the center of the sediment control volumes.

2.2.3.2 Transport

The transport equation is formulated in a conservative form (finite-volume approximation) and is solved using the so-called “cyclic method” (Stelling and Leenderstse, 1991). In addition, a horizontal Forester filter (Forester, 1979) based on diffusion along σ -planes is applied to remove any negative concentration values that may occur. The Forester filter is mass conserving and does not cause significant amplitude losses in sharply peaked solutions.

2.3 WAVE model

The WAVE model is introduced to the integrated model for two objectives. One is to take the wave effect on current into account (online-coupling); the other one is the wave induced shear stress is calculated by the model.

In this study, the third-generation SWAN (Simulating WAVes Nearshore) model which is able to simulate the evolution of random, short-crested wind-generated waves in our study area is utilized. The SWAN model is based on the discrete spectral action balance equation and is fully spectral (in all directions and frequencies). Some processes such as refractive propagation due to current and depth, wave generation by wind, dissipation due to whitecapping, bottom friction and depth-induced wave breaking and non-linear wave-wave interactions (both quadruplets and triads) are accounted for in the SWAN model as well.

2.3.1 Basic equations

In SWAN the waves are described with two-dimensional wave action density spectrum, even when non-linear phenomena dominate (e.g., in the surf zone). The rationale for using the spectrum in such highly non-linear is that, even in such conditions it seems possible to predict with reasonable accuracy this distribution of the second order moment of the waves (although it may not be sufficient to fully describe the waves statistically). The spectrum that is considered in SWAN is the action density spectrum $N(\sigma, \theta)$ rather than the energy density spectrum $E(\sigma, \theta)$ since in the presence of currents, action density is conserved whereas energy density is not (e.g., Whitham, 1974). The independent variables are the relative frequency σ (as observed in a frame of reference moving with the current velocity) and the wave direction θ (the direction normal to the wave crest of each spectral component). The action density is equal to the energy density divided by the relative frequency: $N(\sigma, \theta) = E(\sigma, \theta) / \sigma$. In SWAN this spectrum may vary in time and space.

In SWAN the evolution of the wave spectrum is described by the spectral action balance equation which for Cartesian co-ordinates is (e.g., Hasselmann et al., 1973):

$$\frac{\partial}{\partial t} N + \frac{\partial}{\partial x} c_x N + \frac{\partial}{\partial y} c_y N + \frac{\partial}{\partial \sigma} c_\sigma N + \frac{\partial}{\partial \theta} c_\theta N = \frac{S}{\sigma} \quad (2.18)$$

The first term in the left-hand side of this equation represents the local rate of change of action density in time, the second and third term represent propagation of action in geographical space (with propagation velocities c_x and c_y in x - and y -space, respectively). The fourth term represents shifting of the relative frequency due to variations in depths and currents (with propagation velocity c_σ in σ -space). The fifth term represents depth-induced and current-induced refraction (with propagation velocity c_θ in θ -space). The expressions for these propagation speeds are taken from linear wave theory (e.g., Whitham, 1974; Mei, 1983; Dingemans, 1997). The term $S (= S(\sigma, \theta))$ at the right-hand side of the action balance equation is the source term in terms of energy density representing the effects of generation, dissipation and non-linear wave-wave interactions. In addition, wave propagation through obstacles and wave-induced set-up of the mean sea surface can be computed in SWAN as well.

2.3.2 Wave effects on flow

In relatively shallow areas (coastal seas) wave action becomes so important that we can't neglect its effects on the flow because of several processes:

- The vertical mixing processes are enhanced due to turbulence generated near the surface by whitecapping and wave breaking, and near the bottom due to energy dissipation in the bottom layer.
- A net mass flux is generated which has some effect on the current profile, especially in cross-shore direction.
- In the surf zone long-shore currents and a cross-shore set-up is generated due to variations in the wave-induced momentum flux (radiation stress). In case of an irregular surf zone, bathymetry strong circulations may be generated (rip currents).

- The bed shear stress is enhanced; this affects the stirring up of sediments and increases the bed friction.

These processes are accounted for in a wave-averaged manner. Some processes basically act at a specific location or interface, such as the enhanced bed shear-stress or wave breaking at the surface, while others have a (certain) distribution over the vertical, such as the energy dissipation due to bottom friction in the wave boundary layer. Obviously, a vertical distribution can only be accounted for in a 3D computation.

2.4 Cohesive sediment dynamics implemented in FLOW model

2.4.1 Cohesive sediment settling velocity

In salt water cohesive sediment tends to flocculate to form sediment “flocs”, with the degree of flocculation depending on the salinity of the water. These flocs are much larger than the individual sediment particles and settle at a faster rate. In order to model this salinity dependency, there are two settling velocities which must be specified by users. The first one WS0 is the settling velocity of the sediment particle in fresh water (salinity = 0). The second one WSM is the settling velocity of the particle in salt water where the salinity equals SALMAX. The settling velocity of the sediment flocs is calculated as follows:

$$w_{s,0}^{(\ell)} = \frac{w_{s,\max}^{(\ell)}}{2} \left(1 - \cos\left(\frac{\pi S}{S_{\max}}\right) \right) + \frac{w_{s,f}^{(\ell)}}{2} \left(1 + \cos\left(\frac{\pi S}{S_{\max}}\right) \right), \text{ when } S \leq SALMAX$$

$$w_{s,0}^{(\ell)} = w_{s,\max}^{(\ell)}, \text{ when } S > SALMAX \quad (2.19)$$

where:

$w_{s,0}^{(\ell)}$: the (non-hindered) settling velocity of sediment fraction (ℓ).

$w_{s,\max}^{(\ell)}$: WSM, settling velocity of sediment fraction (ℓ) at salinity concentration SALMAX.

$w_{s,f}^{(\ell)}$: WS0, fresh water settling velocity of sediment fraction (ℓ).

S : salinity

S_{\max} : SALMAX, maximal salinity at which WSM is specified.

It is remarked that modelling turbulence induced flocculation or the break-up of sediment flocs is not yet implemented and the influence of flocculation is disregarded by setting WSM = WS0.

2.4.2 Cohesive sediment dispersion

The vertical mixing coefficient for sediment is equal to the vertical fluid mixing coefficient calculated by the selected turbulence closure model, i.e.:

$$\varepsilon_s^\ell = \varepsilon_f \quad (2.20)$$

where:

ε_s^ℓ : vertical sediment mixing coefficient for sediment fraction (ℓ).

ε_f : vertical fluid mixing coefficient calculated by the selected turbulence closure model.

2.4.3 Cohesive sediment erosion and deposition

For cohesive sediment fractions the fluxes between the water phase and the bed are calculated with the well-known Partheniades-Krone formulations (Partheniades, 1965):

$$E^{(\ell)} = M^{(\ell)} S(\tau_{cw}, \tau_{cr,e}^{(\ell)}) \quad (2.21)$$

$$D^{(\ell)} = w_s^{(\ell)} c_b^{(\ell)} S(\tau_{cw}, \tau_{cr,d}^{(\ell)}) \quad (2.22)$$

$$c_b^{(\ell)} = c^{(\ell)} \left(z = \frac{\Delta z_b}{2}, t \right) \quad (2.23)$$

where

$E^{(\ell)}$: erosion flux [kg/m²/s]

$M^{(\ell)}$: user specified erosion parameter [kg/m²/s]

$S(\tau_{cw}, \tau_{cr,e}^{(\ell)})$: erosion step function:

$$S(\tau_{cw}, \tau_{cr,e}^{(\ell)}) = \begin{cases} \left(\frac{\tau_{cw}}{\tau_{cr,e}^{(\ell)}} - 1 \right), & \text{when } \tau_{cw} > \tau_{cr,e}^{(\ell)}, \\ 0 & \text{when } \tau_{cw} \leq \tau_{cr,e}^{(\ell)}. \end{cases} \quad (2.24)$$

$D^{(\ell)}$: deposition flux [kg/m²/s]

$w_s^{(\ell)}$: fall velocity (hindered) [m/s]

$c_b^{(\ell)}$: averaged sediment concentration in the near bottom computational layer

$S(\tau_{cw}, \tau_{cr,d}^{(\ell)})$: deposition step function:

$$S(\tau_{cw}, \tau_{cr,d}^{(\ell)}) = \begin{cases} \left(1 - \frac{\tau_{cw}}{\tau_{cr,d}^{(\ell)}}\right), & \text{when } \tau_{cw} < \tau_{cr,d}^{(\ell)}, \\ 0 & \text{when } \tau_{cw} \geq \tau_{cr,d}^{(\ell)}. \end{cases} \quad (2.25)$$

τ_{cw} : mean bed stress due to current and waves as calculated by the wave-current interaction model

$\tau_{cr,e}^{(\ell)}$: user specified critical erosion shear stress [N/m²]

$\tau_{cr,d}^{(\ell)}$: user specified critical deposition shear stress [N/m²]

(ℓ) : sediment fraction (ℓ)

The calculated erosion or deposition flux is applied to the near bottom computational cell by setting the appropriate sink and source terms for that cell. Advection, particle settling, and diffusion through the bottom of the near bottom computational cell are all set to zero to prevent double counting these fluxes.

2.4.4 Influence of waves on cohesive sediment transport

The vertical mixing coefficient for sediment calculated by the selected turbulence closure model implies the extra turbulent mixing due to waves will not be taken into account in the suspended sediment transport calculation except by way of the enhancement of the bed shear stress caused by wave-current interaction.

2.5 Morphodynamics model

2.5.1 Feedback to hydrodynamics (update bathymetry during flow simulation)

The depth to the bed in water level and velocity is also updated every half time step. This accounts for the total change in mass of all sediment fractions present in a computational cell. To ensure stability of the morphological updating procedure, it is important to ensure one-to-one coupling between bottom elevation changes and changes in the bed shear stress used for bedload transport and sediment source and sink terms. This is achieved by using a combination of upwind and downwind techniques as follows:

- Depth in water level points is updated based on the changed mass of sediment in each control volume.
- Depth in velocity points is taken from upwind water level points.
- Bed shear stress in water level points (used for computing bedload sediment transport and suspended sediment source and sink terms) is taken from downwind velocity points.
- Bedload transport applied at velocity points is taken from upwind water level points.

2.5.2 Effect of sediment on fluid density

In the current version of Delft3D-FLOW, it uses an empirical relation (Eckart, 1958) to adjust the density of water in order to take into account varying temperature and salinity. For sediment transport this relation is extended to include the density effect of sediment fractions in the fluid mixture. This is achieved by adding (per unit volume) the mass of all sediment fractions, and subtracting the mass of the displaced water. As a mathematical statement this translates as:

$$\rho_{mix}(S, c^{(\ell)}) = \rho_w(S) + \sum_{\ell=1}^{l_{sed}} c^{(\ell)} \left(1 - \frac{\rho_w(S)}{\rho_s^{\ell}} \right) \quad (2.26)$$

where:

ρ_w : specific density of water with salinity concentration S [kg/m³]

S: salinity concentration [ppt]

ρ_s^{ℓ} : specific density of sediment fraction (ℓ) [kg/m³]

l_{sed} : number of sediment fractions

Horizontal density gradients (now also due to differences in sediment concentrations) can create density currents. Vertical density gradients can also have a significant effect on the amount of vertical turbulent mixing present.

2.6 Water quality model (Delft3D-WAQ)

Water quality model implemented in Delft3D solves the equations for transport and physical, (bio)chemical and biological processes. There are a number of processes we can choose. We need to define our required processes and the model will simulate them.

2.6.1 Mass balances

Delft3D-WAQ guarantees the mass balance of selected state variables, such as dissolved oxygen, nitrate or sediment. It does so for each computational cell. By combining computational cells in one, two or three dimensions each water system can be represented and substances can be transported through computational cells and hence through the water column. In addition, there are some other processes we need to take into account such as conversion between substances and exchange of substance between water column and seabed.

To proceed one in time ($t + \Delta t$), Delft3D-WAQ solves equation (2.27) for each computational cell and for state variable. Equation (2.27) is a simplified representation of the advection-diffusion-reaction equation which will be discussed in following part.

$$M_i^{t+\Delta t} = M_i^t + \Delta t \times \left(\frac{\Delta M}{\Delta t} \right)_{Tr} + \Delta t \times \left(\frac{\Delta M}{\Delta t} \right)_p + \Delta t \times \left(\frac{\Delta M}{\Delta t} \right)_s \quad (2.27)$$

The mass balance has the following components:

- the mass at the beginning of a time step: M_i^t
- the mass at the end of a time step: $M_i^{t+\Delta t}$
- changes by transport: $\left(\frac{\Delta M}{\Delta t}\right)_{Tr}$
- changes by physical, bio(chemical or biological processes): $\left(\frac{\Delta M}{\Delta t}\right)_p$
- changes by sources (e.g. waste loads, river discharges): $\left(\frac{\Delta M}{\Delta t}\right)_s$

Changes by transport include both advective and dispersive transport, that is the transport by flowing water and the transport as a result of concentration differences respectively.

Changes by processes include physical processes such as reaeration and settling, (bio)chemical processes such as adsorption and denitrification and biological processes such as primary production and predation on phytoplankton.

Changes by sources include the addition of mass by waste loads and the extraction of mass by intakes. Mass entering over the model boundaries can be considered a source as well.

2.6.2 Mass transport by advection and dispersion

If the advective and dispersive terms are added and the terms at a second surface are included, the one dimensional equation results:

$$M_i^{t+\Delta t} = M_i^t + \Delta t \times \left(v_{x_0} C_{x_0} - v_{x_0+\Delta x} C_{x_0+\Delta x} - D_{x_0} \left. \frac{\partial C}{\partial x} \right|_{x_0} + D_{x_0+\Delta x} \left. \frac{\partial C}{\partial x} \right|_{x_0+\Delta x} \right) \times A \quad (2.31)$$

where:

M_i^t : mass in volume i at time t (g)

Δt : time step (s)

$\left. \frac{\partial C}{\partial x} \right|_{x_0}$: concentration gradient at $x = x_0$ (g/m⁴)

A : surface area (m²)

v_{x_0} : velocity at $x = x_0$ (m/s)

C_{x_0} : concentration at $x = x_0$ (g/m³)

instead of this equation, Delft3D-WAQ uses the following equivalent equation:

$$M_i^{t+\Delta t} = M_i^t + \Delta t \times \left(Q_{x_0} C_{x_0} - Q_{x_0+\Delta x} C_{x_0+\Delta x} - D_{x_0} A_{x_0} \frac{\partial C}{\partial x} \Big|_{x_0} + D_{x_0+\Delta x} A_{x_0+\Delta x} \frac{\partial C}{\partial x} \Big|_{x_0+\Delta x} \right) \quad (2.32)$$

where:

Q_{x_0} : flow at $x = x_0$ (m³/s)

If the previous equation is divided by the volume $V (= \Delta x \Delta y \Delta z)$ and the time span Δt , then the following equation results in one dimension.

$$\frac{C_i^{t+\Delta t} - C_i^t}{\Delta t} = \frac{D_{x_0+\Delta x} \frac{\partial C}{\partial x} \Big|_{x_0+\Delta x} - D_{x_0} \frac{\partial C}{\partial x} \Big|_{x_0}}{\Delta x} + \frac{v_{x_0} C_{x_0} - v_{x_0+\Delta x} C_{x_0+\Delta x}}{\Delta x} \quad (2.33)$$

Taking the asymptotic limit $\Delta t \rightarrow 0$ and $\Delta x \rightarrow 0$, the advection-diffusion equation for one dimension results:

$$\frac{\partial C}{\partial t} = \frac{\partial}{\partial x} \left(D \frac{\partial C}{\partial x} \right) - \frac{\partial}{\partial x} (vC) \quad (2.34)$$

Thus, the finite volume method for transport is a computational method to solve the advection-diffusion equation. The accuracy of the method will be related to the size of Δx , $A (= \Delta y \Delta z)$ and Δt .

By adding terms for transport in the y and z -direction a 3-dimensional model is obtained. Taking the asymptotic limit again, will lead to a 3-dimensional advection-diffusion equation:

$$\frac{\partial C}{\partial t} = D_x \frac{\partial^2 C}{\partial x^2} - v_x \frac{\partial C}{\partial x} + D_y \frac{\partial^2 C}{\partial y^2} - v_y \frac{\partial C}{\partial y} + D_z \frac{\partial^2 C}{\partial z^2} - v_z \frac{\partial C}{\partial z} \quad (2.35)$$

$$\frac{\partial C}{\partial t} = D_x \frac{\partial^2 C}{\partial x^2} - v_x \frac{\partial C}{\partial x} + D_y \frac{\partial^2 C}{\partial y^2} - v_y \frac{\partial C}{\partial y} + D_z \frac{\partial^2 C}{\partial z^2} - v_z \frac{\partial C}{\partial z} + S + f_R(C, t) \quad (2.36)$$

with dispersion coefficients taken for every direction. If functions ‘ S ’ and ‘ f ’ are added as shown in the equation above, the so-called advection-diffusion-reaction equation emerges. The additional terms are so-called source terms. They stand for:

1. Dispersion or ‘waste loads’ (S): these source terms are additional inflows of water or mass that were not present in Delft3D-FLOW as velocity terms in the impulse equations. They may be present in Delft3D-FLOW’s continuity equation, but this is not strictly required. As many source terms as required may be added by users.

They are usually used for small rivers, discharges of industries, sewage treatment plants, small waste load outfalls, etc.

2. Reaction terms or ‘processes’ (f_R).

There are some physical process examples listed as following:

- settling of suspended particular matter
- water movement not affecting substances, like evaporation
- volatilisation of the substance itself at the water surface

2.6.3 Boundary conditions

2.6.3.1 Closed boundaries

Closed boundaries are those boundaries that have zero flow and dispersion for all time steps. No transport is associated with these exchange surfaces.

2.6.3.1 Open boundaries

Open boundaries are required for solution of the advection-diffusion equation. Without specification of the open boundaries the model does not know what to do at its borders. Concentrations of all substances and dispersion coefficients must be specified at all open boundaries for all time-steps. Flows are automatically taken from Delft3D-FLOW.

2.6.4 Sediment module implemented in Delft3D-WAQ

2.6.4.1 Modelling framework

In this study, as an inorganic substance, the cohesive sediment that can be modelled in the Delft3D-WAQ in relation to particular matter is:

Name	Description	Unit
IM1	suspended inorganic matter fraction 1	g/m ³
IM2	suspended inorganic matter fraction 2	g/m ³
IM1S1	inorganic matter fraction 1 in bed layer 1	g
IM2S1	inorganic matter fraction 2 in bed layer 1	g
IM1S2	inorganic matter fraction 1 in bed layer 2	g
IM2S2	inorganic matter fraction 2 in bed layer 2	g

The mass balances for particulate (suspended matter in the water column (c_w) and particulate matter in the sediment (c_b) is given in equation (2.37) and (2.38) respectively.

$$\frac{\Delta c_w}{\Delta t} = loads + transport - settling + resuspension \tag{2.37}$$

$$\frac{\Delta c_b}{\Delta t} = \text{loads} + \text{settling} - \text{resuspension} - \text{burial} + \text{digging} \quad (2.38)$$

2.6.4.2 Processes

A schematic situation with a water column with depth h , a near bed layer with depth δ_{nb} and bed layer with thickness δ_b in a domain with surface area A is assumed. Fine sediment depositing in the near-bed layer can be remobilized by tidal currents, fine sediment entrained into the bed can be released during storm condition only. The amount of fines in the near-bed layer is not limited, but shall not be large in general. No fines accumulate in the near-bed layer through out a spring-neap cycle. The amount of fines can be entrained into the bed is limited by the permeability of the bed, and limited to p_{cr} .

Within the 1DV domain, fines are released at a rate of S [kg/s], because of sand mining and fines are transported into the domain from the outside world, which is characterized by a concentration c_0 and a diffusion coefficient k [m²/s]. All concentrations are by mass [kg/m³]. Of course, c , c_{nb} , nor p can become smaller than zero.

Then the system can be sketched as:

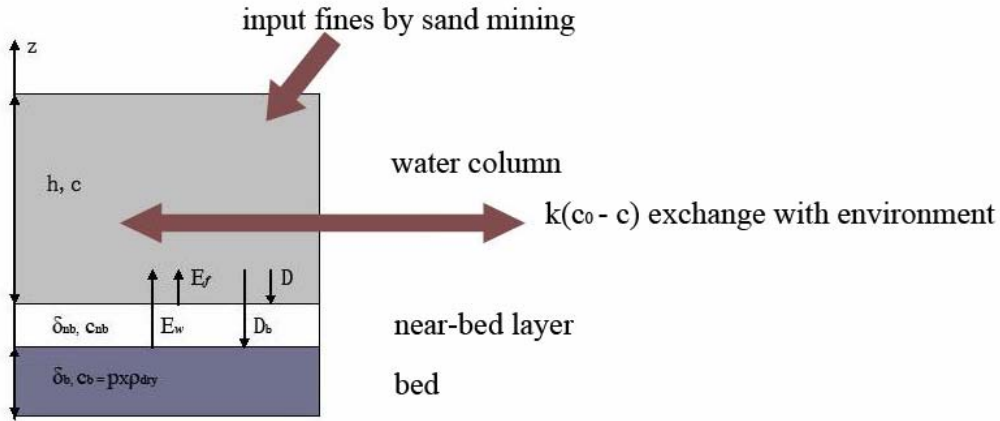


Fig 2.4 The sketch of sediment processes

Then there are several balance equations obtained for the three layers:

$$Ah \frac{\partial c}{\partial t} = hk(c_0 - c) + S + AE_f + AE_w - AD - AD_b \quad (2.39)$$

$$\delta_{nb} \frac{\partial c_{nb}}{\partial t} = D - E_f \quad (2.40)$$

$$\rho_b \delta_b \frac{\partial p}{\partial t} = D_b - E_w \quad (2.41)$$

The vertical exchange processes are modelled as following. Erosion by tidal flow according to Patheniades formula with a threshold shear stress:

$$E_f = M \left(\frac{\tau_{b,f}}{\tau_{c,f}} - 1 \right) \text{ for } \tau_{b,f} > \tau_{c,f} \quad (2.42)$$

for the wave-induced erosion during storm we use Van Rijn's pick-up function, which describes the gross pick-up of sand from the seabed:

$$E_s = p \times 3.3 \cdot 10^{-7} \rho_s \left((s-1) g D_{50} \right)^{0.5} D_*^{0.3} T^{1.5} \text{ [kg/m}^2\text{s]} \text{ for } \tau_b > \tau_{c,w} \quad (2.43)$$

where $s = \rho_s - \rho_w$, $D_* = D_{50} \left[(s-1) g / v^2 \right]^{1/3}$, and $T = (\tau_{b,w} - \tau_{c,w}) / \tau_{c,w}$. The gross deposition of sand follows from

$$D_s = W_s c_{a,e} \text{ with } W_s = \frac{10v}{D_{50}} \left[\left(1 + \frac{0.01(s-1)gD_{50}^3}{v^2} \right)^{0.5} - 1 \right] \text{ and} \quad (2.44)$$

$$c_{a,e} = 0.015 \frac{D_{50}}{a} \frac{T^{1.5}}{D_*^{0.3}} \rho_w$$

in which a = reference height, equal to the roughness height k_s , which follows from for instance the Chezy value. The net pick-up function E_w then reads:

$$E_w = \max \left[0, (E_s - D_s) \right] \quad (2.45)$$

Deposition on the bed (i.e. in the near-bed layer) is given by:

$$D = (1 - \alpha) W_s c \quad (2.46)$$

And entrainment of fines into the bed is given by:

$$D_b = \alpha W_s c \quad (2.47)$$

in which α equals the value defined by user for $p < p_{cr}$ otherwise: $\alpha = 0$.

2.7 Conclusions

In this chapter, some basic knowledge about cohesive sediment has been introduced. Several relevant modules such as flow, wave, and water quality implemented in Delft3D are presented respectively. Delft3D as a primary tool in this study will play an important role in the research about cohesive sediment. However, the numerical model based on Delft3D doesn't cover all the processes involved in the cohesive sediment behaviour, about which some correct understanding is still in discussion.

In the following chapter, ZUNO coarse grid model which covers the most part of North Sea is used first to obtain hydrodynamic boundary conditions for the smaller scale model RIJMAMO model with finer grid.

Chapter 3 Developing the Simplified ZUNO Model

3.1 Introduction to the Dutch coastal zone

In the past decades, there were various projects developed along the Dutch coast which have changed the morphology of this area. These projects included Closure works, harbour construction and extension, and maintenance dredging. In addition to these historic developments, a large number of new developments are in the blueprint.

Sediment properties in the Dutch coast have been of interest by researchers. From the analysis based on about 500 surface samples from the North Sea bed, it shows that illite is the dominant clay mineral with mean content of 51%, followed by smectite (27%), chlorite (12%) and kaolinite (10%). However, there is few available data on the grain size and settling velocity of the suspended sediment. In recent period, a number of physically-based modelling studies on the North Sea have been finalized and a settling velocity of 0.25 mm/s yielded best results (WL | Delft Hydraulics, 2005) based on calibration of the transport and fate of SPM against the DONAR database which contains chemical and physical data from the so-called MWTL programme (Monitoring Programme of the National Water Systems). Even so, for the coarser fraction of the SPM, a settling velocity of about 0.5 mm/s should be more reasonable from an analysis of data collected (Van Kessel, 2006).

The origin of the mud and suspended particulate material of the Dutch coast remains controversial. McManus and Prandle (1997) showed that only the Dover Strait, the northern boundary (56° N), the Wash and Suffolk coast of UK are statistically significant sources of suspended sediments in the Southern North Sea. The smectite content in the fine-grained surface sediment in the Belgian coastal zone is high, which points to the Cretaceous formations in the Dover Strait as a source area. It is reported that the erosion and resuspension of Tertiary clay, Holocene mud and peat layers along the Flemish Banks served as a local source of suspended material in the Belgian/Dutch coastal area, although quantities are not provided (Fettweis, 2003). In addition, dumped sediments, riverine inputs have been also taken into account as sources of the sediment. Their contributions and impacts on the sediment are still in investigation.

As hydrodynamic forcing, tides, density differences (due to river inflow), wind stress and waves play a determinant role on the transport of SPM on a wide range of time scales. The tide in the southern North Sea is characterized as being predominately semi-diurnal. Residual flows in the entire North Sea are counterclockwise. In the Dutch coastal zone the depth-averaged residual flow velocities reach a few (5-10) cm/s. Moreover, riverine waters also have a great impact on the Dutch coastal zone. Because of salinity-induced density gradients and Coriolis effects, a relative narrow band of a width of 20 to 30 km, governed by the river flow and wind conditions, of fresh/brackish water is formed along the Dutch coast. This band of fresh/brackish water is known as the Coastal River. The annual mean wind in this area is from southwest with a mean speed of around 7-9 m/s. However, there are frequent winds from other directions at much higher speeds. In particular North-Northwest winds are pronounced for waves and set-up they can produce. The waves within the North Sea can be classified as short

waves ($T_s < 10$ s) and long waves or swell ($T_s > 10$ s) where T_s is wave period. Holthuijsen (1996) showed that on the basis of wave computation, short waves are depth-limited in the southern part of the North Sea for extreme conditions, with maximum wave heights of about $0.4 h$, where h is the local water depth.

The patterns and paths of the suspended sediment transport largely depend on the water movement. The suspended material and mud layer are carried by the residual current from south to north along the Belgian-Dutch coast. On the way of transportation northwards, the complex coastal hydrodynamics, consisting of gyres, divergences or convergence's of currents, mixing of the freshwater, or geological traps, results in the accumulation of cohesive sediments along the coastal zone.

3.2 Model setup

In this research, the objective of setting up the large-scale hydrodynamic model is to provide hydrodynamic boundary conditions to the finer model. This large-scale model which entirely covers the southern part of North Sea, is provided by WL | Delft Hydraulics and had been calibrated well.

3.2.1 Grid and bathymetry

To reach a good compromise between the covering area and computation time, the ZUNO model grid is relatively coarse. It is a curvilinear, boundary fitted grid which contains 8,710 computational elements to cover about $1,000 \text{ km} \times 800 \text{ km}$ area with cell size around 8 km by 6 km (Fig 3.1). The bathymetry used for the model is provided by WL | Delft Hydraulics, also shown as Fig 3.1.

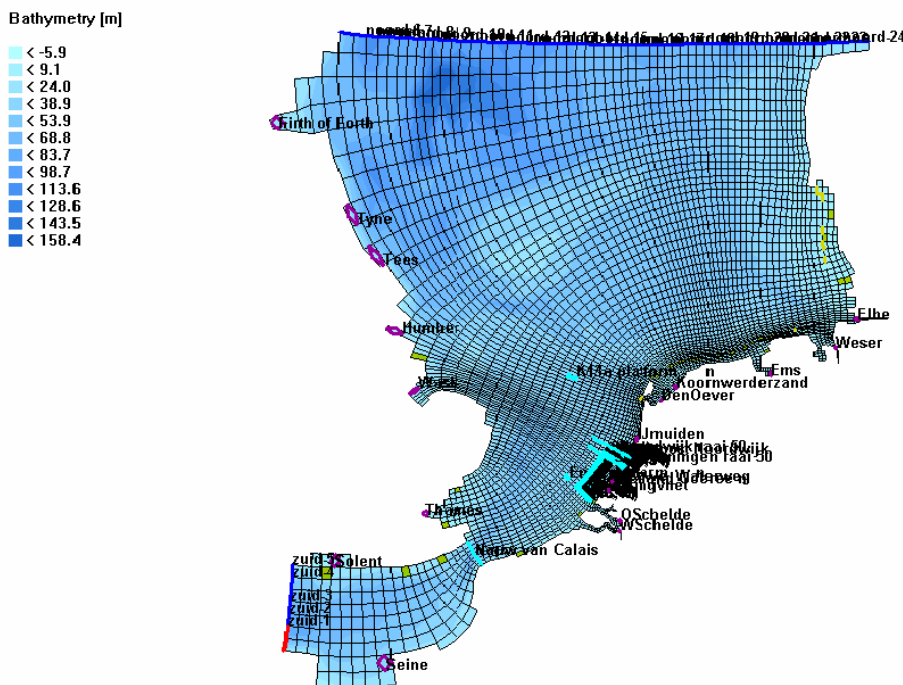


Fig 3.1 ZUNO coarse grid and bathymetry

In vertical direction, Delft3D uses “Sigma grid”, which means the total water depth is divided into a number of layers each of which covers a percentage of the total water depth. These sigma layers result in the same vertical resolution in the entire model domain regardless of the local water depth. In this study, there are 10 computational layers defined along the water depth. The layer distribution and thickness of layer is shown as Table 3.1

Table 3.1 The distribution of layers along vertical depth in ZUNO model

Layer	1	2	3	4	5	6	7	8	9	10
Relative thickness of total depth (%)	4.0	5.9	8.7	12.7	18.7	18.7	12.7	8.7	5.9	4.0

The logarithmic layer distribution provides relatively high resolution near the surface and near the bed. Near the surface a high resolution is required to take the impact of wind into account; while near the bed, a high resolution is needed in view of sediment transport computation within the model (Roelvink, 2001a).

3.2.2 Open boundary condition

The model has two open boundaries. A southern open boundary is situated at the south of the Dover Strait and a northern open boundary is situated between Scotland and the most northern part of Denmark. Each open boundary is divided into a number of boundary conditions, which need to be prescribed.

Through the open boundary, the behaviour of large scale system can be simulated inside the ZUNO model domain. The water levels, specified at the open boundaries, are obtained from a larger scale hydrodynamic model covering the entire continental Shelf, up to the 2000 m depth contour (Roelvink, 2005a; Roelvink, 2001a). The water levels in grid elements which combine of different tide components are defined in both boundaries.

3.2.3 River discharge

Fresh water discharge from rivers into the saline North Sea leads to significant density difference, and in turn affects the hydrodynamics in the nearshore area.

During the simulation period of ZUNO model, actual measured discharges along the Dutch coast are used in this model. But those discharges along the French, British, and Danish coasts which are far away from our interested area don't have pronounced effects on the hydrodynamics of our interested area. So we keep them as original values which represent long-term average discharges at those locations.

3.3 Simplified model verification

The original ZUNO model includes salinity, temperature process (heat flux model) and space varying wind and atmospheric pressure processes on a coarse grid (Fig 3.2). However, SILTMAN data starts from November 1995, the relevant data required by those processes is absent in 1995 and starts from January 1996. Therefore, the original model has to be simplified by removing the temperature, salinity and space varying

atmosphere pressure processes and using uniform wind data from one observed location instead of space varying wind data. In this simplified model, the wind data we use is from K13a platform (Fig 3.3).

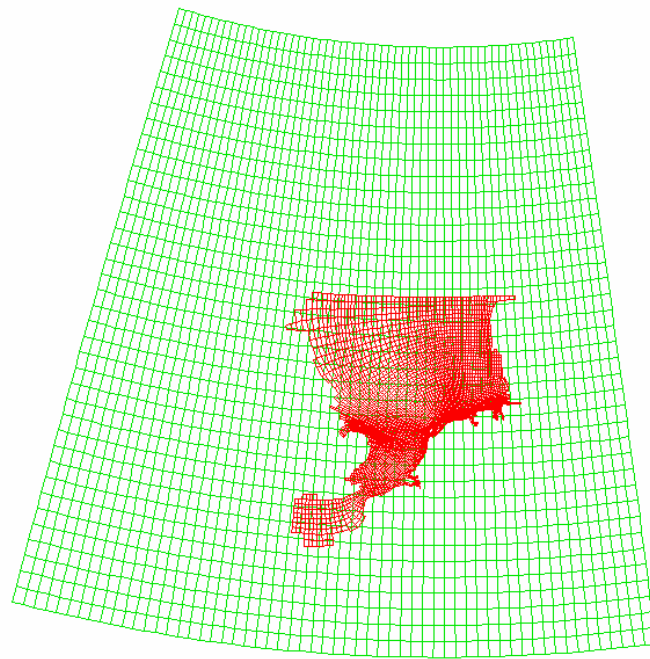


Fig 3.2 A coarse grid and ZUNO grid

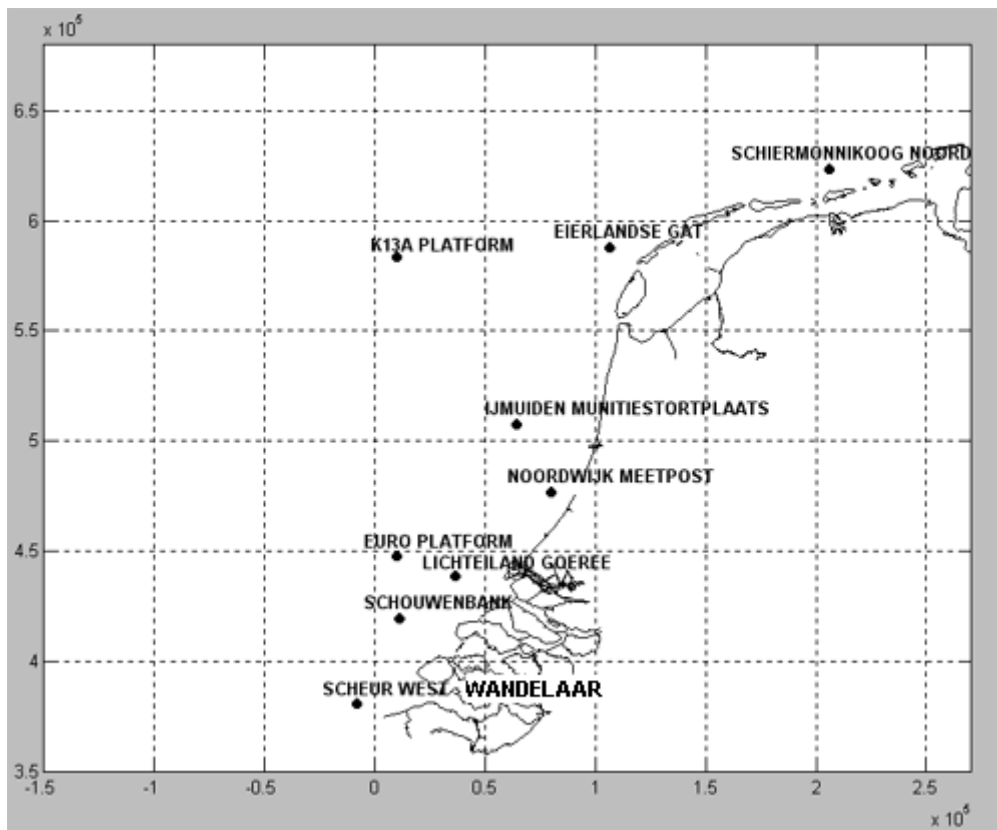


Fig 3.3 Distribution of observed locations

The verification period is about half of a month from *15 December 1995* to *31 December 1995*, during which the water level is compared with observed data from three locations which are Lichteiland Goeree, Euro Platform and K13a Platform respectively (Fig 3.3).

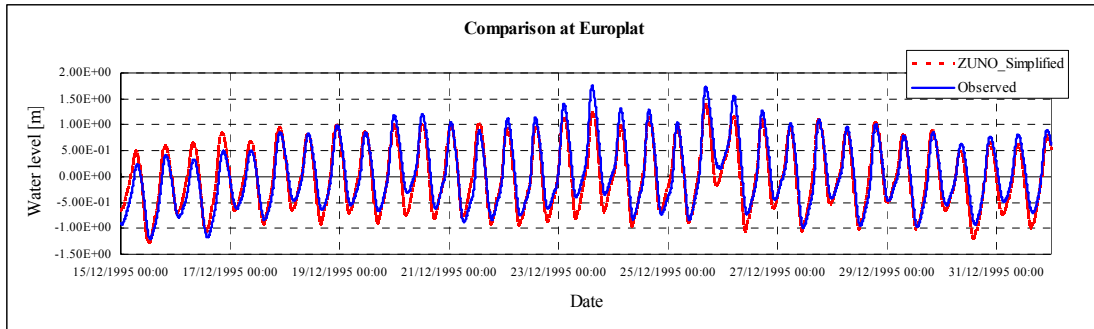


Fig 3.4 Comparison between simulated water level by ZUNO simplified model and observed water level at Euro platform

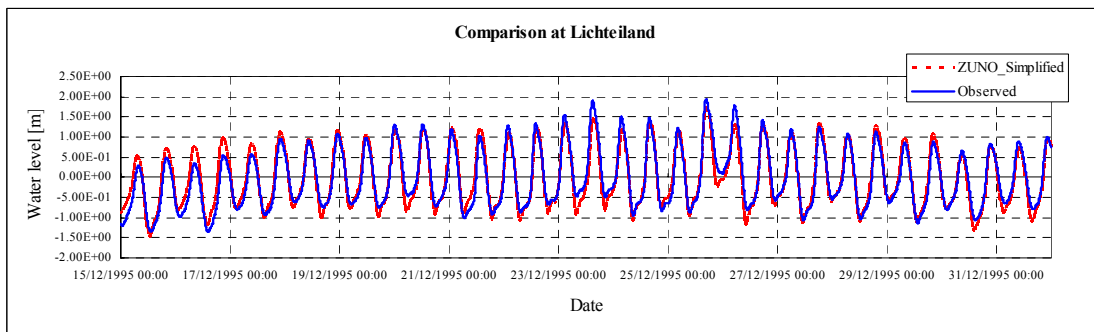


Fig 3.5 Comparison between simulated water level by ZUNO simplified model and observed water level at Lichteiland Goeree

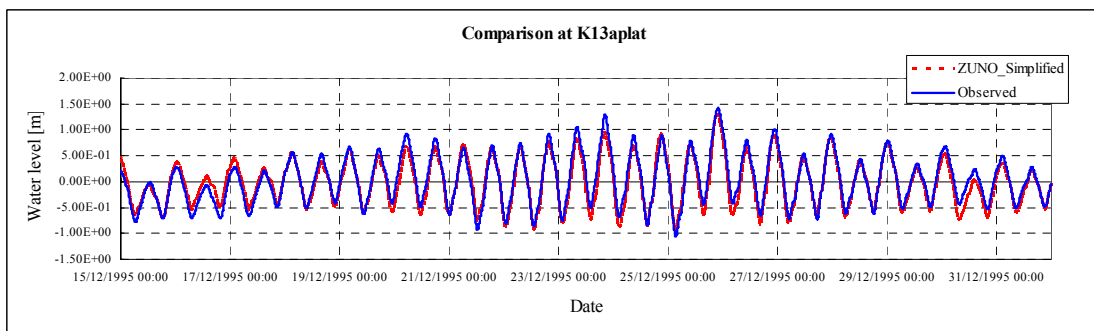


Fig 3.6 Comparison between simulated water level by ZUNO simplified model and observed water level at K13a platform

Table 3.2 Statistical measures between simplified ZUNO model and observed data

Criterion / Location	R ²	RMSE
EuroPlat	0.95	0.21
Lichteiland	0.97	0.19
K13aPlat	0.96	0.13

As to the comparison of water level (Fig 3.4-3.6), the simulated results present a good agreement with the observed ones. But during the period of half a month, there are a few days in which the model doesn't catch the highest and lowest water level during the flood and ebb tides. Both of the largest differences between the simulated and observed on the highest and lowest water level appear on the same day *24 December 1995*. The largest differences on the highest and lowest water level are both about 0.5 m, which can be inspected at Euro platform (Fig 3.4). Moreover, some little phase differences exist as well. In view of the three Figures, the model performs better at Lichteiland and K13a platform than that at Euro platform, which is also confirmed in Table 3.2. Based on the statistical measures (Table 3.2), the performance of the simplified ZUNO model is satisfactory.

Some similar comparisons are carried out between the simplified and original models and both of them are compared with the observed data from the three locations during the period from *15 January 1996 to 31 January 1996*.

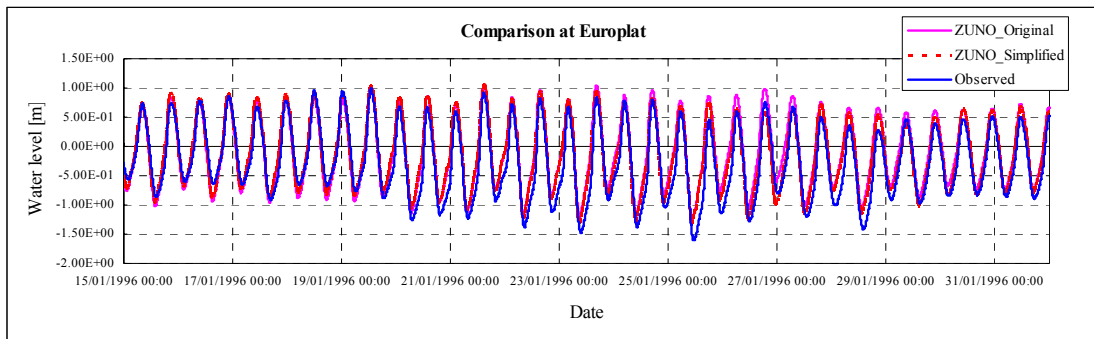


Fig 3.7 Comparison among simulated water level respectively by ZUNO simplified and original model and observed water level at Euro platform

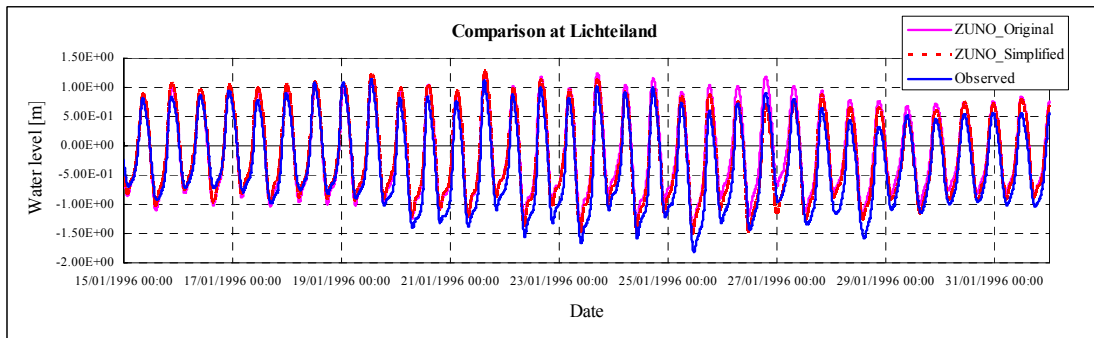


Fig 3.8 Comparison among simulated water level respectively by ZUNO simplified and original model and observed water level at Lichteiland Goeree

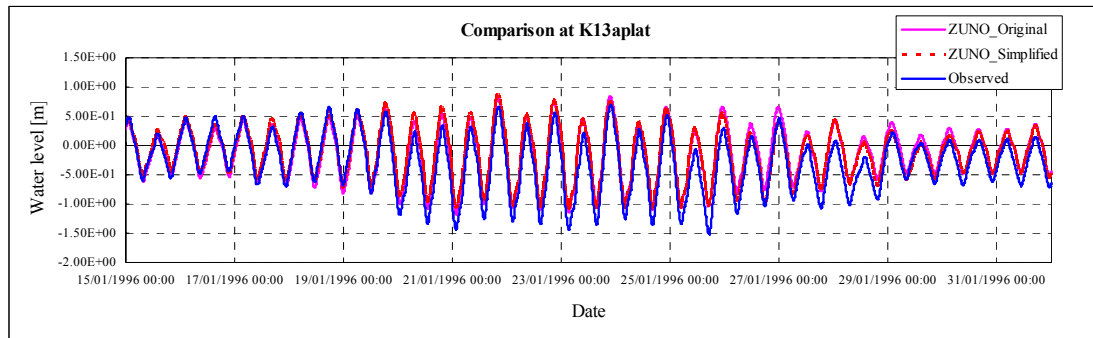


Fig 3.9 Comparison among simulated water level respectively by ZUNO simplified and original model and observed water level at K13a platform

Table 3.3 Statistical measures between simplified model & observed data and between original model & observed data

Criterion Location	R ²		RMSE	
	Simplified & Observed	Original & Observed	Simplified & Observed	Original & Observed
EuroPlat	0.96	0.95	0.21	0.25
Lichteiland	0.98	0.97	0.21	0.27
K13aPlat	0.96	0.95	0.22	0.22

It seems there is not significant difference between the simplified and original models for most time of this period (Fig 3.7-3.9). But it is noticeable around 27 *January 1996* the simplified model has a better performance on catching the highest and lowest water level than the original one at Lichteiland and Euro platform (Fig 3.7, 3.8). For the whole period, the simplified model shows a little better result than the original one according to the statistical measures in Table 3.3. Nevertheless, there are still a few highest and lowest water levels during flood and ebb tides both of the models can't capture. The most significant is the largest difference on the lowest water level which appears around 25 *January 1996* at K13a platform (Fig 3.9). The difference reaches 0.5 m.

Based on the comparisons and the statistical measures, we can see that the results reproduced by the simplified model are quite good, which performs well in catching the variation pattern of the observed water level even though there are some highest and lowest water levels during flood and ebb tides the model is not able to capture very accurately on the magnitude. In addition, there are some tiny differences between the simplified and original ZUNO models, which can be attributed to the different wind fields applied in these two models and the unavailability of space varying atmospheric pressure process in the simplified model. According to the statistical measures, the simplified model even performs a little better than the original one during the selected period. This is probably the advantage simplified model performs in the local area, and this superiority is not very significant compared with the original model.

3.4 Original model verification

Due to the lack of relevant data, the original ZUNO model has to be simplified for providing boundary conditions to a finer model in *November* and *December 1995*. But after this period, boundary conditions of the finer model are still provided by the

original model which has been verified by WL | Delft Hydraulics. In this study, the original model verification is carried out during the period from 15 March 1996 to 31 March 1996.

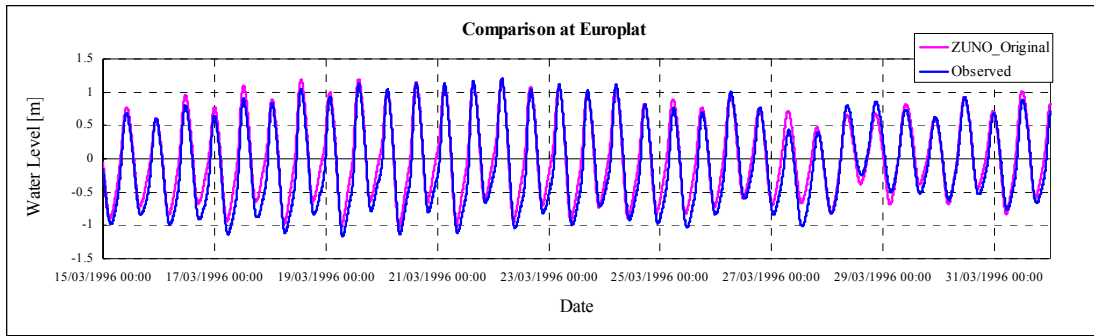


Fig 3.10 Comparison between simulated water level by ZUNO original model and observed water level at Euro platform

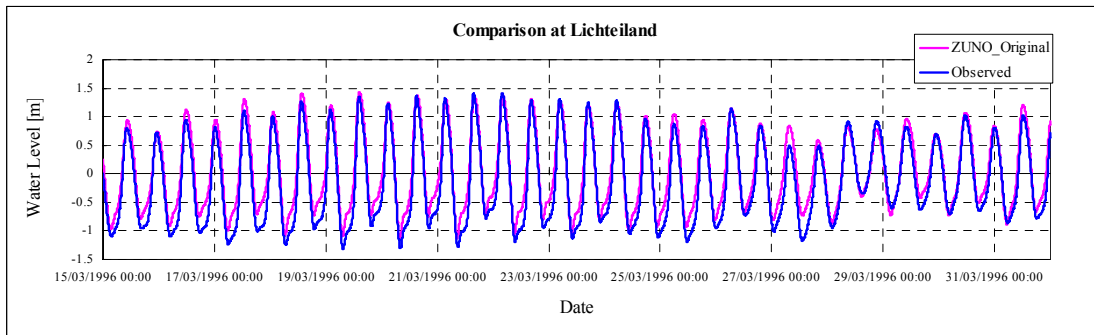


Fig 3.11 Comparison between simulated water level by ZUNO original model and observed water level at Lichteiland Goeree

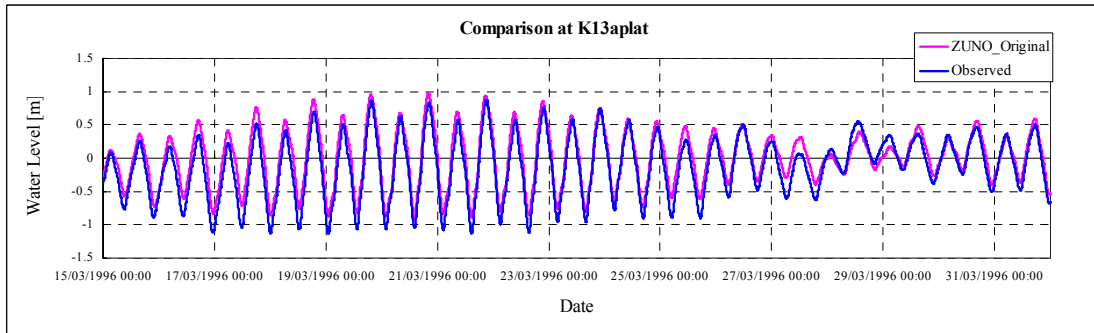


Fig 3.12 Comparison between simulated water level by ZUNO original model and observed water level at K13a platform

Table 3.4 Statistical measures between original ZUNO model and observed data

Criterion Location	R^2	RMSE
EuroPlat	0.97	0.20
Lichteiland	0.98	0.23
K13aPlat	0.97	0.17

During the verification period, the simulated results follow the observe values very well as shown as the figures (Fig 3.10-3.12). A significant difference appears on 27 March

1996 at all of the three observed locations. On this day, the simulated water levels are both higher than the observed highest and lowest ones, and difference is around 0.5 m. According to the statistical measures in Table 3.4, this is obviously successful verification. The original ZUNO model performs well as we expect, which lays down a solid basis for the work at next step.

3.5 Conclusion

The simplified ZUNO model successfully reproduces the variation pattern of water level at three observed points, of which Lichteiland is in the area RIJMAMO model covers, Euro platform and K13a platform are suited southwest and northwest to the area respectively. Through the comparison between the simplified and original model, it is found that their simulated results are almost same for the whole period although some differences exist on few time points. In addition, the original model reproduces the observed value as well. Thus, it is possible to provide appropriate boundary conditions to the finer model with the results calculated by the simplified and original ZUNO models.

The next chapter will present hydrodynamics results calculated by RIJMAMO model, which are compared with measured data in terms of water level and velocity.

Chapter 4 RIJMAMO Model Calibration and Verification

In order to obtain the more detailed information in our study area, a finer model based on RIJMAMO grid is introduced in this chapter. Firstly, hydrodynamics of the RIJMAMO model is calibrated and verified against SILTMAN data with the boundary condition extracted from the simplified and original ZUNO models which are verified in the last chapter. Subsequently, WAVE and cohesive sediment models are introduced successively and the modelled SPM concentration is calibrated and verified against SILTMAN data as well.

4.1 Introduction to the Maasmond area

As shown as Fig 4.1, the port of Rotterdam is located in the bank of the River Rhine. As one of the largest ports of the world, it has its approach channel through Maasmond where the navigable depth is 24 m. The River Rhine discharges to the North Sea, and the area near to its confluence is known as Maasmond, which is our study area.

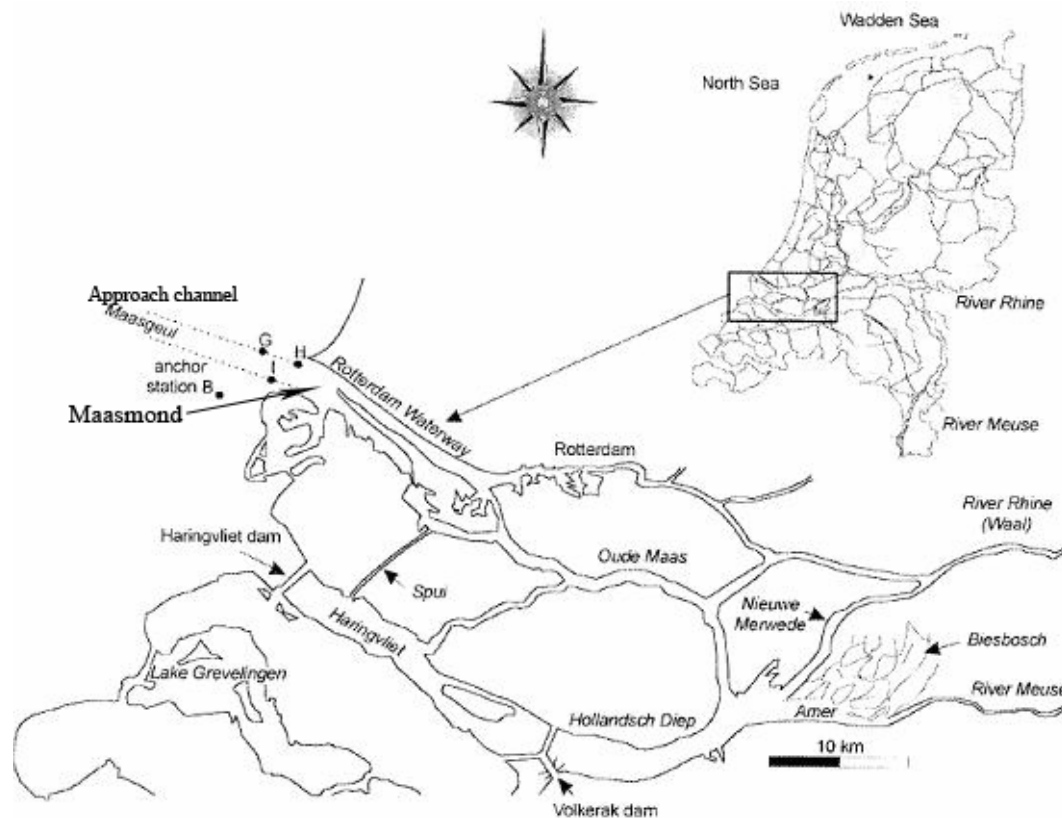


Fig 4.1 Location of approach channel to the Port of Rotterdam and the harbour basin at Maasmond

The sedimentation characteristics in the Maasmond area are largely dependant upon the sedimentation and meteorological conditions of the North Sea. Almost the entire amount of sediment that is deposited in the Maasmond area comes from the North Sea. According to investigation, around 80% of the sediment volume that accumulates in the Maasmond area has its origin in the British Channel and the French coast (Vuurens,

2001). In this region enormous amounts of material become available every year due to coastal erosion. Along with the northerly long-shore currents, this material is transported along the French, Belgian and Dutch coastlines into the North Sea basin. On its way northward the material encounters several 'sedimentation traps'. Maasmond, as a major entrapment area, large amounts of sediment are deposited in the basins and navigational channels of the Port of Rotterdam. To safeguard navigation, large amounts of sediment have to be dredged. The annual variation is large as a result of contributions from capital work and variations in hydro-meteo conditions. It is estimated that about 37% of all sediments deposited on the Loswal (about 5 km northwest of Hook of Holland) locations consists of marine mud, and 10% of riverine mud. This would imply that lately about 2.4 Mton of marine mud is dredged and dumped yearly. Only part of the deposited material remains at its dumping location, estimated by De Kok (2004) at 0.5 Mton/yr. About 0.3 Mton/yr is recirculated back to the Maasmond, and remaining 1.6 Mton/yr is transported northward along the Dutch coast with the Coastal River. Note that said 0.5 Mton/yr does not stay in/on the seabed forever, as discussed below.

The seabed can serve as a sediment buffer by storing sediment during calm weather periods and releases this sediment during storm. Winterwerp (1998) estimated that during storm conditions with $H_s = 4.5$ m, sediment layers with a thickness of 5 – 10 cm are stirred from the seabed. It can be assumed that all fine-grained sediments within that layer are then mobilised and mixed over (a part of) the water column.

Moreover, sediments in the Maasmond are mainly marine with some fluvial sediments. The marine sediments originate from erosion of downstream coastal areas whereas the fluvial sediments originate from the Alps and the low-altitude mountain ranges in the Northern France and Belgium. Vuurens (2001) reported that bed material in the Maasmond is silty-sand with a D_{50} of 0.055mm. Chen and Eisma (1995) found sediment sizes in the North Sea bed between 0.1 and 0.4 mm. Chen and Eisma (1995) reported that organic components of the sediments in the North Sea bed vary between 8 to 23%. Landward side of Maasmond contains more silt than the sea-side.

Transport of this sediment to Maasmond area is additionally influenced by the Rhine discharge apart from tidal currents, wind-induced currents and wave-induced stirring. Ninety five percent of the sediments that is deposited in the Maasmond area comes from the North Sea; the contribution of sediments carried by Rhine is limited to only 5%. At further upstream areas (such as Botlek) the portion of sediments carried by the North Sea decreases. Sediments carried from the downstream coastal erosion are deposited in the North Sea bed to be eroded later.

Biological activity can initiate flocculation which can increase the settling velocity and thus affects the sediment dynamics. This is particularly important for deeper water which is indeed the case with Maasmond. During the calm periods of summer flora and fauna cause consolidation of deposited sediment over the sea bed increasing the impermeability substantially, which results in easier erosion of sediment during the early summer than during the early winter.

Winterwerp *et al.* (2001) investigated the formation of rapid siltation in the Maasmond area. With simulation studies they argued that during the rough weather conditions the suspended sediment concentration reaches its saturation limits (for most areas of coast). During slack water a thin, temporal layer of fluid mud is formed, which is entrained rapidly during accelerating tides. These dynamics are governed strongly by the

interaction of tides, surface waves and vertical fresh-saline water induced stratification. When this sediment fluid mixture reaches the approach channel almost in perpendicular direction, the depth of flow suddenly increases from 16 m to 24 m causing a sharp fall in velocity. The fluid in the approach channel becomes super-saturated, and the vertical turbulence and concentration profile collapse, forming a fluid mud layer. Sediment-induced density current along the approach channel carry this collapsed mud layer to the harbour basins causing serious sedimentation.

4.2 Model setup

The model setup starts with FLOW model which is a considerably important basis for calculating the SPM concentration at a later stage even for WAQ model in the next chapter.

4.2.1 FLOW model

Grid

The grid for the FLOW model is much finer than ZUNO model, which is shown as Fig 4.2. The green one is RIJMAMO model and the blue line is land boundary. The grid resolution is $(M, N, K) = (137, 160, 13)$. The length of the model section is about 60 km, the width about 30 km excluding the channel and harbour.

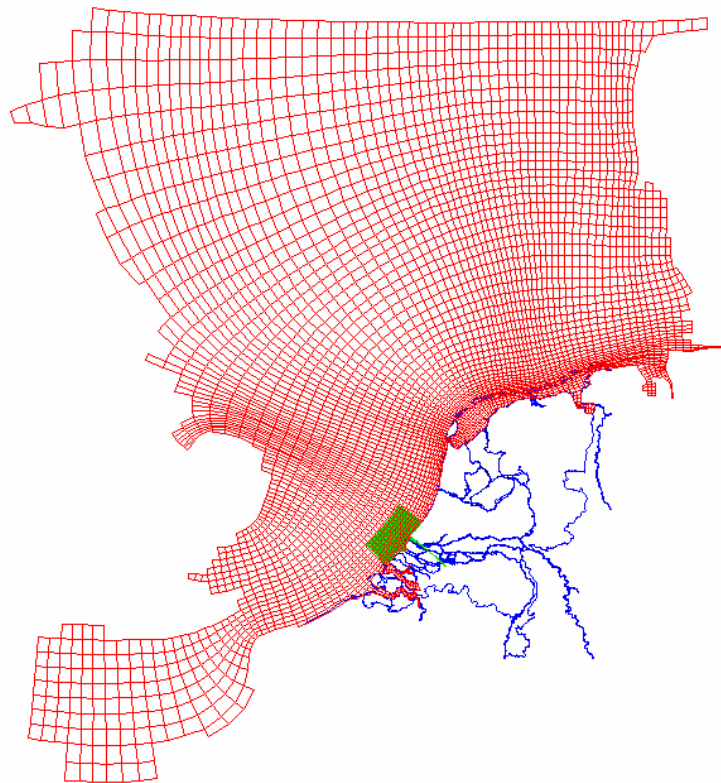


Fig 4.2 ZUNO coarse grid and RIJMAMO fine grid (blue line is land boundary)

In order to compare the simulated velocity and sediment concentration with the observed data as accurate as possible, higher vertical resolution is required near to the

seabed. So the local depth near to seabed is divided into more layers along the vertical direction. The new layer distribution and thickness of layer is listed in Table 4.1.

Table 4.1 The distribution of layers along vertical depth in RIJMAMO model

Layer	1	2	3	4	5	6	7	8	9	10	11	12	13
Relative thickness of total depth (%)	4.0	5.9	8.7	12.7	18.7	18.7	12.7	8.7	5.9	1.0	1.0	1.0	1.0

Bathymetry

The original bathymetry (Fig 4.3) is provided by WL | Delft Hydraulics. In this study, the morphodynamics is taken into account partly, the bathymetry is only updated during continuous running of one scenario. In the next scenario, the model starts with the original bathymetry again, and the initial sediment thickness will not be taken into account of bathymetry.

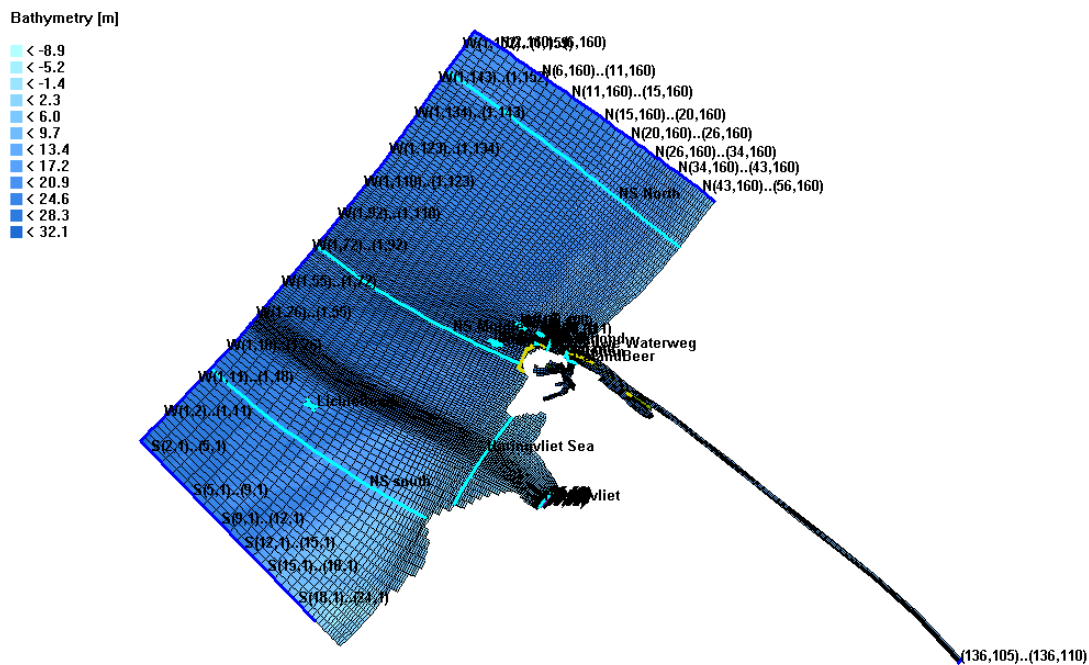


Fig 4.3 RIJMAMO model grid and bathymetry

Open boundary

The boundary conditions defined in this finer model are obtained from ZUNO model, only the river discharge is measured. All these boundary conditions are time-series. The time interval of the three seaside boundary conditions is 5 minutes and the time interval of the measured river discharge is 1 day. Moreover, water level is applied to the southern and western boundaries and current velocity to the northern boundary.

Salinity boundary

Along the southern and northern boundaries, the salinity decreases linearly from 34.5 ppt to 28 ppt landward. At the west, 34.5 ppt is defined at the whole boundary. Besides, the salinity is set at 1 ppt for the river discharge.

Suspended sediment boundary

The sediment concentration increases linearly from 0.01 g/l to 0.05 g/l landward along the southern and northern boundaries. 0.01 g/l is defined at the whole western boundary. The sediment concentration in the river discharge is set following the observed value

4.2.2 WAVE model

The wave grid covers larger area than the flow grid and is extended westward to Euro platform. The green one is the wave grid in Fig 4.4.

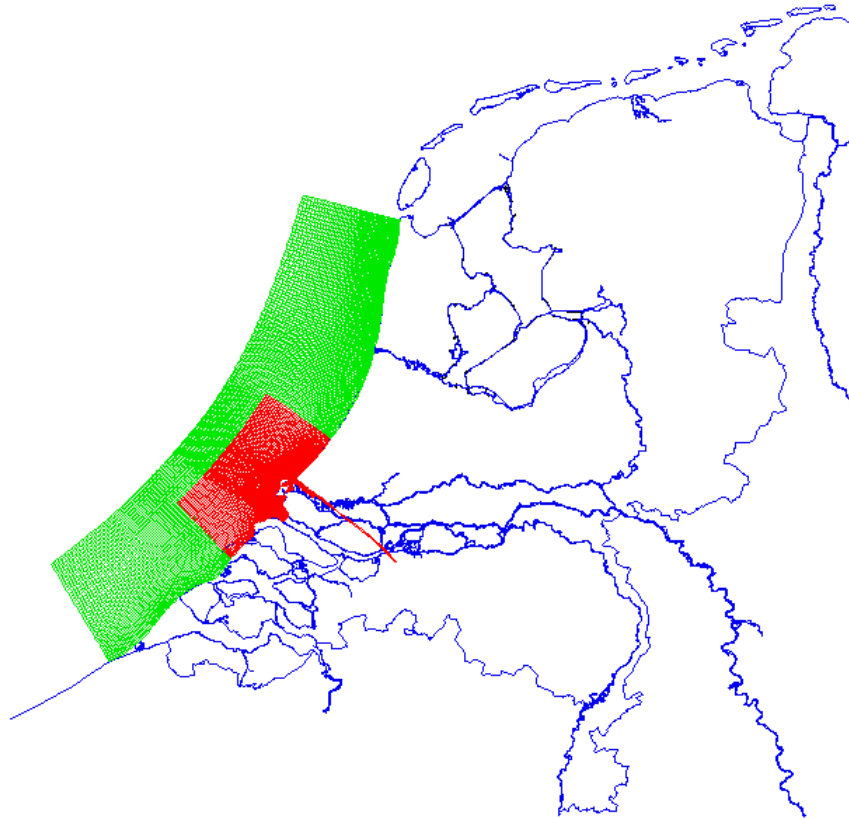


Fig 4.4 Smaller flow grid and wider wave grid

The original bathymetry provided by RIJMAMO model is applied to the area covered by flow model, and for the extended area, the bathymetry from ZUNO model is used.

Observed wave (www.golfklimaat.nl/data) and wind data (www.knmi.nl) from Euro Platform during the simulated period are used as the wave boundary.

4.3 Model calibration

4.3.1 Calibration of hydrodynamic model

The parameters used for the FLOW model are listed as Table 4.2

Table 4.2 Parameters calibrated in FLOW model

Parameter	Value	Lower limit	Upper limit	Unit
Gravity	9.81	9.5	12	m/s ²
Water density	1023	900	1500	kg/m ³
Air density	1.205	0.5	1.5	kg/m ³
Temperature	10	0	60	°C
Salinity	31	0	100	ppt
Wind drag coefficient 1	0.00063	0	1	-
Wind drag coefficient 2	0.0072	0	1	-
Wind speed 1	0	0	100	-
Wind speed 2	100	0	100	-
Roughness Manning	0.026	0	0.04	-
Horizontal Eddy viscosity	1	0	100	m ² /s
Horizontal Eddy diffusivity	1	0	1000	m ² /s
Vertical eddy viscosity	0.0001	0	100	m ² /s
Vertical eddy diffusivity	0.0001	0	1000	m ² /s

In the framework of SILTMAN project, measurements were carried out during 9 distinct periods. In this study, due to the limitation on time, 3 periods are selected for calibration, 2 periods for verification, of which periods for calibration are explained as Table 4.3, periods for verification are explained in the next section.

Table 4.3 Periods selected for calibration in FLOW model

	From	To
Period 1 of calibration	16 November 1995	13 December 1995
Period 2 of calibration	22 December 1995	30 January 1996
Period 3 of calibration	09 February 1996	13 March 1996

The comparison of the velocity magnitude and direction is carried out at the four observed points (B, I, G and H) from SILTMAN data in which the flow velocity is measured at 0.35 m above the bottom (Fig 4.5).

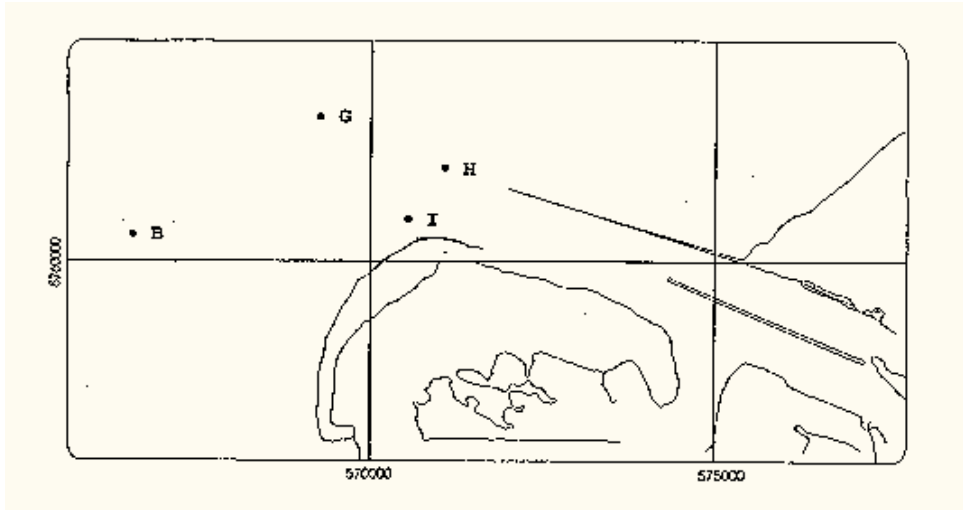


Fig 4.5 Distribution of the four observed points of SILTMAN data measurement campaign

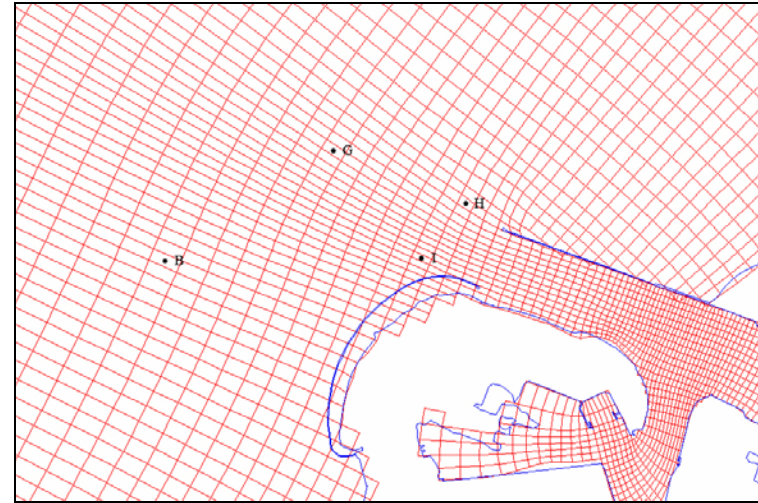


Fig 4.6 Location of the four observed points in the RIJMAMO grid

Accordingly, we can find the corresponding points in the model grid (Fig 4.6). But some of the depths at the corresponding points in this model are quite different from the depths recorded in SILTMAN data. So it is meaningful to investigate surrounding points around the corresponding ones in the model. According to their positions, they are denoted with `_left`, `_right`, `_up`, `_down`. For instance, the point left to the B point is denoted as `B_left`, the point up to I point denoted as `I_up`, the point right to G point denoted as `G_right`, the point down to H denoted as `H_down`. So the rest surrounding points can be deduced by analogy. Thus, there are totally 16 points around the 4 observed points (B, I, G and H). The corresponding depths at these 20 points are listed in Table 4.3.

Table 4.4 Depth identification between RIJMAMO model and SILTMAN data (Unit: m)

	B	B_left	B_right	B_up	B_down	I	I_left	I_right	I_up	I_down	G	G_left	G_right	G_up	G_down	H	H_left	H_right	H_up	H_down
RIJMAMO model	18.6	19	18.2	18.8	18.5	15.9	16.8	15.9	19.3	15.1	21.6	20.8	22.7	19	25.1	25	20	26.9	19.9	26.4
SILTMAN data	16					16.3					19.5					18.15				

The simulated data is compared with the observed data at the four points B, I, G and H as well as with that at the neighbouring points. In comparison with the observed data, a surrounding point is also chosen, at which the depth is the closest to SILTMAN data. It is remarked that during the first and second calibration periods *16 November 1995 – 13 December 1995 and 22 December 1995 – 30 January 1996*, hydrodynamic boundary conditions of RIJMAMO model are provided by the simplified ZUNO model. Due to the limitation on space, not all the results for every calibration period are presented in this chapter. Accounting for there are a lot of measured values which were missing at I point during period 1 of calibration, thus the modelled results during period 2 of calibration are displayed as follows (Fig 4.7-4.19).

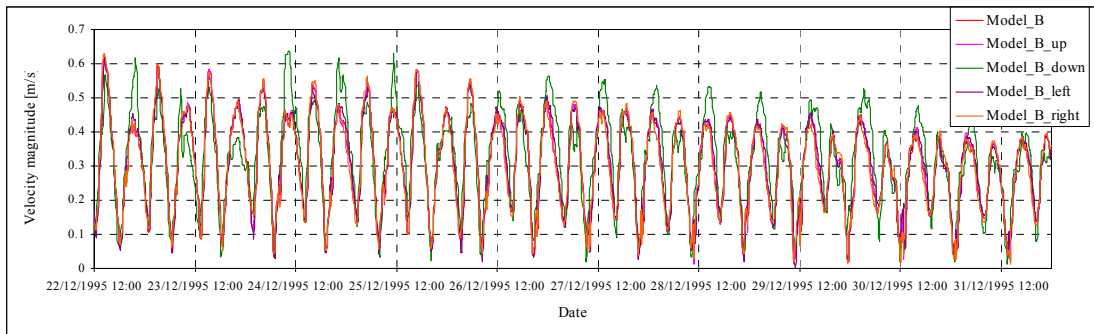


Fig 4.7 Modelled velocity magnitude at B point and four points surrounding B (Period 2 of calibration)

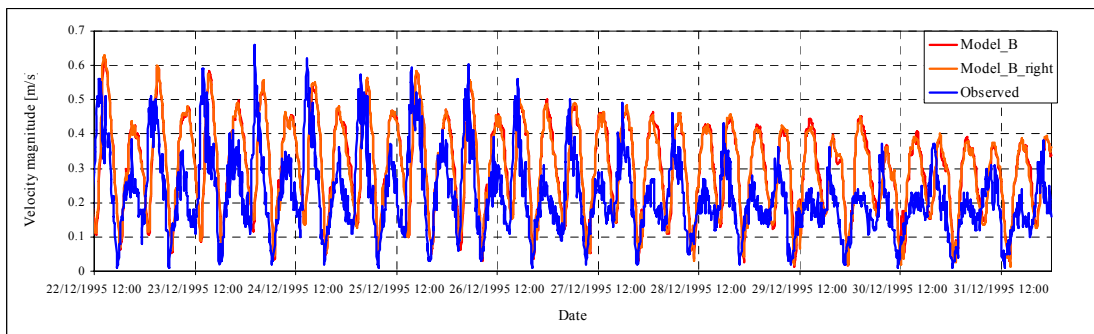


Fig 4.8 Comparison of velocity magnitude at B point (Period 2 of calibration)

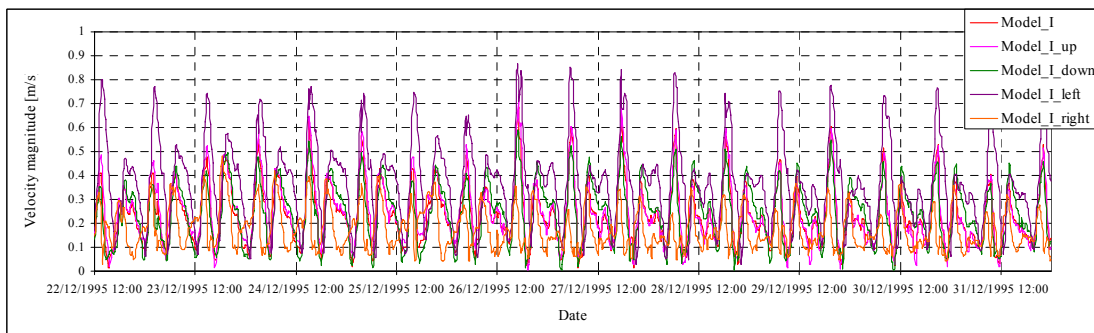


Fig 4.9 Modelled velocity magnitude at I point and four points surrounding I (Period 2 of calibration)

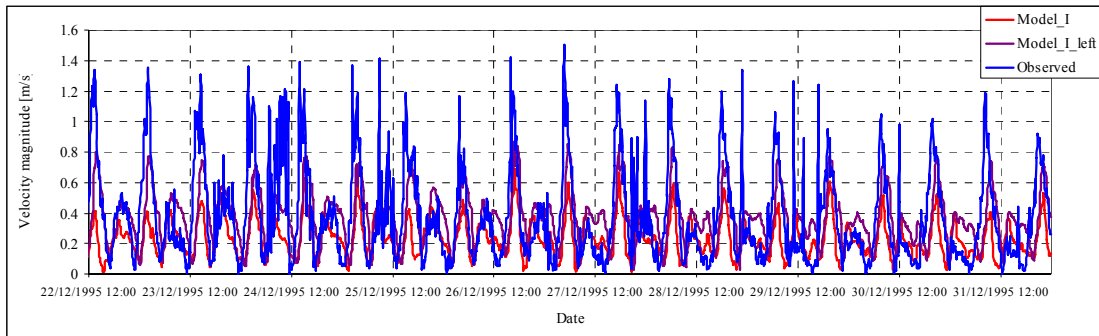


Fig 4.10 Comparison of velocity magnitude at I point (Period 2 of calibration)

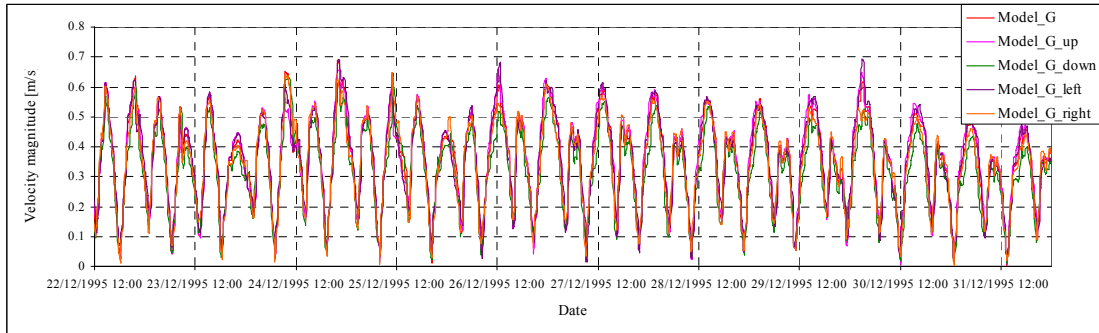


Fig 4.11 Modelled velocity magnitude at G point and four points surrounding G (Period 2 of calibration)

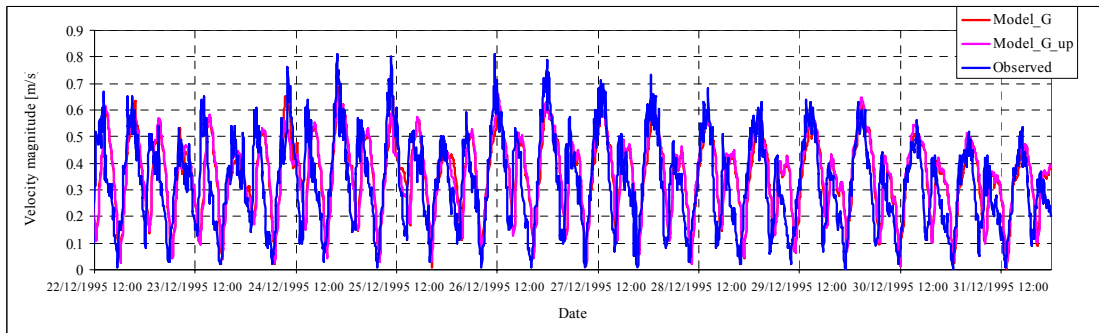


Fig 4.12 Comparison of velocity magnitude at G point (Period 2 of calibration)

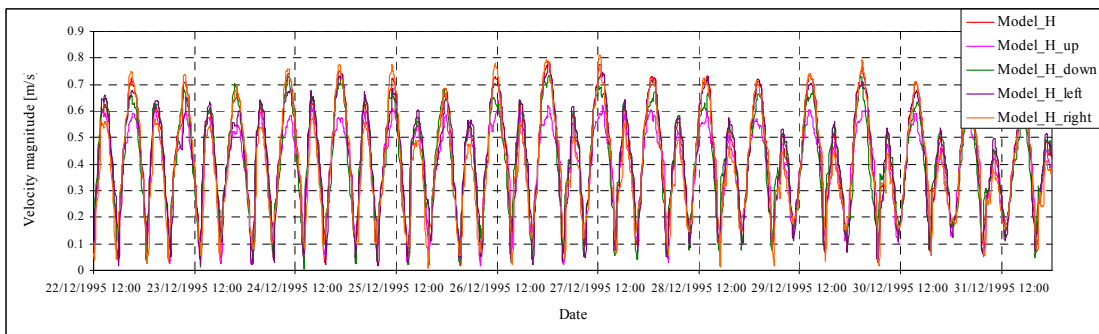


Fig 4.13 Modelled velocity magnitude at H point and four points surrounding H (Period 2 of calibration)

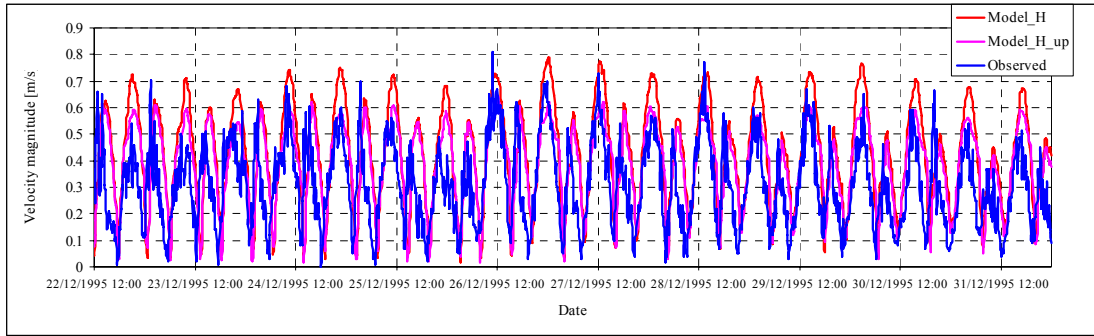


Fig 4.14 Comparison of velocity magnitude at H point (Period 2 of calibration)

Through the comparison of the velocity magnitude (Fig 4.7-4.14) we can come to some conclusions. In all four points, the difference in velocity magnitude at a point to its four surrounding ones is not significant except for point I (Fig 4.9). During the comparison with the observed data, the velocity magnitude is reproduced well by the model at B, G and H points, and the modelled result at H_up point where the depth is closer to SILTMAN data is in better agreement with the SILTMAN data. With regard to I point, it seems to be quite difficult to catch the peak of the velocity magnitude, but the variation pattern is reproduced well. Moreover, at I_left point, the modelled result is closer to the observed peak than that at I point.

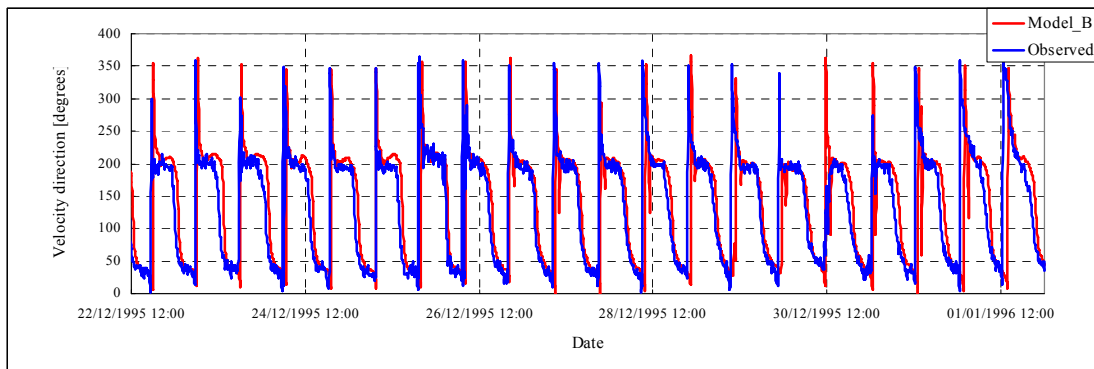


Fig 4.15 Modelled and observed velocity direction at B point (Period 2 of calibration)

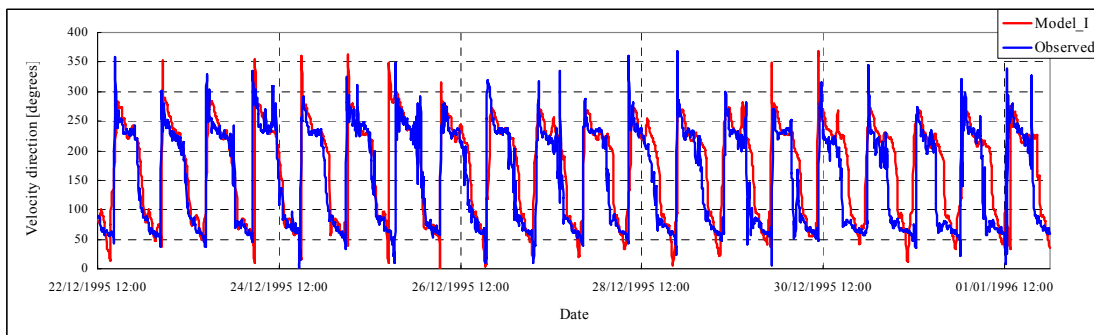


Fig 4.16 Modelled and observed velocity direction at I point (Period 2 of calibration)

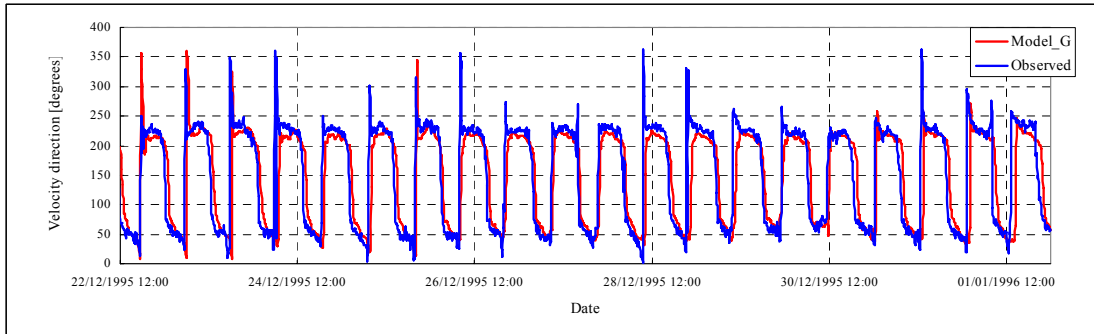


Fig 4.17 Modelled and observed velocity direction at G point (Period 2 of calibration)

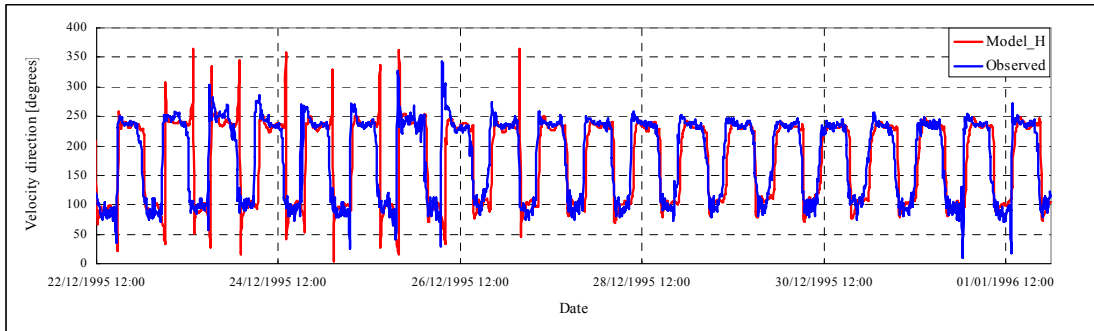


Fig 4.18 Modelled and observed velocity direction at H point (Period 2 of calibration)

Although there is some phase difference which can be inspected from the figures above (Fig 4.15-4.18). In particular, it is more significant at I point again (Fig 4.16). But generally the difference is small enough to be acceptable.

Moreover, in the area RIJMAMO model covers, there is only one observation point (Lichteiland Goeree) which can be used for comparison of water level with the model.

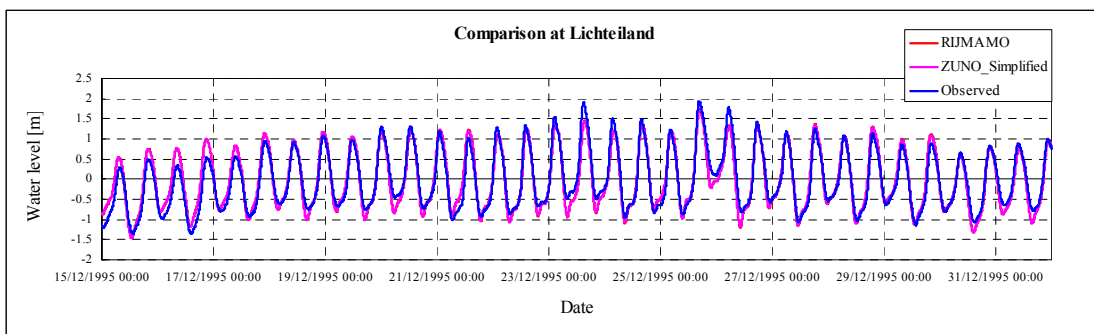


Fig 4.19 Water level at Lichteiland Goeree (Period 2 of calibration)

Fig 4.19 displays a good agreement between the modelled and observed water level. It is remarked that water level curve reproduced by RIJMAMO model is almost overlapped by ZUNO model. That's why the red curve is not visible in the figure (Fig 4.19).

In the third calibration periods *09 February 1996 – 13 March 1996*, hydrodynamic boundary conditions for RIJMAMO model are extracted from the results computed by the original ZUNO model. During the third calibration period, some hydrodynamic results calculated by RIJMAMO model can be compared with observed values collected in SILTMAN data as well. The similar comparison is carried out as follows:

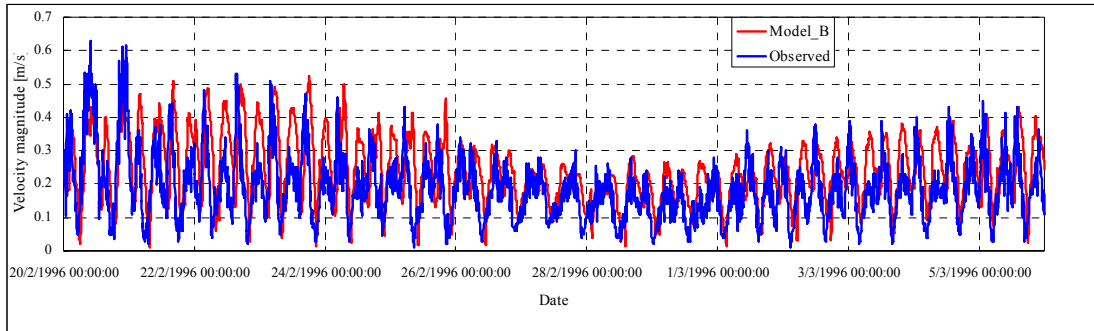


Fig 4.20 Comparison of velocity magnitude at B point (Period 3 of calibration)

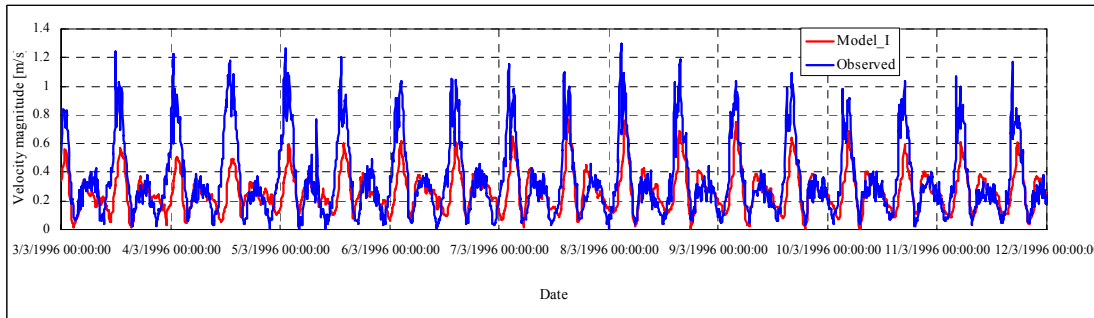


Fig 4.21 Comparison of velocity magnitude at I point (Period 3 of calibration)

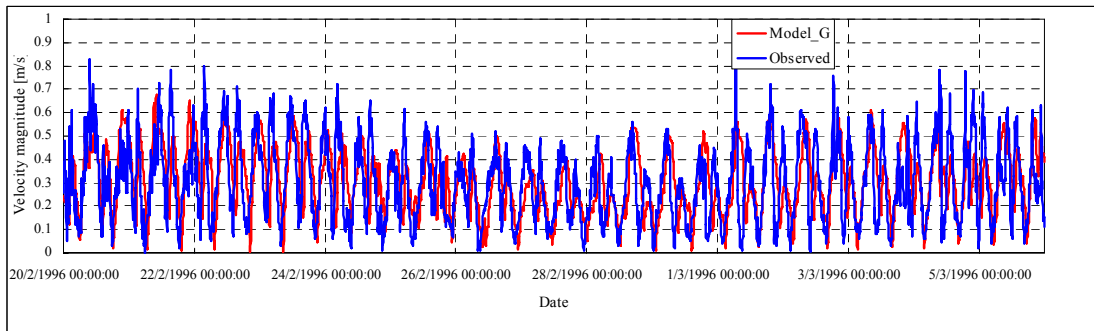


Fig 4.22 Comparison of velocity magnitude at G point (Period 3 of calibration)

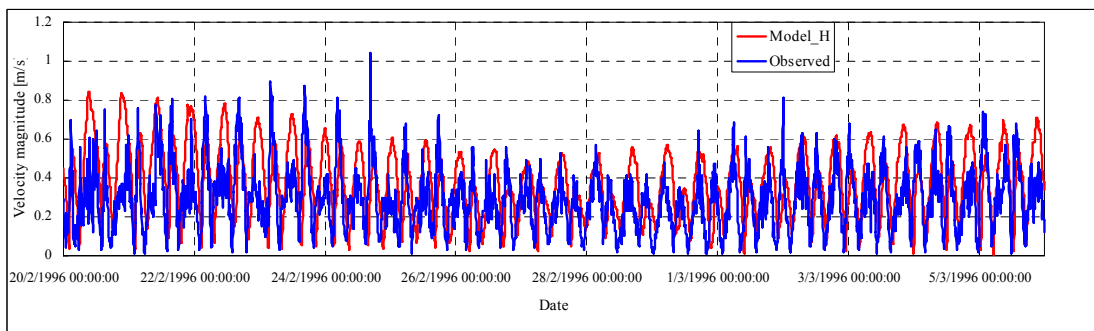


Fig 4.23 Comparison of velocity magnitude at H point (Period 3 of calibration)

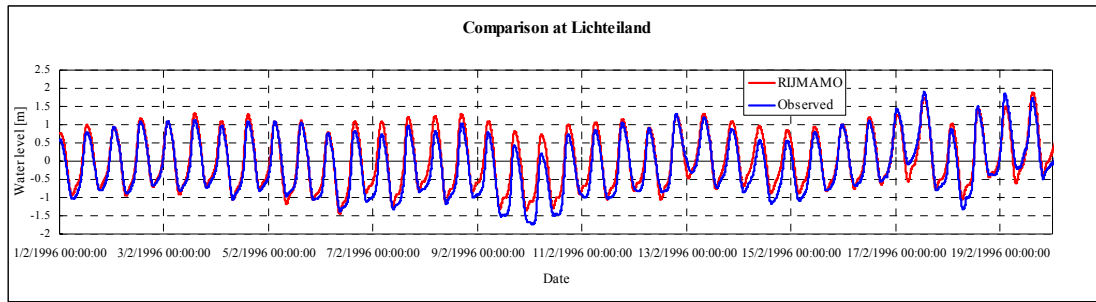


Fig 4.24 Water level at Lichteiland Goeree (Period 3 of calibration)

In this calibration period, the comparison of velocity direction is not presented here any more although it is carried out in this study. In view of the comparison during the third calibration period (Fig 4.20-4.24), some similar conclusions can be drawn as the foregoing comparison during the second calibration period. At I point, it seems to be still difficult to capture the peak of velocity magnitude (Fig 4.21) but the velocity direction is reproduced well by model. In terms of the other points B, G and H, the velocity magnitude and direction are simulated within sufficient accuracy by model (Fig 4.20, 4.22 and 4.23) although there are some significant differences on a few time points. The water level at Lichteiland Goeree is simulated in a good agreement with observed value as we expect. The largest difference is about 0.5 m, which appears around 10 February 1996 (Fig 4.24).

Through the comparison of velocity magnitude during the two calibration periods, it is presented that the hydrodynamics at B point is the weakest in the four points according to the modelled and observed results. The hydrodynamics is underestimated quite a lot by the model at I point. However, the cohesive sediment model has not been introduced in this FLOW model. Accounting for the effect of sediment-driven density flow and the position of I point which is quite close to the mouth, the velocity magnitude at I point is probably increased after introducing sediment process.

4.3.2 Calibration of cohesive sediment model

In order to investigate wave-induced effects on the dynamics of cohesive sediment, the wave model is coupled with the flow model in which the cohesive sediment transport is implemented as a process.

The WAVE model is built with the parameters and processes listed in Table 4.5 and Table 4.6.

Table 4.5 The parameters used in the wave model

Parameters	Options	Value	Unit
Hydrodynamics involved in wave	Bathymetry	Yes	-
	Water level	Yes	-
	Current	No	-
Gravity	9.8-10	9.81	m/s ²
Water density	950-1050	1025	kg/m ³
North	-	90	deg
Minimum depth	-	0.05	m

Table 4.6 The processes involved in the wave model

Processes	Options	Value
Wave setup	Activated/None	None
Generation model for physics	1 st /2 nd /3 rd	2 nd
Wind growth	Activated/De-activated	Activated
White capping	Activated/De-activated	Activated
Quadruplet	Activated/De-activated	Activated
Refraction	Activated/De-activated	Activated

Besides, the measured data with the time interval of 3 hours at Euro platform is taken as boundary condition of the wave model.

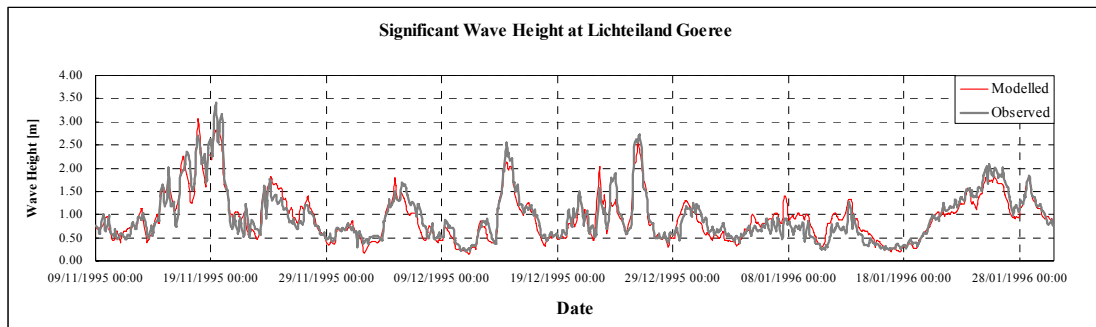


Fig 4.25 Comparison of significant wave height at Lichteiland Goeree (The whole calibration period)

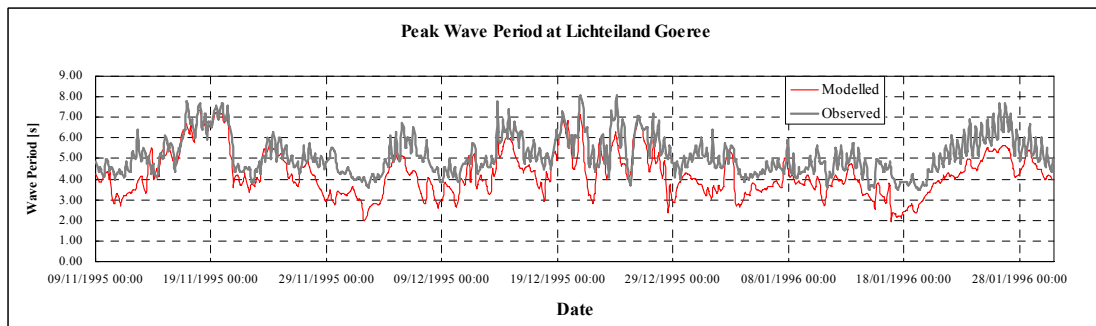


Fig 4.26 Comparison of peak wave period at Lichteiland Goeree (The whole calibration period)

The wave model reproduces the significant wave height quite well at Lichteiland Goeree (Fig 4.25). But for the peak wave period, the difference between the modelled and observed result is larger. In view of Fig 4.26, apparently the peak wave period is underestimated and smoothed by the model compared with the observed result. But its variation trend is caught appropriately by the model. Therefore, the modelled results can be regarded as a good representation for the real situation. The performance of the wave model is highly important for the following cohesive sediment model.

Under the boundary condition suspended sediment concentration increases linearly from 0.01 g/l to 0.05 g/l landward, the cohesive sediment model is fulfilled with the parameters listed in Table 4.7.

Table 4.7 The parameters calibrated in the sediment model

Parameter	Value	Lower limit	Upper limit	Unit
Reference density	1600	100	–	kg/m ³
Specific density	2650	100	4000	kg/m ³
Dry bed density	500	100.0	3000	kg/m ³
Settling velocity	0.5	>0	30	mm/s
Critical shear stress for sedimentation	0.1/1000	0	1000	N/m ²
Critical shear stress for erosion	0.6	0.001	100	N/m ²
Sediment erosion rate	0.0002	0	1	kg/m ² /s

During the observational period from 1995 to 1996, there are four time windows, which are *16 November 1995 – 13 December 1995*, *22 December 1995 – 30 January 1996*, *09 February 1996 – 13 March 1996*, and *20 March 1996 – 01 May 1996* respectively. As explained in Table 4.3, *16 November 1995 – 13 December 1995*, *22 December 1995 – 30 January 1996* and *09 February 1996 – 13 March 1996* are taken as calibration periods.

It is remarked that *_layer13* and *_layer11* represent the result from the 13th and 11th computational layer respectively in the 3-dimensional model. We will select modelled results from the corresponding layers which are the closest to the observed points such as 0.15 m and 0.55 m above the seabed. The selected layer is denoted as *_layerNo*. In addition, all the significant wave heights at the observed four points (B, I, G and H) shown in figures and tables are modelled results. The comparison of sediment concentration during the first calibration period is carried out as shown as follows (Fig 4.27-4.34):

➤ ***16 November 1995 – 13 December 1995:***

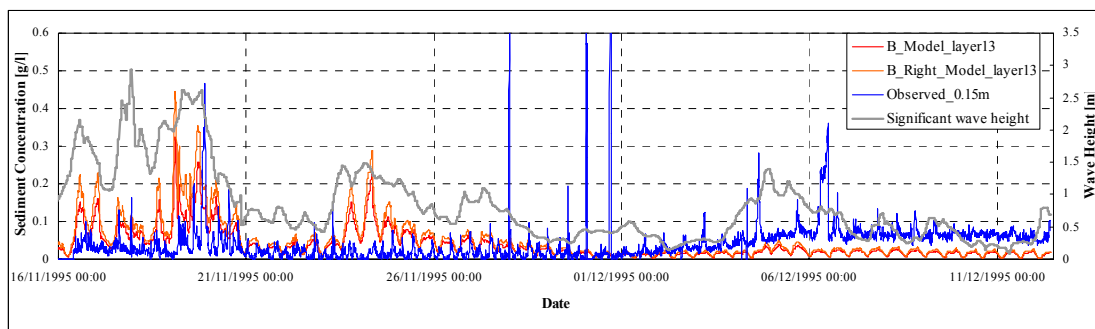


Fig 4.27 Modelled and observed SPM concentration at 0.15 m above the seabed at B point (Period 1 of calibration)

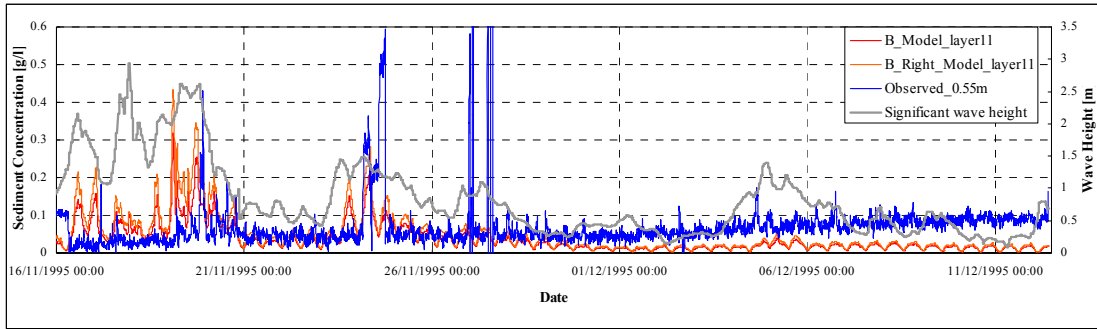


Fig 4.28 Modelled and observed SPM concentration at 0.55 m above the seabed at B point (Period 1 of calibration)

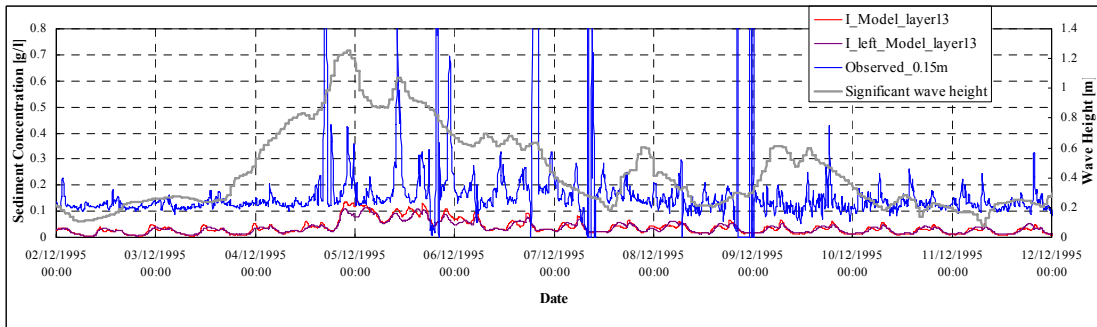


Fig 4.29 Modelled and observed SPM concentration at 0.15 m above the seabed at I point (Period 1 of calibration)

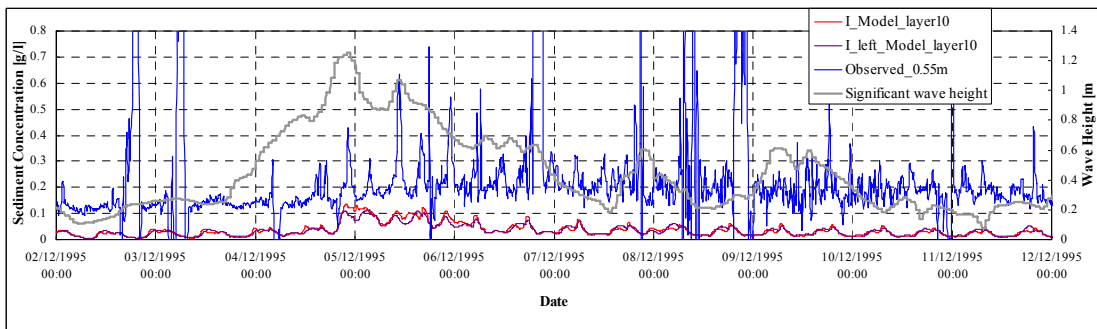


Fig 4.30 Modelled and observed SPM concentration at 0.55 m above the seabed at I point (Period 1 of calibration)

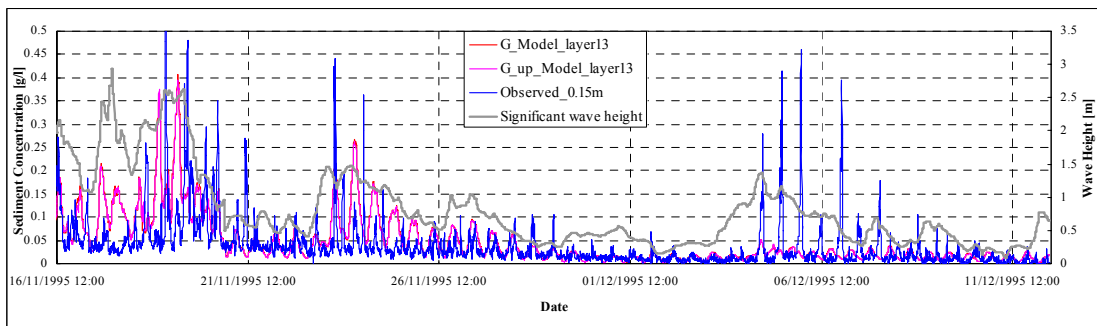


Fig 4.31 Modelled and observed SPM concentration at 0.15 m above the seabed at G point (Period 1 of calibration)

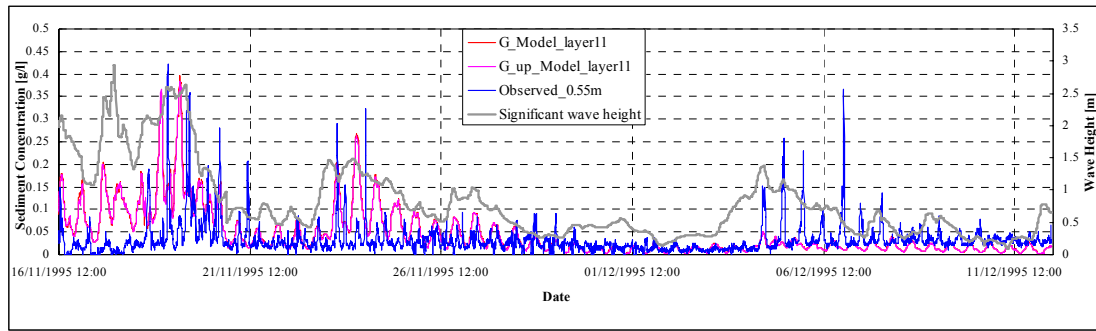


Fig 4.32 Modelled and observed SPM concentration at 0.55 m above the seabed at G point (Period 1 of calibration)

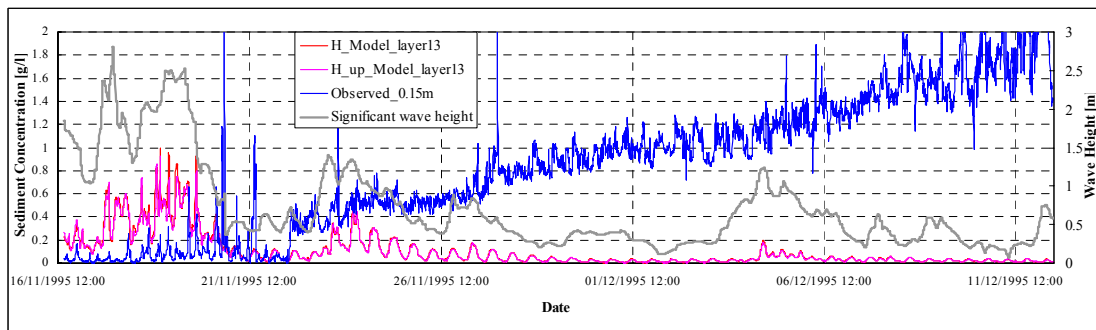


Fig 4.33 Modelled and observed SPM concentration at 0.15 m above the seabed at H point (Period 1 of calibration)

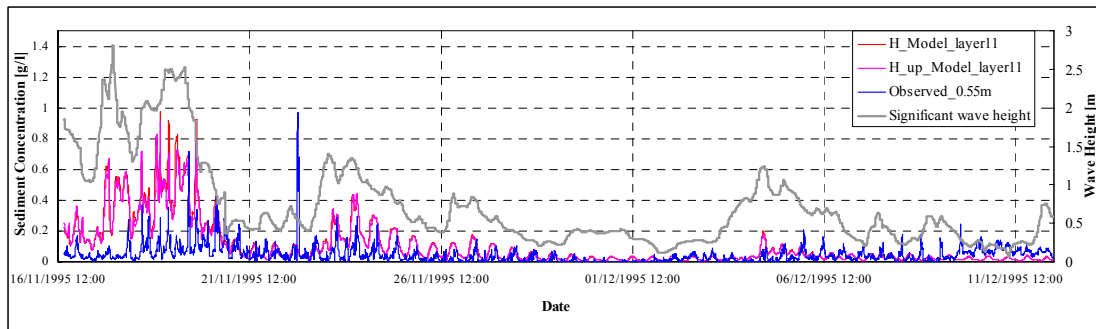


Fig 4.34 Modelled and observed SPM concentration at 0.55 m above the seabed at H point (Period 1 of calibration)

Table 4.8 Means of Significant wave height and SPM concentration in period 1 of calibration (Unit: m and mg/l)

Location	Mean Significant wave height	Observed 0.15m	Modelled layer13	Observed 0.55m	Modelled layer11/10
B	0.83	41.6	38.1	74.7	36.8
I	0.44	179	35.6	238	34.1
G	0.81	37.5	47.8	32.2	46.3
H	0.72	847	105.5	45.7	102.8

As shown in the comparison between the modelled and observed value during the first period in calibration, the difference is significant. At B point (Fig 4.27, 4.28), in the storm period during which the maximum significant wave height reaches 3 m, the modelled SPM concentration is very high compared to the measured one. There is a phase difference on peak value between the modelled and the observed concentration.

At a later stage, which is relatively calm, the concentration is underestimated by model. At I point (Fig 4.29, 4.30), the SPM concentration is observed for only ten days during which the maximum significant wave height reaches to 1 m. In this observational period, the modelled concentration is significantly lower than the observed, and the observed concentration does not seem to follow the variation of wave height at all. At G point (Fig 4.31, 4.32), there is a good agreement between the observed and modelled concentration. However, at a later time the peak of significant wave height reaches to 1 m, the modelled value does not respond too much compared to the observed one. At H point, the observed value at 0.15 m above bottom is probably incorrect (Fig 4.33), which is not taken into our investigation. At 0.55 m above bottom, the modelled result is higher than the observed and some phase difference on peak still exists (Fig 4.34).

Through the statistical measure of the first calibration period (Table 4.8), it is found that the model performs well at B and G points which are a little farther away from the mouth compared with I and H points. In addition, the SPM concentration at I point is underestimated quite a lot by the model during the calm period, whereas the SPM concentration at H point is somehow overestimated by model. In overview of the statistical measures, the modelled concentrations from the 13th and 11th/10th layers do not exhibit significant difference. However, the concentration at 0.55 m is larger than that at 0.15 m for I and B points, indicating the range of (in) accuracy of the observed data.

In the comparison of the next calibration periods, the SPM concentrations at 0.55 m for the four observed points will not be presented unless the observed SPM concentration at 0.15 m looks abnormal.

➤ **22 December 1995 – 30 January 1996:**

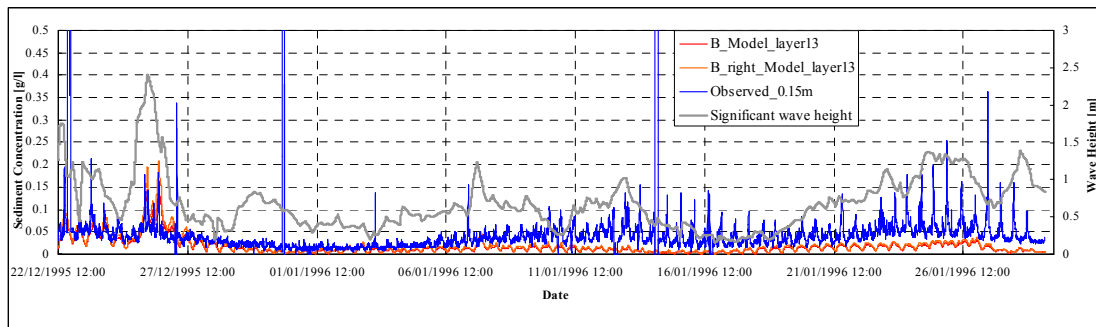


Fig 4.35 Modelled and observed SPM concentration at 0.15 m above the seabed at B point (Period 2 of calibration)

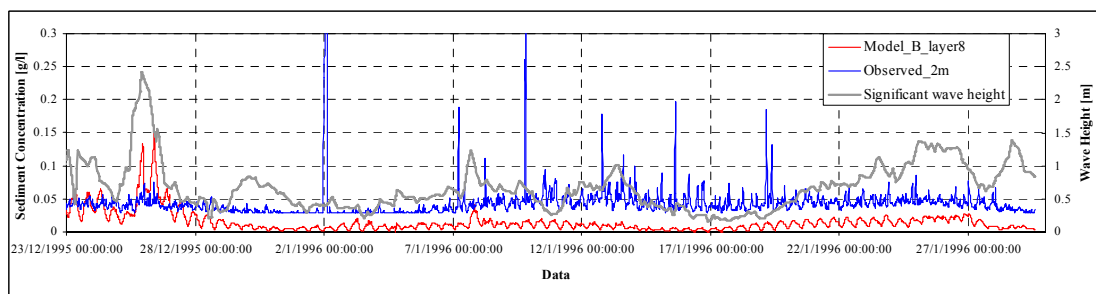


Fig 4.36 Modelled and observed SPM concentration at 2 m above the seabed at B point (Period 2 of calibration)

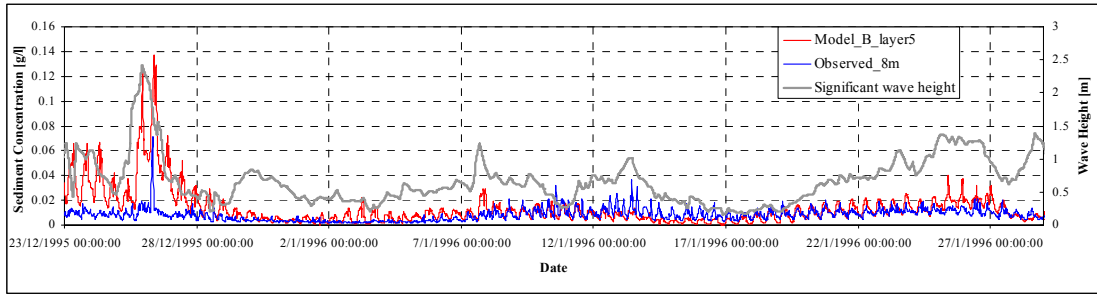


Fig 4.37 Modelled and observed SPM concentration at 8 m above the seabed at B point (Period 2 of calibration)

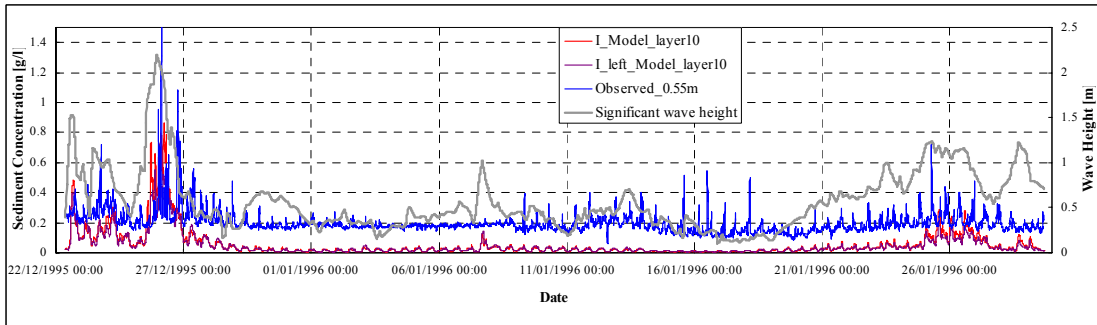


Fig 4.38 Modelled and observed SPM concentration at 0.55 m above the seabed at I point (Period 2 of calibration)

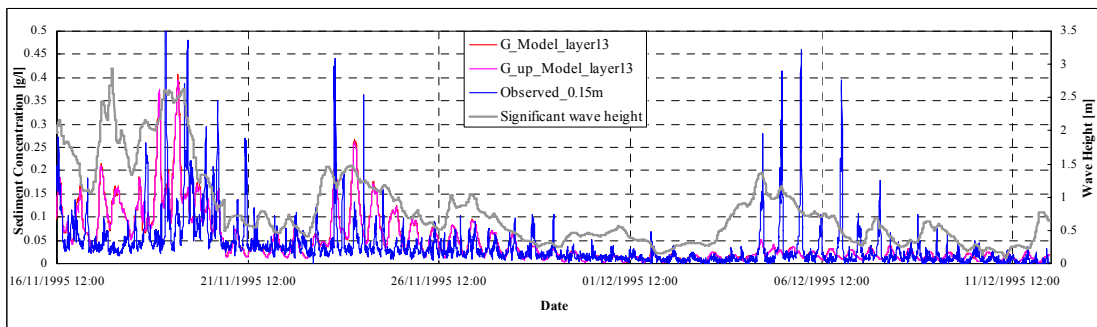


Fig 4.39 Modelled and observed SPM concentration at 0.15 m above the seabed at G point (Period 2 of calibration)

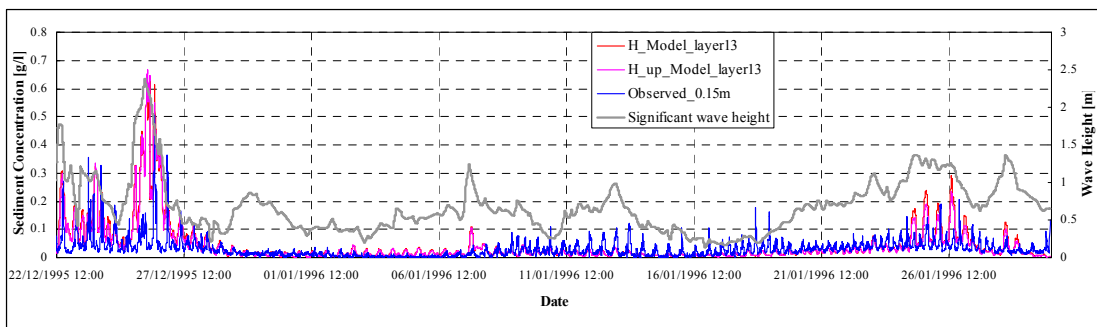


Fig 4.40 Modelled and observed SPM concentration at 0.15 m above the seabed at H point (Period 2 of calibration)

Table 4.9 Means of Significant wave height and SPM concentration in period 2 of calibration (Unit: m and mg/l)

Location	Mean Significant wave height	Observed 0.15m	Modelled layer13	Observed 0.55m	Modelled layer11/10
B	0.69	50.5	16.6	65.3	16.1
I	0.57	212	58.6	197	55.8
G	0.68	28.8	18.6	18.9	18.1
H	0.60	30.7	44.9	36.6	44.0

During the second period of calibration, the model shows a good agreement with observed value at G point (Fig 4.39). But for I point, the SPM concentration is still underestimated too much by the model (Fig 4.38). In this calibration period, there are four vertical observational points which are 0.15 m, 0.55 m, 2 m and 8 m above the seabed at B point (Fig 4.35-4.37). It is noticed that at 2 m above bottom the modelled concentration is much lower than the observed one which does not seem to be remarkably relevant with the variation on significant wave height (Fig 4.36). At 8 m above bottom, the concentration is overestimated by model during the storm period, whereas the concentration is reproduced well during the calm period (Fig 4.37). At H point, it is shown that the modelled concentration is a little higher than the observed one during the storm period while lower during the calm period (Fig 4.40).

According to the statistical measures of the second calibration period (Table 4.9), it is found the SPM concentrations at B and I are underestimated so much by the model. However, the modelled SPM concentrations appear to be good at G and H points through the comparison with observed ones.

➤ **09 February 1996 – 13 March 1996**

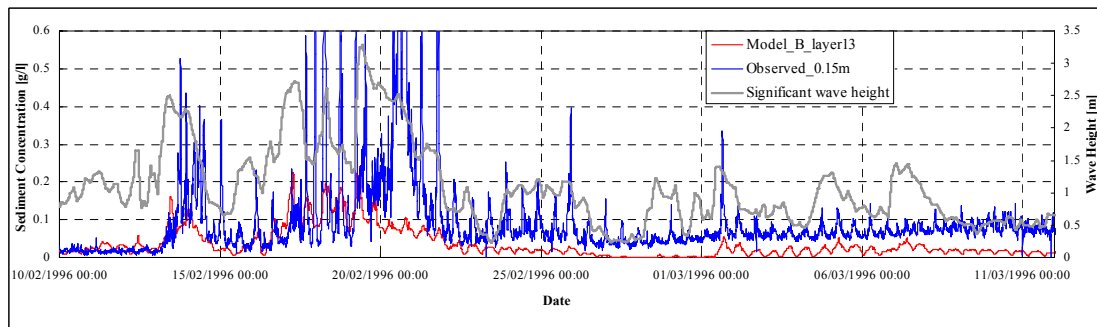


Fig 4.41 Modelled and observed SPM concentration at 0.15 m above the seabed at B point (Period 3 of calibration)

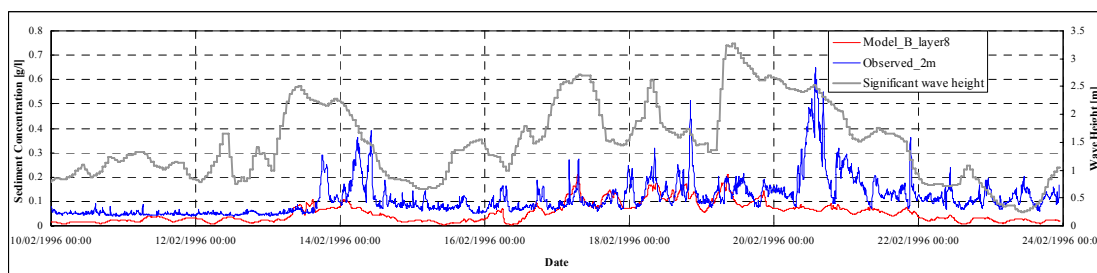


Fig 4.42 Modelled and observed SPM concentration at 2 m above the seabed at B point (Period 3 of calibration)

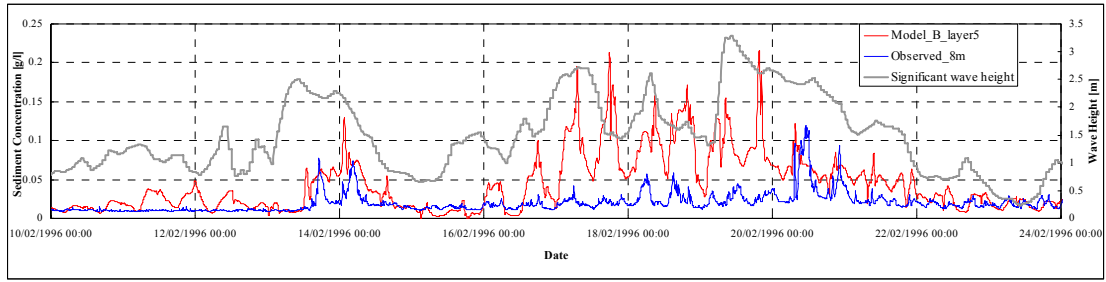


Fig 4.43 Modelled and observed SPM concentration at 8 m above the seabed at B point (Period 3 of calibration)

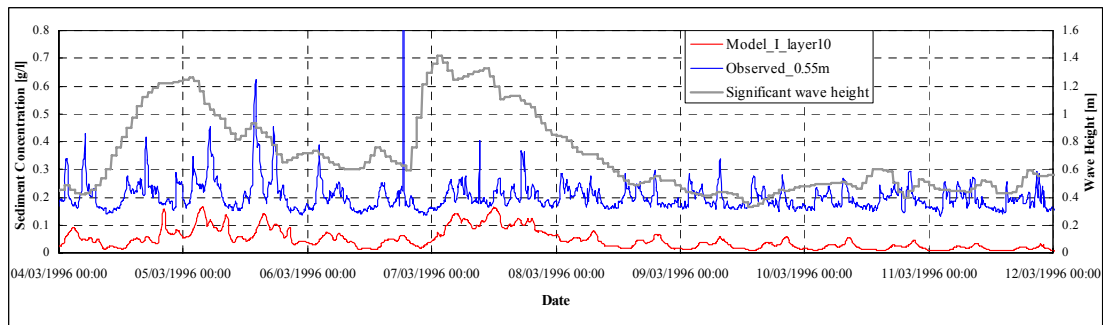


Fig 4.44 Modelled and observed SPM concentration at 0.55 m above the seabed at I point (Period 3 of calibration)

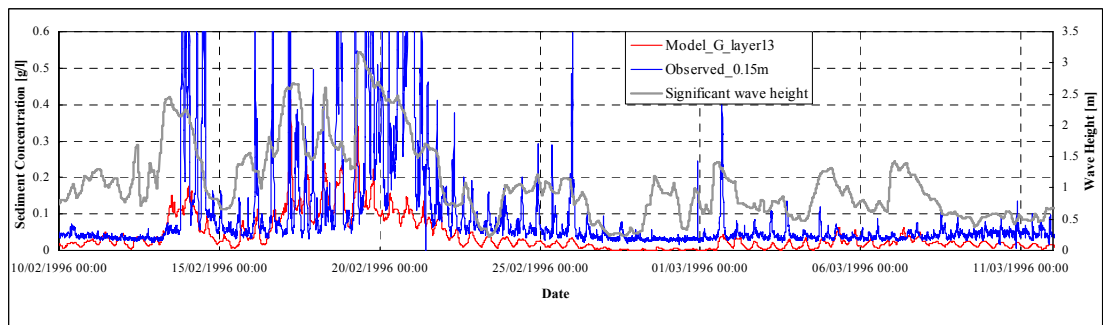


Fig 4.45 Modelled and observed SPM concentration at 0.15 m above the seabed at G point (Period 3 of calibration)

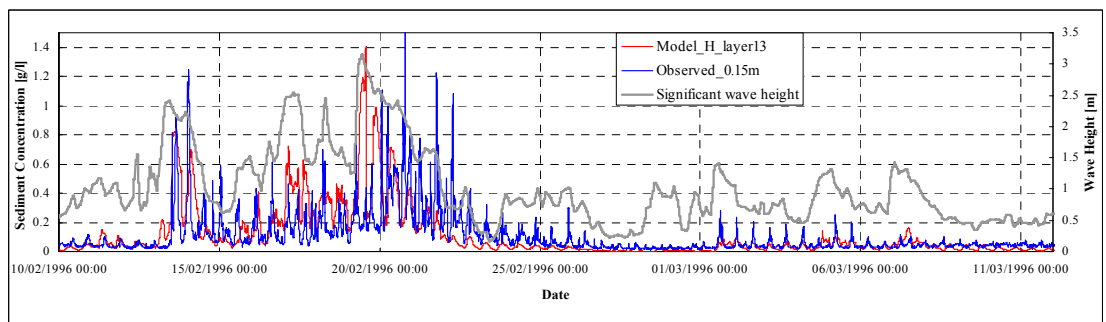


Fig 4.47 Modelled and observed SPM concentration at 0.15 m above the seabed at H point (Period 3 of calibration)

Table 4.8 Means of Significant wave height and SPM concentration in period 3 of calibration (Unit: m and mg/l)

Location	Mean Significant wave height	Observed 0.15m	Modelled layer13	Observed 0.55m	Modelled layer11/10
B	1.09	101	34.6	67.3	33.5
I	0.69	277	46.7	202	44.5
G	1.08	102	39.7	96.4	38.5
H	1.01	107	109	126	106

In the third period of calibration, the significant wave height reaches to nearly 3.5 m, so there can be more sediment which is resuspended from the bed. This can be easily seen from the observed value. However, the modelled results do not have a similar response to the large wave height. Thus, the modelled SPM concentration is much less than the observed one at B, I, and G points (Fig 4.41, 4.44, 4.45). Only at H point, the modelled SPM concentration peaks at 1 g/l, which is close to the observed one but some phase difference still exists, and during the calm period the modelled one is lower than the observed one as well (Fig 4.7). In addition, at B point, the modelled concentration at 2 m and 8 m above the seabed indicates a similar result of comparison to that in the second calibration period (Fig 4.42, 4.43).

In view of the statistical measures of the third calibration period, the SPM concentrations are underestimated by the model so much at B, I and G points. During the period, the mean of the significant wave height reach over 1 m, but the modelled results do not respond sufficiently to the large wave height except for H point.

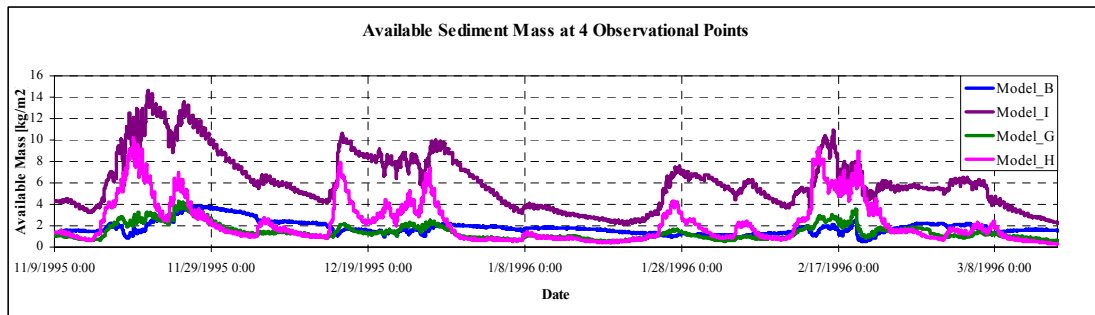


Fig 4.48 The modelled available sediment mass at 4 observational points (The whole calibration period)

In reality, available sediment mass is a critical factor for the SPM concentration. During the whole calibration period shown as Fig 4.49, it is noticeable that the available sediment mass at B point is generally larger than that at G and even H points during calm period, which indicates a part of sediment delivered from south can not arrive at G and H points in the calm weather.

4.4 Model verification

The verification is carried out with the same parameter sets configured in calibration. The verification contains two periods *12 November 1996 – 27 November 1996* and *06 December 1996 – 08 January 1997* (Table 4.9), during which the modelled results are compared with the observed data recorded in SILTMAN data.

Table 4.9 Periods selected for verification in FLOW model

	From	To
Period 1 of verification	12 November 1996	27 November 1996
Period 2 of verification	06 December 1996	08 January 1997

4.4.1 Verification of hydrodynamic model

In the verification periods, there are only two points I and G, at which the velocity magnitude and direction are available in SILTMAN data. Besides, comparison on water level can be carried out at Lichteiland Goeree as well.

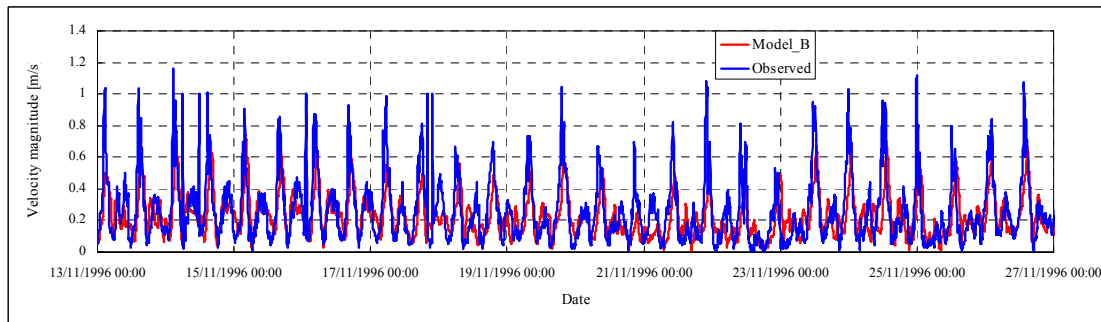


Fig 4.49 Comparison of velocity magnitude at I point (Period 1 of verification)

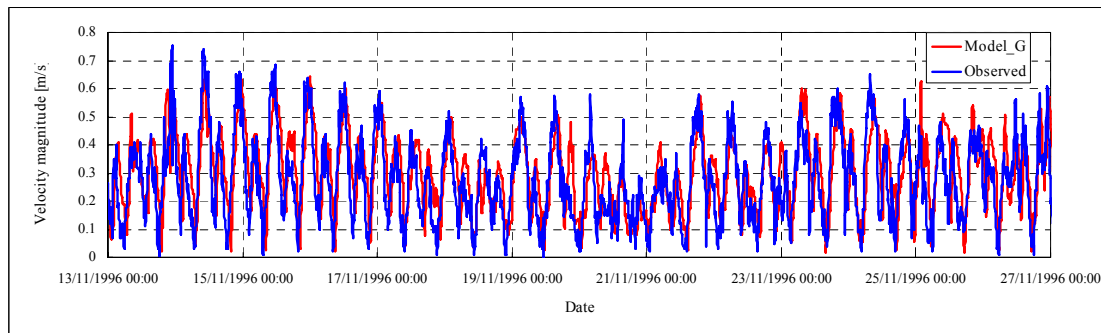


Fig 4.50 Comparison of velocity magnitude at G point (Period 1 of verification)

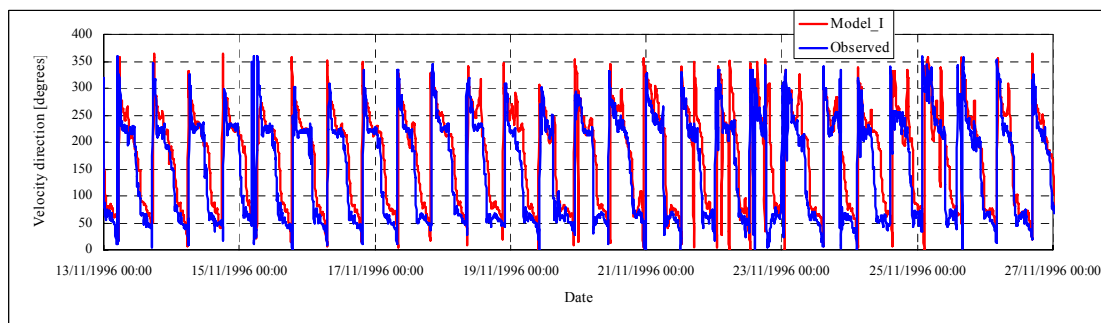


Fig 4.51 Comparison of velocity direction at I point (Period 1 of verification)

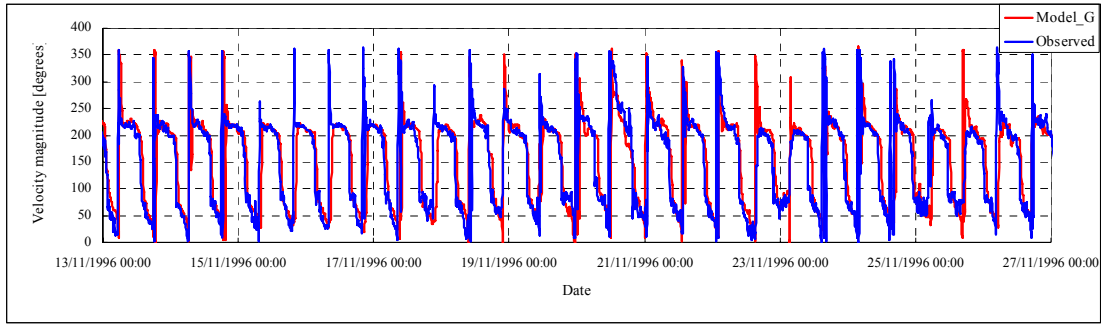


Fig 4.52 Comparison of velocity direction at G point (Period 1 of verification)

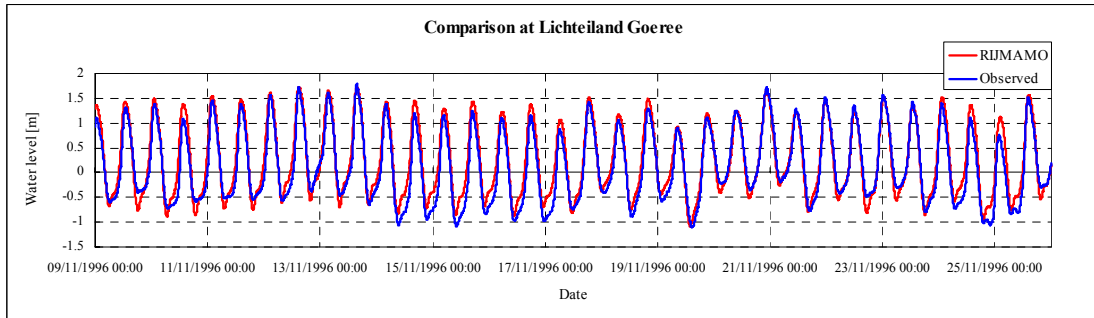


Fig 4.53 Water level at Lichteiland Goeree (Period 1 of verification)

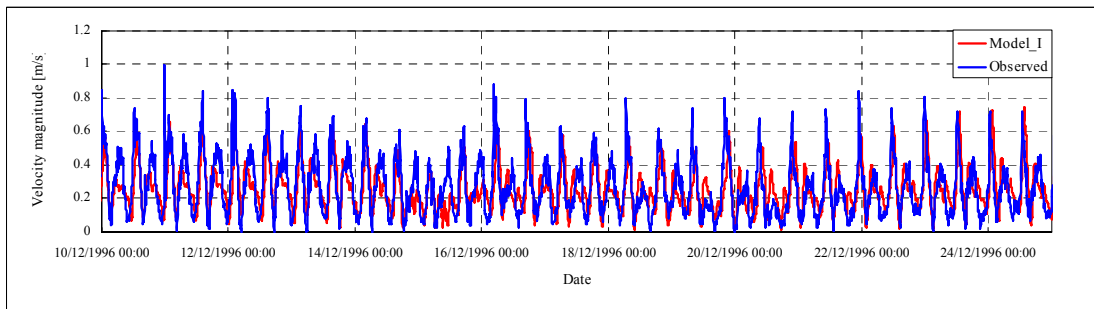


Fig 4.54 Comparison of velocity magnitude at I point (Period 2 of verification)

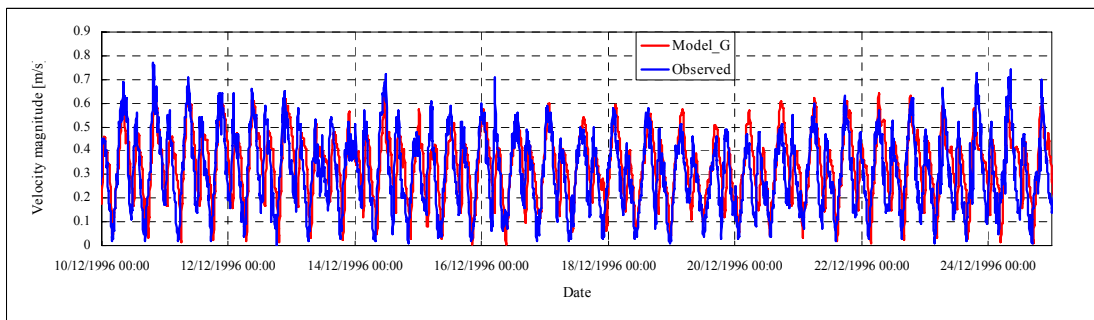


Fig 4.55 Comparison of velocity magnitude at G point (Period 2 of verification)

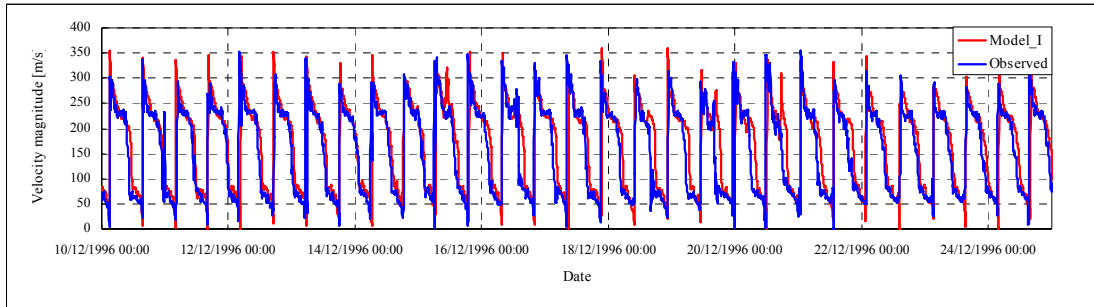


Fig 4.56 Comparison of velocity direction at I point (Period 2 of verification)

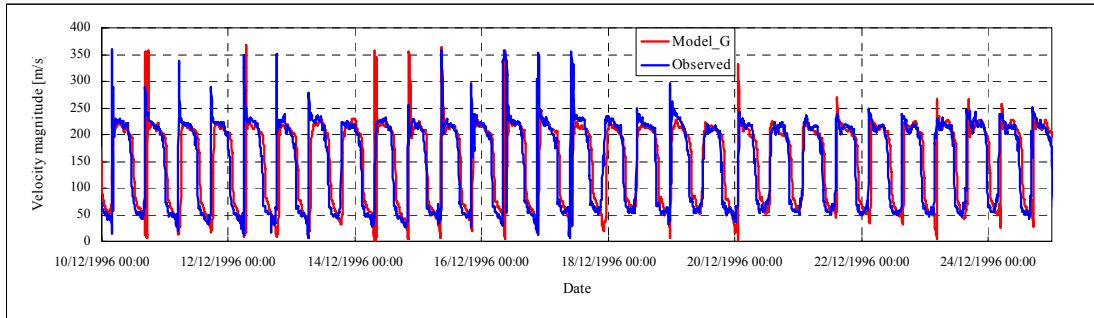


Fig 4.57 Comparison of velocity direction at G point (Period 2 of verification)

In the verification period, the modelled results present a good agreement with the observed values. But in terms of velocity magnitude at I point, the discrepancy is still significant. The peak velocity may exceed 1 m/s, but for the modelled result, the peak value can only reach up to around 0.7 m/s. Moreover, the modelled velocity direction at I point happens to change quite a lot at two time points during the first verification period without any possible explanation. In the second verification period, the modelled velocity magnitude at I point seems to be more close to the observed value. But it is remarked that the observed value seldom reaches 1 m/s compared with the prior periods. In view of the comparison, the modelled hydrodynamics results are quite reliable.

4.4.2 Verification of cohesive sediment model

Before we start to verify the cohesive sediment model, it is favourable to look through the results calculated by wave model which is online-coupled with flow model.

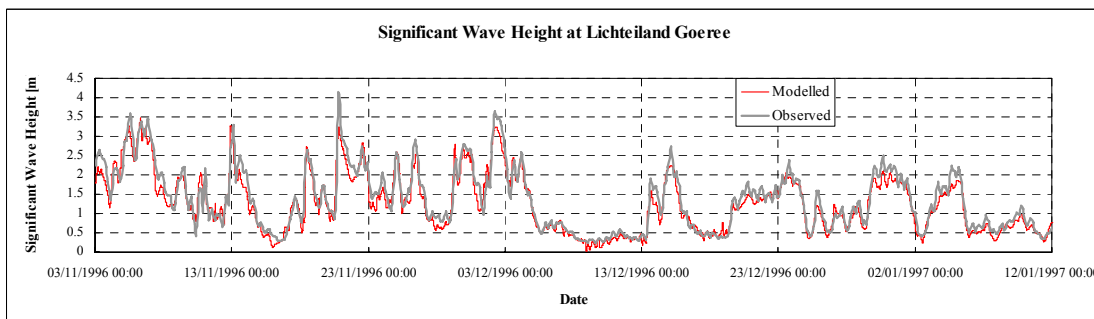


Fig 4.58 Comparison of significant wave height at Lichteiland Goeree (The whole verification period)

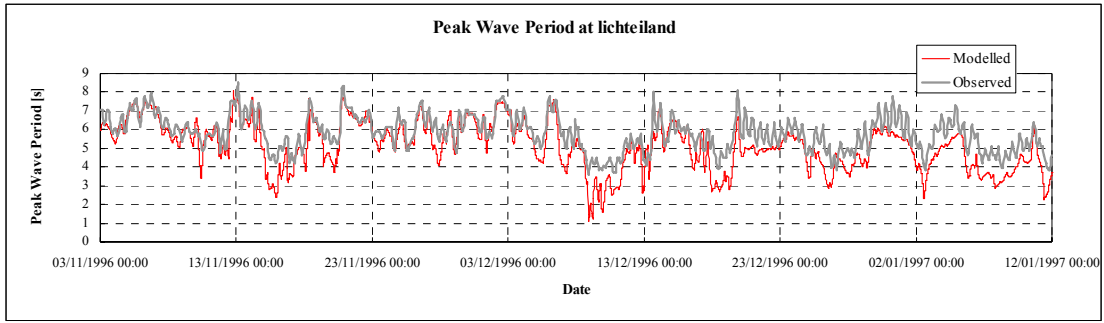


Fig 4.59 Comparison of peak wave period at Lichteiland Goeree
(The whole verification period)

Similar to the calibration results, the significant wave height is reproduced well by wave model although the modelled result is a little lower than the observed value. But with regard to the peak wave period, it is underestimated by model to a large extent. In addition, the variation pattern is captured well by the model.

There are two periods *12 November 1996 – 27 November 1996* and *06 December – 08 January 1997* during which verification of SPM concentration is carried out.

➤ ***12 November 1996 – 27 November 1996***

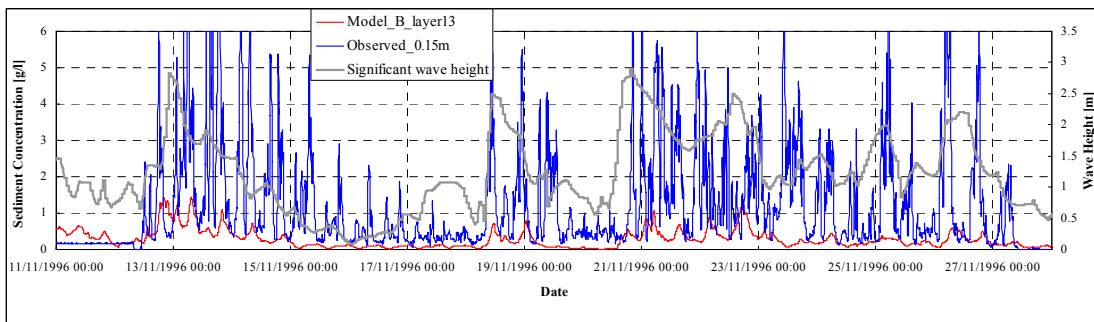


Fig 4.60 Modelled and observed SPM concentration at 0.15 m above the seabed at B point (Period 1 of verification)

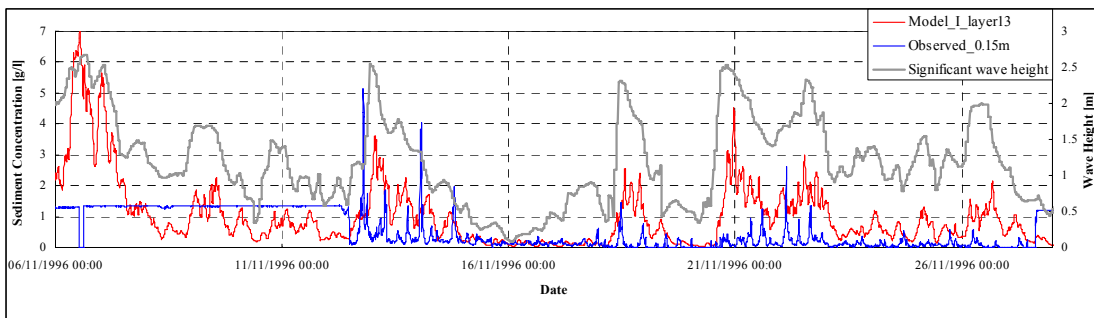


Fig 4.61 Modelled and observed SPM concentration at 0.15 m above the seabed at I point (Period 1 of verification)

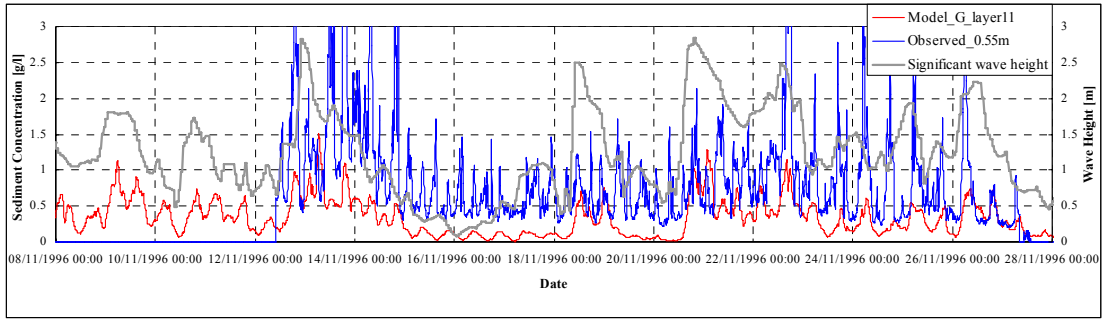


Fig 4.62 Modelled and observed SPM concentration at 0.55 m above the seabed at G point (Period 1 of verification)

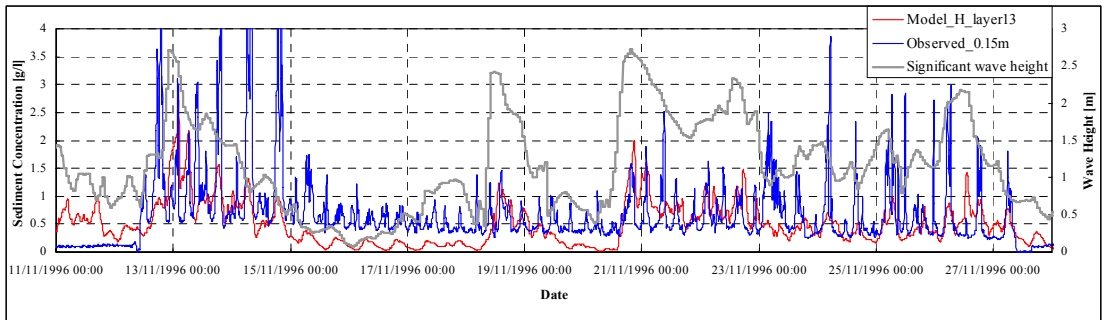


Fig 4.63 Modelled and observed SPM concentration at 0.15 m above the seabed at H point (Period 1 of verification)

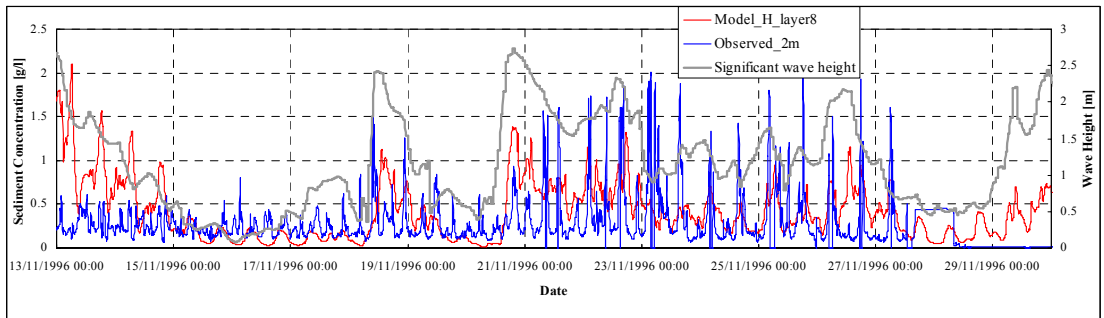


Fig 4.64 Modelled and observed SPM concentration at 2 m above the seabed at H point (Period 1 of verification)

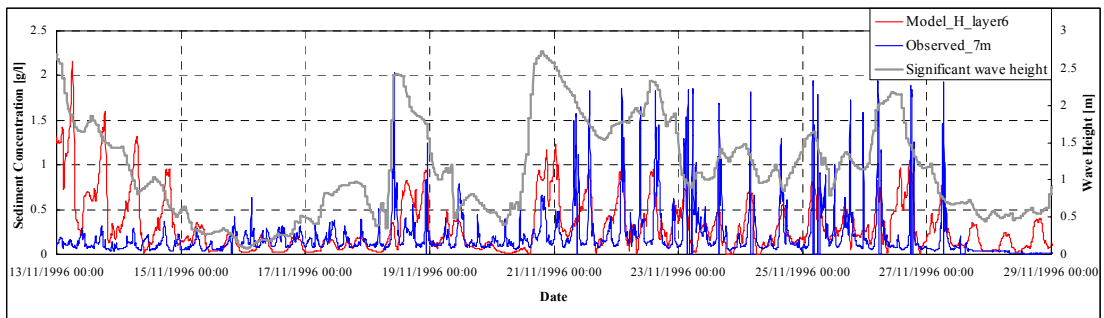


Fig 4.65 Modelled and observed SPM concentration at 7 m above the seabed at H point (Period 1 of verification)

Table 4.10 Means of Significant wave height and SPM concentration in period 1 of verification (Unit: m and mg/l)

Location	Mean Significant wave height	Observed 0.15m	Modelled layer13	Observed 0.55m	Modelled layer11/10
B	1.22	1209	274	2000	261
I	1.21	575	1042	641	948
G	1.23	943	353	942	340
H	1.15	642	489	742	475

The observed values look strange in the first verification period. At B point (Fig 4.60), the observed SPM concentration is extremely high, which never occurred before, even though the significant wave height is less than 3 m. There are large differences between the modelled and observed concentration. At I point (Fig 4.61), initially the observed concentration almost remains constant, which is apparently unrealistic in the case of continuous change on the significant wave height. Contrary to the calibration periods, the modelled concentration is significantly larger than the observed especially during the storm period. However it is remarked that in the calibration periods most of the observed values at I point are available only in relatively calm period during which the largest significant wave height is not more than 1.5 m. At G point (Fig 4.62), there are some observed values which are missing at the initial stage. But for the other times of this period, the modelled results are lower than the observed values. At H point (Fig 4.63), during the calm periods, the modelled concentration is remarkably lower than the observed one at 0.15 m above the seabed; at 2 m above seabed (Fig 4.64), the modelled one is a little lower than the observed one while at 7 m above seabed (Fig 4.65), the modelled one looks better. At last, it is noticeable that in the first verification period, the number of times the significant wave height exceeds 2 m equals to six.

Upon the statistical measures of the first verification period (Fig 4.10), the significant wave height is substantially higher than before. As a result, the observed values have much more response to the significant wave height at all four points (B, I, G and H), all of which are 1-3 times larger than the modelled ones except for H point., where the modelled concentration appears to be closer to the observed one and about 30% lower than the observed one.

➤ **06 December 1996 – 08 January 1997**

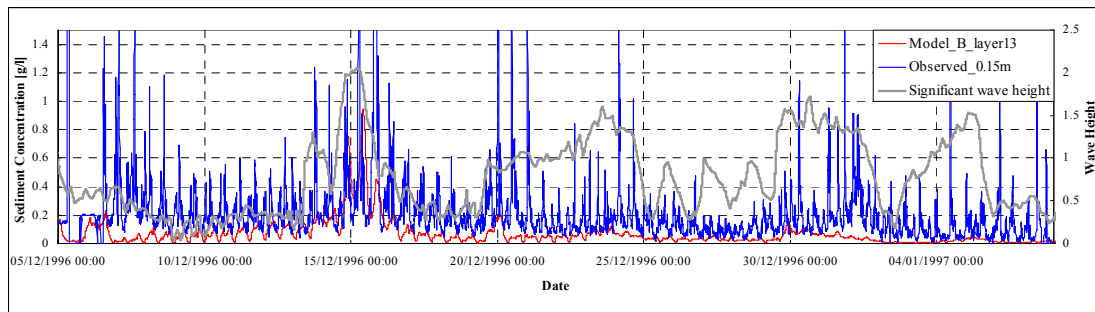


Fig 4.66 Modelled and observed SPM concentration at 0.15 m above the seabed at B point (Period 2 of verification)

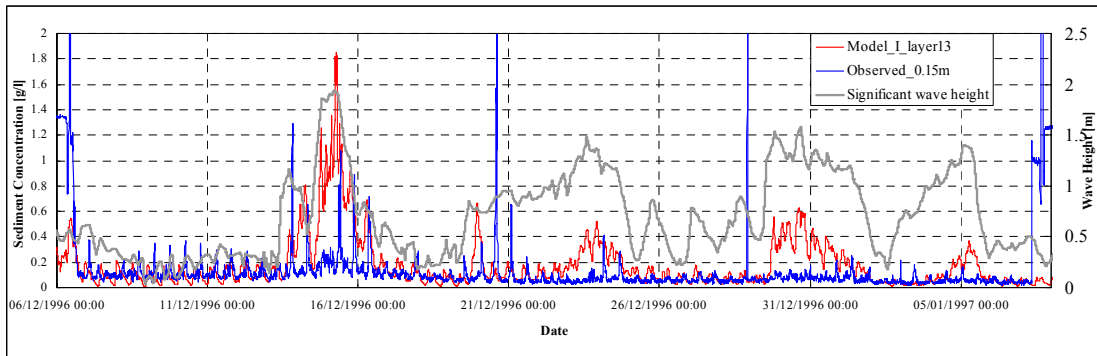


Fig 4.67 Modelled and observed SPM concentration at 0.15 m above the seabed at I point (Period 2 of verification)

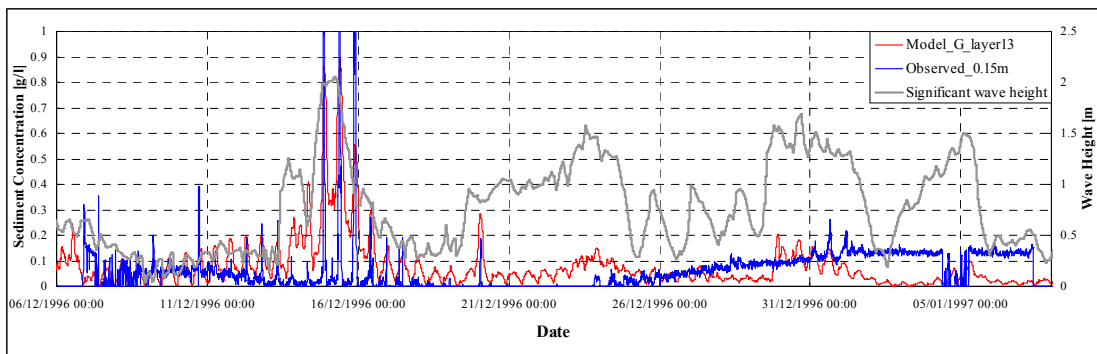


Fig 4.68 Modelled and observed SPM concentration at 0.15 m above the seabed at G point (Period 2 in verification)

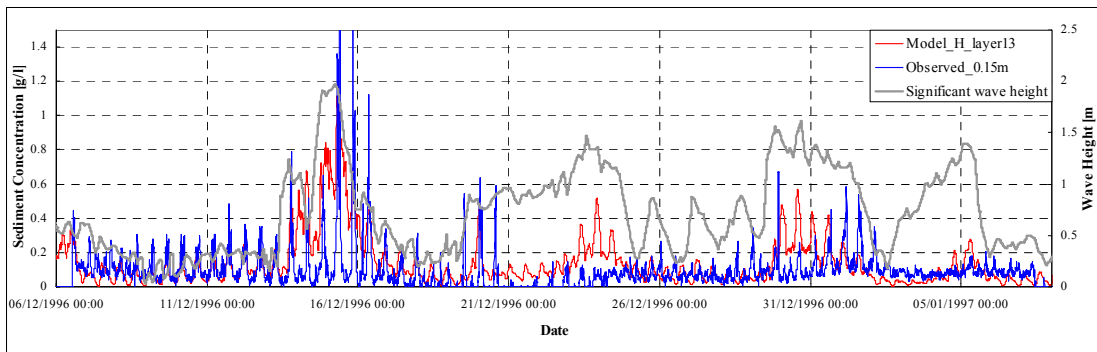


Fig 4.69 Modelled and observed SPM concentration at 0.15 m above the seabed at H point (Period 2 of verification)

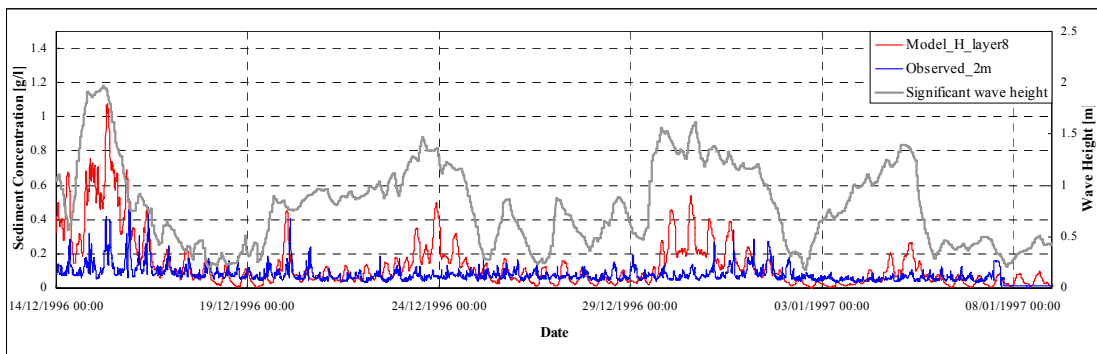


Fig 4.70 Modelled and observed SPM concentration at 2 m above the seabed at H point (Period 2 of verification)

Table 4.11 Means of Significant wave height and SPM concentration in period 2 of verification (Unit: m and mg/l)

Location	Mean Significant wave height	Observed 0.15m	Modelled layer13	Observed 0.55m	Modelled layer11/10
B	0.78	232	68.6	220	66.1
I	0.70	189	176	129	166
G	0.76	67.1	77.5	153	75.2
H	0.71	91.5	136	179	132

In the second verification period which is relatively calm, there is only one time the significant wave height reaches 2 m. At B point (Fig 4.66), the observed concentration is always higher than the modelled one irrespective of storm or calm periods. At I point (Fig 4.67), the modelled concentration is much higher than the observed one during the storm periods. But during the calm periods, the modelled one is a little lower than the observed one. At G and H point (Fig 4.68, 4.69), the modelled concentration is lower than the observed one as well during the calm periods, however the modelled one responds well during the storm periods despite some discrepancies on peak values. As to H point, at 2 m above seabed (Fig 4.70), the modelled concentration is significantly higher than the observed one which sometimes does not respond to the significant wave height during storm periods, whereas the modelled one is lower than the observed one during the calm periods.

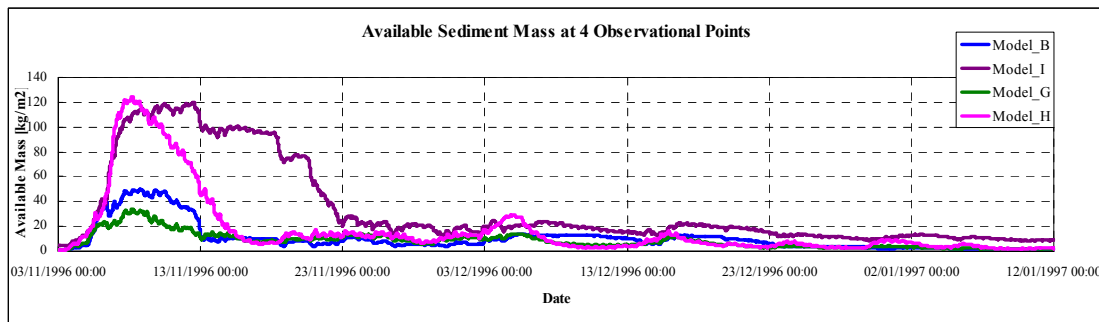


Fig 4.71 The modelled available sediment mass at 4 observational points (The whole verification period)

During the verification period shown in Fig 4.49, there are large increases in sediment availability at all of the 4 points during the initial period, The main reason behind this is that the amount of sediment delivered from the river is quite large during that period. In addition, similar to the result of the calibration period, the available sediment mass at B point is larger than that at G and even H point during calm periods. But in this verification period the difference is the available mass at B point is also larger than that at G point during the initial storm period.

4.5 Conclusions

In this chapter, the calibration and verification results of a coupled model consisting of flow, wave and sediment module are presented.

The following conclusions can be drawn for the modelling of hydrodynamics, wave and cohesive sediment:

- The hydrodynamic results are reproduced quite well by RIJMAMO model in terms of water level, velocity magnitude and direction both in calibration and verification. That means the boundary conditions extracted from large-scale model ZUNO model is appropriate. However, some discrepancies can't be neglected. At I point, the observed peak velocity usually reaches over 1 m/s, which is almost impossible to be captured by the model. The reason should be some local effects. In reality, I point is quite close to the dike which has the shape of a circle (Fig 4.5, 4.6). During the schematization for the reality, although the model can be boundary-fitted with curvilinear grids, in the existing flow grid the dike is schematized by several segments of straight line (Fig 4.6). In addition, some phase differences on velocity direction between the modelled and observed values may be attributed to the boundary condition applied at the river boundary. The boundary condition is a day averaged discharge which is automatically interpolated to 1 minute time interval by the model. Generally speaking, the modelled hydrodynamic results are judged sufficient to contribute to a study on sediment dynamics.
- In the wave model, there is only one observational point at which we can make comparison. According to the comparison, the wave model shows a good performance on simulating the significant wave height. Moreover, the variation pattern of the peak wave period is captured by the model, but the value is underestimated by the model. Some errors should be from generating bathymetry of wave grid which is established on the extension of flow grid (Fig 4.4). However, the bathymetry data for the whole wave grid consists of two parts, of which one is from the RIJMAMO model and the other is from ZUNO model for the extension of flow grid. After putting them together, there appears to be a sudden change on topography at the joint of two parts although some work is done on smoothing.
- The performance of the hydrodynamics and wave models lays down a solid basis for the cohesive sediment model. Based on the calibration and verification of the cohesive sediment model, it is found that the modelled SPM concentration is always lower than the observed one during most of the calm periods. Especially at I point, the modelled one is significantly lower than the observed one, but which is not difficult to explain. In view of the observed velocity at I point, the peak value usually reaches over 1 m/s, which is can't be reproduced by the hydrodynamics model. As a result, the hydrodynamics at I point is underestimated a lot by the model. In addition, during the extreme storm periods such as those in the third calibration and first verification periods the SPM concentration is underestimated by the model so much except for H point where the modelled concentration reaches a level close to the observed one. During normal storm periods such as those in the first, second calibration periods and the second verification period, the modelled concentration has a good agreement with the observed one except for B point, where the concentration is underestimated by the model to a large extent. However, in view of the observed velocity magnitude in SILTMAN data and the modelled one, the hydrodynamics at B point is the weakest in the four observational points. Moreover, some phase differences still exist. The modelled SPM concentration always follow the variation pattern of significant wave height, but the observed one does not follow it completely and sometimes exhibits a characteristic of being strongly stochastic.
- Through the comparison between the observed value and modelled result, it is not advisable to fully believe the observed value which does not depict the real case

sometimes. It is remarked that all of the observed value in SILTMAN data is raw without being processed. So some noises from measurement usually appear in the comparison. Sometimes we can identify them by comparing the observed values at 0.15 m and 0.55 m above the seabed. In principle, they should keep in same variation trend, and in normal condition the concentration at 0.15 m should be a little larger than that at 0.55 m according to vertical profile (Fig 2.1). Besides, the observed concentration appears to change very rapidly, usually after one peak, and then it falls down to a low level in a quite short time. So the shape of its varying curve seems to be much steeper than the modelled one.

- In the flow model, there is only one sediment layer and one sediment component, thus the involved processes are relatively simple for describing the sediment dynamics. In order to achieve a compromise between the calm period and storm period, the critical shear stress is set a little larger, which is a principal factor causing the modelled SPM concentration to be lower than the observed one during most of the calm periods. Therefore, for the sake of solving this problem about the compromise between the calm and storm periods, WAQ (WATER Quality) model involving two layers, two sediment components and more processes will be applied in this study.

Chapter5 WAQ Model

In reality, cohesive sediment dynamics involves a number of processes, which are simplified in the flow model. But due to the fact that some important processes are missing in the flow model, it is difficult to describe the reality only by the cohesive sediment process implemented in the flow model. Therefore, in order to describe the reality better, WAQ model involving more processes is introduced to this study, which is used for versatile water quality modelling including physical, (bio)chemical and biological processes. Moreover, in the last chapter, the calibration and verification are presented with the parameter set with which the best modelled results are obtained. However, it is quite probable to find out a better parameter set for the flow model. The problem is the computation of the flow model is quite time-consuming, requiring 13 days to do simulation for 83 days on a high-speed computer. Obviously, the calibration is quite time-consuming within the flow model. But within WAQ model the computational time is only 1 day for the same simulation period 83 days after the hydrodynamic computation is done by the flow model. Then the WAQ model can calculate the cohesive sediment dynamics based on the hydrodynamic results such as flow pattern, vertical dispersion, and total bed shear stress. Therefore, in order to understand the mechanics dominating cohesive sediment dynamics in a more comprehensive way, and to get more reasonable modelled results referring to the observed values collected in SILTMAN data, it is worthwhile to apply WAQ model in this study.

5.1 Calibration of WAQ model

This calibration starts with the same parameter (Table 5.1) set which has been verified against to SILTMAN data within ZUNO model (Van Kessel, 2006). Additionally, the same boundary conditions as that for the FLOW model are used for WAQ model. It is defined that the sediment concentration increases from 10 mg/l to 50 mg/l gradually onshore. Moreover, there are two periods selected for the calibration of WAQ model (Table 5.2).

Table 5.1 Parameters used in WAQ model

Parameter	Description	Value	Unit
TauShields	Shields shear stress for resusp. pick-up	1.5	N/m ²
GRAIN50	Grain size (D50)	0.0003	m
GRAV	Gravitational acceleration	9.8	m/s ²
KinViscos	Kinematic viscosity	1.00E-06	m ² /s
RHOSAND	bulk density sand	2.60E+06	g/m ³
RhoWater	density of water	1020	kg/m ³
PORS2	porosity of sediment layer S2	0.4	-
ThickS2	Thickness of layer S2 van Rijn pick-up resusp.	0.1	m
MinDepth	minimum waterdepth for sedimentation	0.1	m
MaxResPup	Maximum resuspension pick-up	3600	g/m ² /d
FactResPup	Factor resuspension pick-up	3.50E-07	-
VSedIM1	sedimentation velocity IM1	10.8	m/d
TaucSIM1	critical shear stress for sedimentation IM1	1000	N/m ²
FrIM1SedS2	fraction sedimentation IM1 towards S2	0.05	-

VResIM1	first order resuspension velocity IM1	0.5	1/d
SWResIM1	switch resuspension IM2 (0=resdm, 1=resim2)	1	-
SWResIM2	switch resuspension (0=z+f, 1=min(z,f))	1	-
VSedIM2	sedimentation velocity IM2	86.4	m/d
TaucSIM2	critical shear stress for sedimentation IM2	1000	N/m ²
FrIM2SedS2	fraction sedimentation IM2 towards S2	1.25E-02	-
VResIM2	first order resuspension velocity IM2	2	1/d
FrTIMS2Max	maximum fraction TIM in layer S2 pick-up	0.6	-
TaucRS1DM	critical shear stress for resuspension DM in layer S1	1000	N/m ²
TaucRS1IM1	critical shear stress for resuspension IM1S1	0.1	N/m ²
TaucRS1IM2	critical shear stress for resuspension IM2S2	0.1	N/m ²
TaucRS2DM	critical shear stress for resuspension DM in layer S2	1000	N/m ²
TaucRS2IM1	critical shear stress for resuspension IM1S2	1000	N/m ²
TaucRS2IM2	critical shear stress for resuspension IM2S2	1000	N/m ²

Table 5.2 Periods selected for calibration in WAQ model

	From	To
Period 1 of WAQ calibration	16 November 1995	13 December 1995
Period 2 of WAQ calibration	22 December 1995	30 January 1996

With the parameter set, modelled results during two periods *16 November 1995 – 13 December 1995* and *22 December 1995 – 30 January 1996* are calculated by WAQ model after adequate spin-up of the model. Moreover, the total bed shear stress which is a critical factor to determine the dynamics of cohesive sediment is exported from the WAQ model and its values are inserted into the comparison figures instead of the previous significant wave height. Besides, the SPM concentration modelled by FLOW is added to the comparison figures as well.

➤ **16 November 1995 – 13 December 1995**

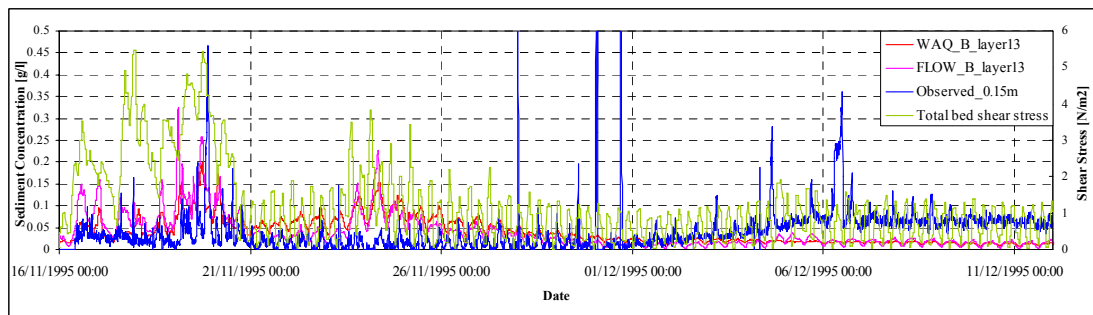


Fig 5.1 Modelled and observed SPM concentration at 0.15 m above the seabed at B point (Period 1 of WAQ calibration)

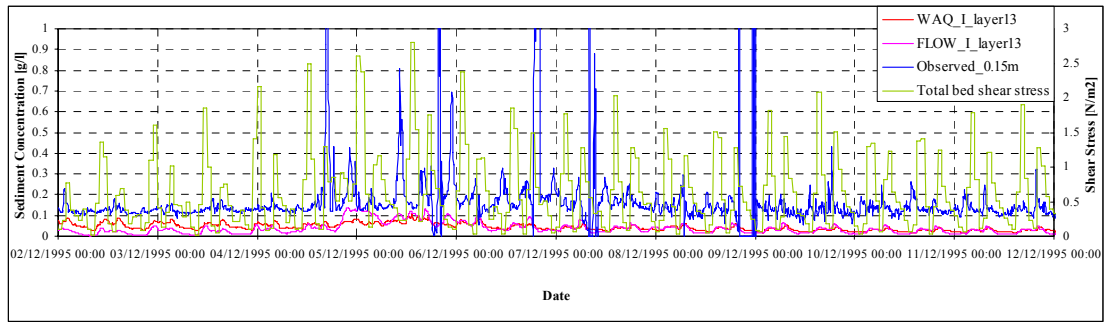


Fig 5.2 Modelled and observed SPM concentration at 0.15 m above the seabed at I point (Period 1 of WAQ calibration)

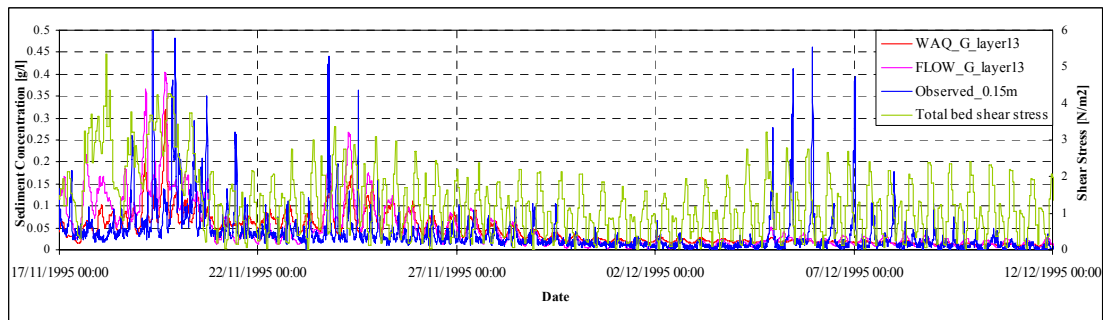


Fig 5.3 Modelled and observed SPM concentration at 0.15 m above the seabed at G point (Period 1 of WAQ calibration)

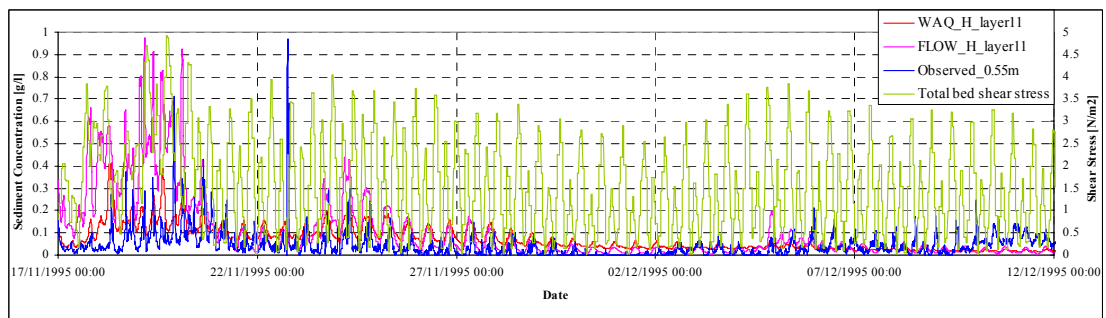


Fig 5.4 Modelled and observed SPM concentration at 0.55 m above the seabed at H point (Period 1 of WAQ calibration)

Table 5.3 Means of Total bed shear stress and SPM concentration in period 1 of WAQ calibration (Unit: N/m² and mg/l)

Location	Mean Shear stress	Observed 0.15m	Modelled layer13		Observed 0.55m	Modelled layer11/10	
			WAQ	FLOW		WAQ	FLOW
B	1.15	41.6	39.7	38.1	74.7	37.1	36.8
I	0.62	179	42.9	35.6	238	39.2	34.1
G	1.12	37.5	42.3	47.8	32.2	39.9	46.3
H	1.55	847	74.8	105.5	45.7	70.7	102.8

Through the comparison of the first calibration period (Fig 5.1-5.4), it is found at B point (Fig 5.1), the modelled SPM concentration of WAQ has right response to the wave-induced bed shear stress during the storm period, but its value is lower than the observed one and the modelled one of FLOW. During most of the calm periods, the modelled concentration of WAQ is lower than the observed one but a little higher than

the modelled one of FLOW. At I point (Fig 5.2), during this measurement period which is relatively calm, the total bed shear stress is not more than 3 N/m². The modelled concentration of WAQ is a little larger than the one of FLOW but still significantly lower than the observed one, which is also indicated in Table 5.3. At G point (Fig 5.3), similar to B point, the observed concentration is also underestimated by WAQ during the storm period, whereas the modelled concentration of WAQ has a good agreement with the observed one during the calm period. At H point (Fig 5.4), compared to the FLOW result, the WAQ seems to be closer to the observed concentration during the storm period, whereas the observed one is overestimated a lot by the FLOW model (Fig 5.4).

Upon the statistical measures of the first calibration period (Table 5.3), there is not significant difference between the modelled concentrations of WAQ and FLOW except for H point, at which the modelled concentration of FLOW is about 40% larger than the one of WAQ. That is because effects on hydrodynamics caused by sediment are not accounted for in WAQ model, whereas the sediment-flow interactions such as damping of vertical mixing and density current are taken into account in FLOW model. The SPM concentration is higher, these effects are more significant. The WAQ model performs well at B, G and H points. At I point, the large discrepancy still exists, which is similar to the FLOW model.

➤ **22 December 1995 – 30 January 1996**

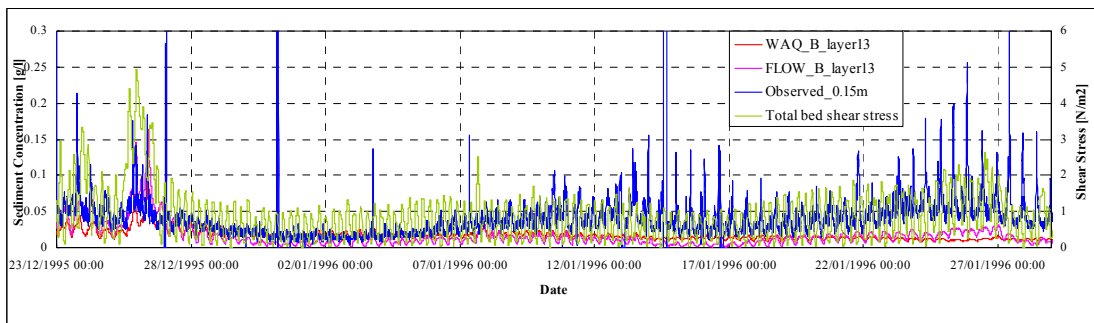


Fig 5.5 Modelled and observed SPM concentration at 0.15 m above the seabed at B point (Period 2 of WAQ calibration)

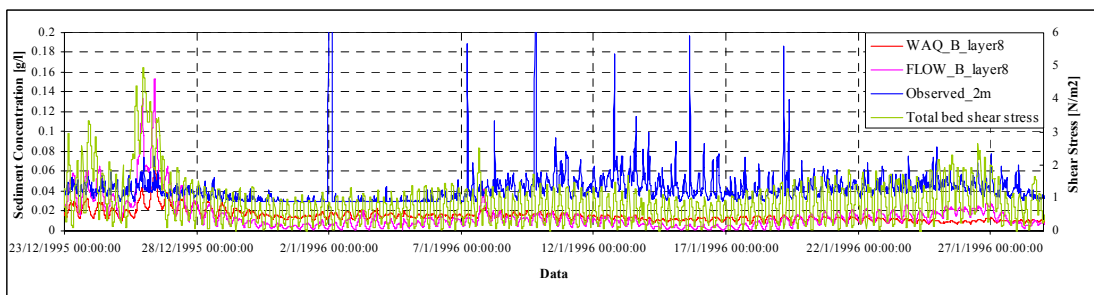


Fig 5.6 Modelled and observed SPM concentration at 2 m above the seabed at B point (Period 2 in WAQ calibration)

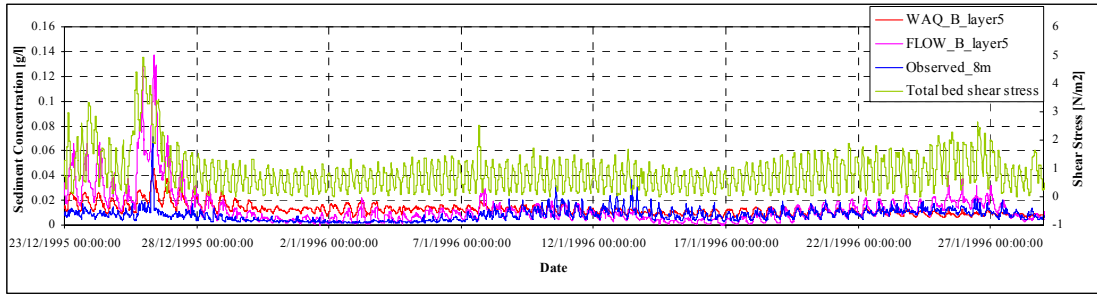


Fig 5.7 Modelled and observed SPM concentration at 8 m above the seabed at B point (Period 2 of WAQ calibration)

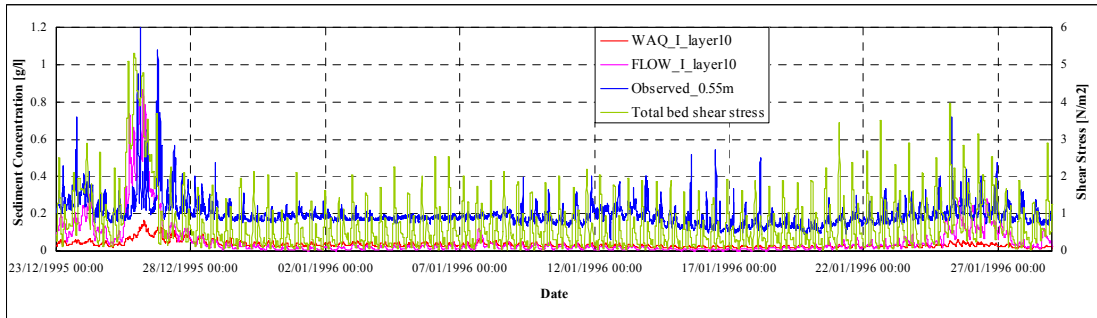


Fig 5.8 Modelled and observed SPM concentration at 0.55 m above the seabed at I point (Period 2 of WAQ calibration)

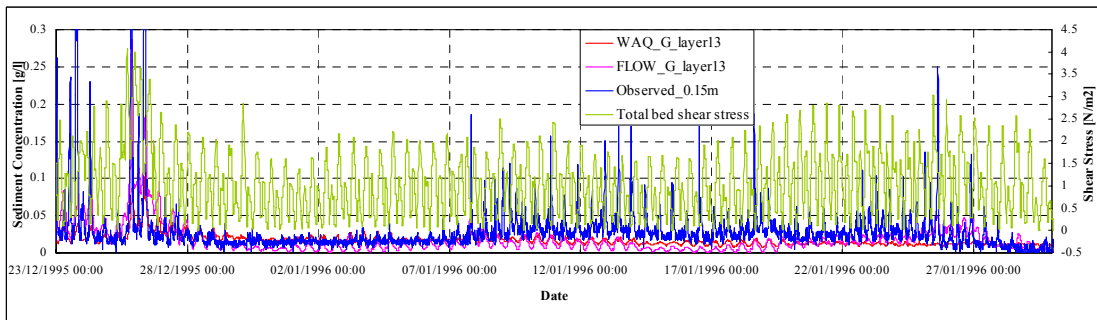


Fig 5.9 Modelled and observed SPM concentration at 0.15 m above the seabed at G point (Period 2 of WAQ calibration)

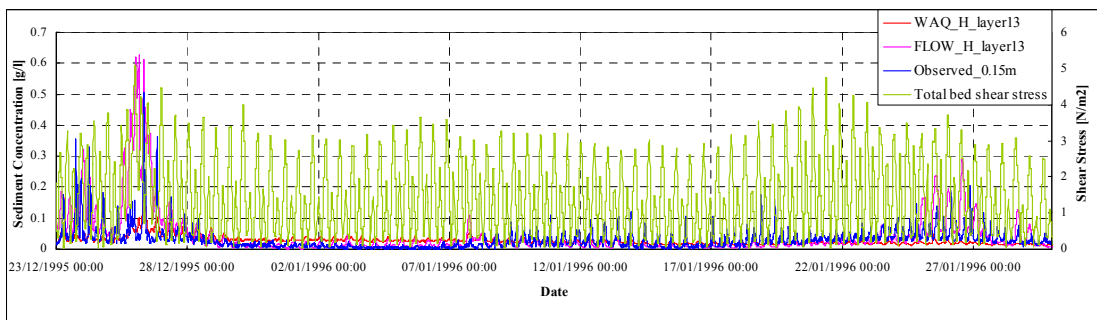


Fig 5.10 Modelled and observed SPM concentration at 0.15 m above the seabed at H point (Period 2 of WAQ calibration)

Table 5.4 Means of Total bed shear stress and SPM concentration in period 2 of WAQ calibration (Unit: N/m² and mg/l)

Location	Mean Shear stress	Observed 0.15m	Modelled layer13		Observed 0.55m	Modelled layer11/10	
			WAQ	FLOW		WAQ	FLOW
B	0.88	50.5	17.3	16.6	65.3	16.4	16.1
I	0.76	212	37.8	58.6	197	34.1	55.8
G	1.07	28.8	17.1	18.6	18.9	16.4	18.1
H	1.47	30.7	27.7	44.9	36.6	26.5	44.0

During the second calibration period (Fig 5.5-5.10), it is found that at B point, firstly at 0.15 m above the seabed (Fig 5.5), the modelled concentration of WAQ is a little lower than the modelled one of FLOW but still close to the observed one. During the calm period, both of the modelled results are lower than the observed value even though the modelled one of WAQ is a little larger than the modelled one of FLOW, which is similar to the comparison at 2 m above the seabed (Fig 5.6). At 8 m above the seabed (Fig 5.7), the observed concentration is overestimated by FLOW model but in a good agreement with the modelled one of WAQ. During the calm period, the modelled concentration of WAQ seems to be a little larger than the modelled one of FLOW. At I point (Fig 5.8), during the storm period, the FLOW model has right response to the wave-induced shear stress, but obviously the WAQ model does not respond sufficiently. During the calm period, both of the modelled results are significantly lower than the observed value. At G point (Fig 5.9), the modelled concentration of WAQ has response to the wave-induced shear stress, but is much lower than the observed one during the storm period. At H point (Fig 5.10), the case is similar to the G point during the storm period. But during the calm period the modelled concentration of WAQ is higher than the modelled one of FLOW and observed one.

According to the statistical measures of the second calibration period (Table 5.3), there is still a large discrepancy at I point, and the observed concentration is underestimated a lot by both of FLOW and WAQ models. The modelled results look better at G and H points. It is addressed that the concentration is higher, the difference between the FLOW and WAQ is larger.

5.2 Conclusions

Based on the comparison presented above, the following conclusions can be drawn:

In overview of the comparison, the SPM concentration modelled by WAQ closely follows that modelled by FLOW under the condition that the concentration is not very high. During storm periods, the WAQ appears to respond much less on the SPM concentration compared to that modelled by FLOW. However, during most of calm periods the concentration modelled by WAQ is a little larger than that modelled by FLOW, which indicates there is more sediment which responds to the tide-induced shear stress. Because in the WAQ model, two sediment components are introduced, one is finer with smaller critical erosion shear stress and the other is coarser with larger critical erosion shear stress, in calm periods the finer one is able to respond to the tide-induced shear stress which is much smaller than the wave-induced one. Moreover, at B point the modelled concentration of WAQ at 2m above the seabed is still significantly lower than the observed one although it is a little higher than the modelled one of

FLOW. At last, the observed concentration changes very rapidly, there are quite steeper fluctuations on the variation pattern, which are difficult to captured by WAQ or FLOW.

Through the application of WAQ model, although it does not seem to be much better than FLOW model in view of the comparison with the observed value, it still displays some positive hints which can guide us to do further calibration. Last but not least, using WAQ model, a large amount of time is saved for the calibration of model.

Chapter 6 Conclusions and Recommendations

The main objective of this study is to understand the underlying mechanics which governs cohesive sediment dynamics in different weather conditions. Of course during the storm periods, the cohesive sediment dynamics is more important. So far, some conclusions can be drawn based on the work which has been done.

6.1 Conclusions

For the sake of providing appropriate hydrodynamic boundary conditions to the finer RIJMAMO model, the study commenced with large-scale ZUNO model. Actually this model has been verified by WL | Delft Hydraulics, but due to the unavailability of the required data for 1995, temperature, salinity and space varying atmospheric pressure processes are removed from the original model. Besides, the wind data is taken from one observational point instead of the space-varying data. With the simplified model, the simulated water level at three observational points is compared with the measured one and another simulated one by the original model. In view of the comparison, the simplified model does not decrease the simulation accuracy on water level at least in the nearshore area, and the original model also behaves well as we expect. Therefore, the simulated hydrodynamic result by the simplified model can be used to provide boundary condition to the finer model as well.

The hydrodynamic boundary condition for RIJMAMO is a time-series with time interval of 5 minutes, which is extracted from the simulated results on corresponding grids in ZUNO model. The modelled velocity magnitude and direction are compared with the observed values at four observation points in SILTMAN data, and the comparison on water level at Lichteiland Goeree is carried out as well. Through the calibration and verification on hydrodynamic model, we can see the modelled hydrodynamic results are quite satisfying except for the velocity magnitude at I point. At this point which is so close to the dike, the peak of velocity magnitude usually reaches over 1 m/s which is nearly impossible to captured by the model in the existing grid structure used in this study.

Within the wave model, the significant wave height is reproduced well although some peaks are underestimated a little. Moreover, the peak wave period is significantly underestimated and smoothed by the model but the variation pattern is still reproduced in a right way. Generally speaking, these modelled results can be applied to cohesive sediment model within sufficient accuracy.

With regard to cohesive sediment model, there are two models FLOW and WAQ which are used in this study. In fact, the observed SPM concentration shows a characteristic of being highly stochastic. But for this study, what the numerical model can explain is deterministic process. In FLOW model, the modelled SPM concentration always follows the variation pattern of significant wave height. Compared with the observed value, the modelled one seems to be a little lower during the calm period, which indicates there is less sediment that responds to tide-induced shear stress. In WAQ model, during the calm period, there appears to be more sediment that responds to tide-induced shear stress than that in FLOW model, however, compared with the observed values, the amount of response is still not enough. Finally, the steep fluctuations on observed concentration seem to be impossible to reproduce by the models.

6.2 Recommendations

Apart from the conclusions listed above, there are some recommendations for the future study:

The hydrodynamic boundary conditions for RIJMAMO model are time-series, with which the model shows a good performance during the calibration and verification. So it is worthwhile to use astronomic type of boundary condition to describe the existing time-series type of that at the three seaside boundaries. After that, we will not need to run ZUNO model any more before we run RIJMAMO model.

During flow simulation, we take morphology into account. The bathymetry is updated and there is feedback to hydrodynamics. However, our calibration period is about half a year long, thus the simulation has to be split to several time windows. The new simulation starts with calculated results of the last time step in the last simulation as initial conditions. However, the model loads bathymetry from original bathymetry file but not from the updated bathymetry in the last simulation. How to update the morphology for segmented simulation is an interesting topic for software developers.

Accounting for the characteristic of cohesive sediment, flocculation in salinity water is an important process which has significant effect on the vertical distribution of sediment concentration. Thus, this is another interesting topic we can study applying an appropriate model to describe the flocculation in the future.

WAQ model displays some advantages, but in view of the modelled results using the same parameter set as ZUNO model, it is not satisfying enough. There should be much more potential we can exploit on WAQ. Firstly, the parameters need to be calibrated further. Secondly, the boundary conditions can be extracted from ZUNO model which has been verified against SILTMAN data, or provided by data-driven model.

In SILTMAN data, the time interval of observation is 10 minutes, but at some time points the observed values are missing. In order to gain clearer insight on the general variation pattern of SPM concentration, the raw observed data should be processed. It is advised to pick up the observed value on every 1 hour or 2 hours from the raw data, and then make comparison with modelled result. The reason of doing so is not only for reaching a better agreement visually but also for filtering some noises from the observed value.

References

- Ariathurai, C.R., 1974. A finite element model for sediment transport in estuaries, University of California, Berkley, USA.
- Bhattacharya, B., 2005. Learning from data for aquatic and geotechnical environments. Taylor & Francis Group, 251 pp.
- Booij, N., Ris, R.C., Holthuijsen, L.H., 1999. A third generation wave model for coastal regions: 1. Model description and validation. *J. Geophys. Res.* 104: 7649-7666.
- Cornelisse, J.M., Vereek, H., 1994. Erosion and liquefaction of natural mud under surface waves. In: Cohesive sediments edited by Burt, N., Parker, R. and Watts, J.: 353-363; Nearshore and estuarine cohesive sediment transport conference, INTERCOH' 94, 4th, Wallingford, England, UK.
- Dingemans, M.W., Radder, A.C., De Vriend, H.J., 1987. Computation of driving forces of wave-induced currents. *Coastal Engineering*, 11: 539-563.
- Dingemans, M.W., 1997. Water wave propagation over uneven bottoms. Part 1 – linear wave propagation. *Advanced Series on Ocean Engineering*, 13. World Scientific, 471 pp.
- Dronkers, J., 2005. Dynamics of coastal systems. *Advanced series on ocean engineering*, Volume 25. World scientific.
- Eisma, D., Kalf, J., 1987. Dispersal, concentration and deposition of suspended matter in the North Sea. *Journal of the Geological Society of London* 144, 161-178.
- Fettweis, M.a.E., Dries Van den, 2003. The mud deposits and the high turbidity in the Belgian-Dutch coastal zone, southern of bright of North Sea. *Continental Shelf Research* 23: 669-691.
- Groeneweg, J., 1999. Wave-current interactions in a generalised Lagrangian Mean formulation, Delft University of Technology, Delft, The Netherlands.
- Groeneweg, J., Klopman, G., 1998. Changes of the mean velocity profiles in the combined wave-current motion in a GLM formulation. *Journal of Fluid Mechanics* 370: 271-296.
- Gerritsen, H., Boon, J.G., Van der Kaaij, T., Vos, R.J., 2001. Integrated modelling of suspended matter in the North Sea. *Estuarine, coastal and shelf science*, 53: 581-594.
- Hartog, J., van de Kreeke, J., Analysis of optical back scatter data observed by the smart buoy at the stations Noordwijk 10, Noordwijk 5 and Noordwijk 2, RIKZ and National Institute for Coastal and Marine Management.
- Hasselmann, K., Barnett, T.P., Bouw, E., Carlson, H., Cartwright, D.E., Enke, K., Ewing, J.A., Gienapp, H., Hasselmann, D.E., Kruseman, P., Meerburg, A., Müller,

- P., Olbers, D.J., Richter, K., Sell, W. and Walden, H., 1973. Measurement of wind-wave growth and swell decay during the Joint North Sea Wave Project (JONSWAP). *Dtsch. Hydrogr. Z. Suppl.*, 12, A8.
- Johan Boon, H.W., Hans Los, 2001. Description and model representation T0 situation part 1: The transport of fine-grained sediments in the southern North Sea.
- Krone, R.B., 1984. The significance of aggregate properties to transport processes; estuarine cohesive sediment dynamics; workshop on cohesive sediment dynamics with special reference to physical processes in estuaries, Lecture notes on coastal and estuarine studies 14, Tampa.
- Lesser, G.R., Roelvink, J.A., van Kester, J.A.Th.M., Stelling, G.S., 2004. Development and validation of a three-dimensional morphological model. *Coastal Engineering*, 51: 883-915.
- Mei, C.C., 1983. *The applied dynamics of ocean surface waves*. Wiley, New York, 740 pp.
- Ris, R.C., Holthuijsen, L.H., Booij, N., 1999. A third generation wave model for coastal regions: 2. Verification. *J. Geophys. Res.* 104: 7667-7681.
- Roelvink, J.A., van der Kaaij T., Ruessink, B.G., 2001a. Calibration and verification of large scale 2D/3D flow models Phase 1, WL | Delft Hydraulics.
- Roelvink, J.A., Walstra, D.J.R., 2005b. Keeping it simple by using complex models. *Advances in Hydro-Science and Engineering*, Vol.VI.
- Ross, M.A., and Mehta, A.J., 1989. On the mechanics of lutoclines and fluid mud. *Journal of Coastal Research (Special Issue 5: High concentration cohesive sediments transport)*: 51-61.
- Ruessink, B.G., Jeuken, M.C.J.L., 2002. Dunefoot dynamics along the dutch coast. *Earth surface processes and landforms* 27, 1043-1056.
- Stelling, G.S., Leendertse, J.J., 1991. Approximation of convective processes by cyclic AOI methods, *Proceeding of the 2nd ASCE Conference on Estuarine and Coastal Modelling*, Tampa. ASCE, New York, pp. 771-782.
- Stelling, G.S., van Kester, J.A.Th.M., 1994. On the approximation of horizontal gradients in sigma coordinates for bathymetry with steep bottom slopes. *International Journal for Numerical Methods in Fluids*, 18: 915-955.
- Terwindt, J.H.J., 1967. Mud transport in the Dutch DELTA area and along the adjacent coastline. *Netherlands Journal of Sea Research*, 3, 4: 505-531.
- Thatcher, M.L., and Harleman, R.F., 1972. A mathematical model for the prediction of unsteady salinity intrusion in estuaries. Report no 144, Massachusetts Institute of Technology.

- Uittenbogaard, R.E., van Kester, J.A.Th.M. and Stelling, G..S., 1992. Implementation of three turbulence models in 3D-TRISULA for rectangular grids. WL | Delft Hydraulics.
- Uittenbogaard, R.E., Winterwerp, J.C., van Kester, J.A.Th.M. and Leepel, H., 1996. 3D Cohesive Sediment Transport. A preparatory study about implementation in DELFT3D, WL | Delft Hydraulics.
- Van Kessel, T., Winterwerp, J.C., 2002. Small-scale 3D mud transport, WL | Delft Hydraulics.
- Van Kessel, T., Brière, C., 2006. Modelling of seasonal SPM variations in the Dutch coastal zone, WL | Delft Hydraulics.
- Van Leussen, W., Cornelisse, J.M., 1993. The role of large aggregates in estuarine fine-grained sediment dynamics. Nearshore and estuarine cohesive sediment transport, A.J. Mehta (Editor), Coastal and estuarine studies, 42: 75-91.
- Van Rijn, L.C., 1993. Principle of Sediment Transport in Rivers, Estuaries, Coastal Seas and Oceans. Aqua Publications, 1993, Amsterdam.
- Van Rijn, L.C., 1986. Sediment pick-up functions. Journal of hydraulic engineering, 112: 867-874.
- Van Rijn, L.C., 1983. Siltation in dredged trenches: two-dimensional mathematical flow model with a two-equation turbulence closure, WL | Delft Hydraulics.
- Verbeek, H., Kuijper C., Cornelisse, J.M. and Winterwerp, J.C., 1991. Deposition of Graded Natural Muds in The Netherlands. Nearshore and estuarine cohesive sediment transport, A.J. Mehta (Editor), Coastal and estuarine studies, 42: 185-204.
- Vos, R.J., 2004. Analysis of suspended matter data from the Minipod deployments, RIKZ werkdocument RIKZ/OS/2004/147w.
- Vriend, H.J.d., 1991. Mathematical modelling and large-scale coastal behaviour. Journal of Hydraulic Research, 29: 727-740.
- Whitham, G.B., 1974. Linear and nonlinear waves. Wiley, New York, 636 pp.
- Winterwerp, J.C., 1998. SILTMAN: analysis of field measurements, Rijkswaterstaat-RIKZ and National Institute for Coastal and Marine Management.
- Winterwerp, J.C., 1999. On the dynamics of high-concentration mud suspensions. Ph.D.-thesis Delft University of Technology.
- Winterwerp, J.C., Kesteren, W.G.M.V, 2004. Introduction to the physicals of cohesive sediment in the marine environment. Developments in Sedimentology, 56. Elsevier, 466 pp.
- Winterwerp, J.C., 2006. Fluxes of fine sediment along the Dutch coast and the impact of

Maasvlakte 2: a system description, Rijkswaterstaat, RIKZ

WL | Hydraulics, 2006. Delft3D-FLOW User Manual.

WL | Hydraulics, 2006. Delft3D-WAQ User Manual.

WL | Hydraulics, 2006. Delft3D-WAVE User Manual.

Ye, Q., 2006. Modelling of cohesive sediment transportation, deposition and resuspension in the Haringvliet Mouth. MSc-thesis UNESCO-IHE Institute for Water Education.